Realistic Forests and the Modeling of Forest-Atmosphere Exchange

Bannister, E. J.; Mackenzie, A. R.; Cai, X.-m.

DOI:
10.1029/2021RG000746

Document Version
Publisher's PDF, also known as Version of record

Citation for published version (Harvard):
Bannister, EJ, Mackenzie, AR & Cai, X 2022, 'Realistic Forests and the Modeling of Forest-Atmosphere Exchange', *Reviews of Geophysics*, vol. 60, no. 1, e2021RG000746. https://doi.org/10.1029/2021RG000746

AGU ADVANCING EARTH AND SPACE SCIENCE

Reviews of Geophysics

REVIEW ARTICLE
10.1029/2021RG000746

Realistic Forests and the Modeling of Forest-Atmosphere Exchange

E. J. Bannister[1,2], A. R. MacKenzie[1,2], and X.-M. Cai[2]

[1]Birmingham Institute of Forest Research (BIFoR), University of Birmingham, Birmingham, UK, [2]School of Geography, Earth and Environmental Sciences, University of Birmingham, Birmingham, UK

Key Points:

- Most forests are naturally patchy. Many are being fragmented by humans. Studies of forest-air exchange rarely consider this heterogeneity
- Gaps, edges, and patchy sources/sinks generate fluxes of momentum and scalars. Scalar quantities are rarely at equilibrium around forests
- Better representations of forest structure, for example, from laser scans, should be included in models, along with more physics and chemistry

Correspondence to:

A. R. MacKenzie,
a.r.mackenzie@bham.ac.uk

Citation:

Bannister, E. J., MacKenzie, A. R., & Cai, X.-M. (2022). Realistic forests and the modeling of forest-atmosphere exchange. *Reviews of Geophysics*, *60*, e2021RG000746. https://doi.org/10.1029/2021RG000746

Received 19 APR 2021
Accepted 20 DEC 2021

Author Contributions:

Conceptualization: E. J. Bannister
Formal analysis: E. J. Bannister, A. R. MacKenzie, X.-M. Cai
Funding acquisition: A. R. MacKenzie
Methodology: E. J. Bannister, A. R. MacKenzie, X.-M. Cai
Supervision: A. R. MacKenzie, X.-M. Cai
Visualization: E. J. Bannister
Writing – original draft: E. J. Bannister
Writing – review & editing: A. R. MacKenzie, X.-M. Cai

Abstract Forests cover nearly a third of the Earth's land area and exchange mass, momentum, and energy with the atmosphere. Most studies of these exchanges, particularly using numerical models, consider forests whose structure has been heavily simplified. In many landscapes, these simplifications are unrealistic. Inhomogeneous landscapes and unsteady weather conditions generate fluid dynamical features that cause observations to be inaccurately interpreted, biased, or over-generalized. In Part I, we discuss experimental, theoretical, and numerical progress in the understanding of turbulent exchange over realistic forests. Scalar transport does not necessarily follow the flow in realistic settings, meaning scalar quantities are rarely at equilibrium around patchy forests, and significant scalar fluxes may form in the lee of forested hills. Gaps and patchiness generate significant spatial fluxes that current models and observations neglect. Atmospheric instability increases the distance over which fluxes adjust at forest edges. In deciduous forests, the effects of patchiness differ between seasons; counter intuitively, eddies reach further into leafy canopies (because they are rougher aerodynamically). Air parcel residence times are likely much lower in patchy forests than homogeneous ones, especially around edges. In Part II, we set out practical ways to make numerical models of forest-atmosphere more realistic, including by accounting for reconfiguration and realistic canopy structure and beginning to include more chemical and physical processes in turbulence resolving models. Future challenges include: (a) customizing numerical models to real study sites, (b) connecting space and time scales, and (c) incorporating a greater range of weather conditions in numerical models.

Plain Language Summary Plants live by an intricate set of exchanges with the atmosphere. They draw carbon dioxide from the air—while being buffeted by the wind—and release water vapor, oxygen, pollen, and a variety of organic compounds. These exchanges are especially intricate in forests, where microbes and animals add to the quantity and variety of exchanges. Forests' patchwork structures mean that trees may experience profoundly different climates to others only meters away. These exchanges are made yet more complicated by the fragmentation of forests by human activity. Here we review recent developments in the understanding of exchanges between the air and realistic, patchy forests. We focus on applying this understanding to improve the realism of computer models. No model can recreate all the exchanges in detail. However, capturing more of the edges, gaps, and patches in real forests, as well as non-ideal weather conditions, will improve our understanding of forest-atmosphere exchanges. This will aid scientific understanding and policy making for forest ecology, meteorology and climatology, and air and water quality.

1. Introduction

1.1. A Sense of Scale

Forests cover about 30% of the Earth's surface and interact with the atmosphere in a variety of ways. Some of these interactions are familiar enough to appear in the poetry and stories of most cultures. Fluttering leaves and swaying branches are among the most obvious visual manifestations of wind. Trees split the wind into flows of different velocities which, if the wind is strong enough, howl when they are reunited. Other interactions, which occur across scales outside of human perception, are apparent only in careful measurements. The time scales of interest in forest-atmosphere interactions begin at approximately 10^{-2} s for leaf fluttering and photosynthetic processes. The period of tree and branch swaying is typically from 10^{-1} to 10 s. Phenomena with longer time scales include boundary-layer turbulence (10^{-1}–10^{4} s), weather systems (10^{3}–10^{6} s), and ecosystem–climate feedbacks (10^{7}–10^{12} s). Similarly, the smallest relevant space scales are roughly 10^{-6} m, which is the order of stomatal openings, airborne spores, and small pollens. Tree elements, such as seeds, leaves, and branches range from 10^{-3} m

(seeds) to 10^2 m (entire large trees). Individual ecosystems scale from 10^2 m (small clumps of trees and plants) to 10^7 m (entire forested landscapes, such as in the Amazon and Congo basins, or the Taiga forests of the Northern Hemisphere). Boundary-layer turbulence contains eddies with diameters 10^{-3}–10^3 m, and processes relevant to meso and synoptic weather systems scale 10^3–10^6 m. No set of mathematical equations describes these various interacting phenomena completely or, often, even approximately. There is also no single correct time or space scale at which to view forest-atmosphere interactions. The most important features of the interactions depend on the scale of interest, as does the theory, experimental methods, and tools available to researchers to study them. In this review, we concentrate on forest-atmosphere interactions across length scales of 10^{-1}–10^3 m and time scales of 1–10^3 s. We refer to this as the "ecosystem scale," which approximately corresponds to the ecological scales from "individuals" to "patches" (Scholes, 2017) and the meteorological micro- and γ-mesoscales (Stull, 1988).

1.2. The Extent of the Literature

At the ecosystem scale, we assume the overall landscape properties to be stationary, because drivers such as fragmentation, tree senescence, and extensive plant growth typically occur on time scales much longer than those of plant movement or boundary-layer dynamics. With these assumptions in mind, researchers typically approach ecosystem-scale forest-atmosphere interactions from one of two directions. The first approach focuses on the effect of the atmosphere on trees and other plants, such as on plant biomechanics (De Langre, 2008, 2019; Gosselin, 2019), leaf microclimates (Vogel, 2009), or water use efficiency (Schymanski & Or, 2016). The second approach, which we use in this review, focuses on the effect of forests on the atmosphere, especially on the structure of the turbulence and the transport of momentum and scalar quantities (Brunet, 2020; Finnigan, 2000; Katul et al., 2013).

Previous reviews of ecosystem–scale turbulent transport around forests have discussed land-atmosphere interactions more generally (e.g., Bou-Zeid et al., 2020; Fisher & Koven, 2020) and ecosystem exchange at long-term monitoring sites (e.g., Baldocchi, 2008; Hicks & Baldocchi, 2020; Oliphant, 2012). These reviews, and the work they discuss, attempt to estimate the net ecosystem exchange of carbon and other scalar quantities, sometimes for scaling up into global-system and other large-scale models. Other reviews focus on the detailed structure and statistics of the turbulence in forests and other vegetated landscapes. The early work in this area was motivated by applied problems in agriculture and forestry, such as minimizing crop lodging and the windthrow of trees (e.g., Inoue, 1955; Ruth & Yoder, 1953). In the 1970s and 1980s, pioneering investigations of the transport equations moved the field from empirical observations to obtaining precise knowledge about certain features of the turbulence, especially in horizontally uniform canopies on flat ground (Finnigan, 2000; Kaimal & Finnigan, 1994; Raupach & Thom, 1981; Raupach et al., 1996; Van Gardingen & Grace, 1991). Katul et al. (2013) supplement these reviews with their survey of scalar turbulence in uniform canopies. Lemone et al. (2019) and Brunet (2020) provide comprehensive background to boundary-layer measurements, including in plant canopies, and update earlier reviews of the flow in homogeneous plant canopies with results obtained using high-performance computers. Other recent reviews discuss the flow and transport of scalar quantities around forest edges (Belcher et al., 2012), the measurement and modeling of ecological processes such as evapotranspiration (e.g., Katul et al., 2012), and hill-induced dynamical effects on the flow and scalar fields around forests and other vegetation (e.g., Belcher et al., 2012; Finnigan et al., 2020).

1.3. The Scope of This Review

The majority of existing work considers forests whose structure has been "idealized" in some way. Often this idealization step occurs when physical and numerical models are configured, although occasionally study sites are chosen on the basis of strict criteria. While there is no single definition of "idealized" in the context of forest-atmosphere exchange, the majority of the literature assumes forests to be horizontally homogeneous, with closed canopies, no large patches or gaps, and without site specific morphological or ecological detail. Below, we describe a forest as "idealized" if most of these properties are assumed. Forests in the real world rarely fit these assumptions. For example, forests around the world are becoming increasingly fragmented (Bogaert et al., 2011; Fahrig, 2003; Taubert et al., 2018). Edge regions differ from the forest interior both in their mean local climate (e.g., less humid) and in the range of meteorological extremes they experience (Magnago et al., 2015). Even in intact ecosystems, most forest canopies comprise a patchwork of openings of many shapes and sizes, formed by senescence, disease, and windthrow (Hirons & Thomas, 2018; Whitmore, 1989). These gaps are significant

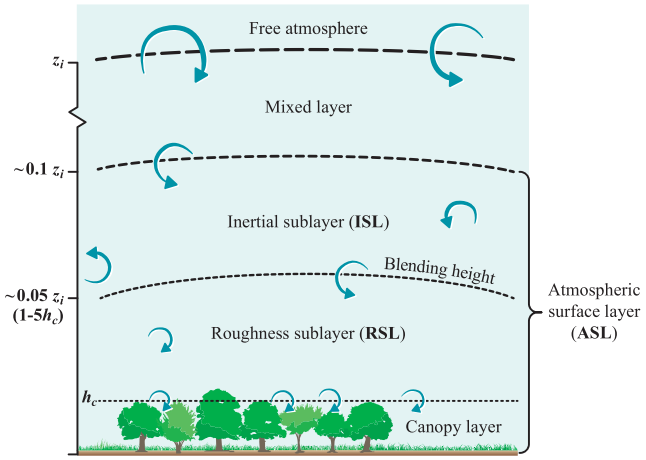

Figure 1. Sublayers of the daytime atmospheric boundary layer (ABL) over a forest. The figure follows the classification in Oke (1988) for an urban boundary layer. The height of the mixed layer, which typically accounts for around 90% of the daytime ABL height, is suppressed to aid presentation. The variables z_i and h_c denote the depth of the ABL and the mean height of the forest, respectively.

ecologically and structurally. The floras of the northern temperate forests, for example, include many species that depend on gaps and patchiness (Fox, 1977; Tinya et al., 2009). The divergence between theory and reality causes, for example, estimates of ecosystem exchange to be inaccurate or biased (Aubinet et al., 2010; Baldocchi, 2008; Stoy et al., 2013; K. Wilson et al., 2002). This is no secret, and most studies end with calls for further experiments in a wider range of ecosystems, using more detailed techniques and models.

We focus our attention on ecosystem-scale exchange of momentum, energy, and mass between the atmosphere and heterogeneous forests. We split our review into two parts. Part I (Sections 2–4) discusses experimental, theoretical, and numerical progress in our understanding of turbulent exchange over realistic, patchy forests. Section 2 summarizes the methodology behind numerical investigations of forest-atmosphere exchange, and the turbulence structure around idealized forests, including the effects of atmospheric stability. The remainder of Part I discusses how structural heterogeneity and patchiness affects the exchange of momentum (Section 3) and scalar quantities (Section 4). We concentrate principally on forests on level ground, although Section 4 briefly discusses recent progress in investigating scalar transport around forested hills. (See Finnigan et al. [2020], for example, for a comprehensive treatment of terrain induced effects on land-atmosphere exchange.) Part II (Sections 5–6) sets out practical ways to make numerical models of forest-atmosphere more realistic, including by accounting for reconfiguration and realistic canopy structure (Section 5) and beginning to include more chemical and physical processes in turbulence resolving models (Section 6). We conclude in Section 7 and provide recommendations for further research under the broader goals of (a) customizing numerical models to real study sites, (b) connecting space and time scales, and (c) incorporating a greater range of weather conditions in numerical models.

Part I: Forest-atmosphere exchange around heterogeneous forests

We begin Part I by summarizing the important fluid dynamical properties of forest-atmosphere exchange in idealized landscapes before moving on to look at exchange in more realistic landscapes.

2. The Flow in and Around Idealized Forests

2.1. Definition of Terms

We use right-handed Cartesian tensor notation, with the Einstein summation convention, and indices (i, j, k) take values (1, 2, 3) respectively. For example, u_i is the velocity in the x_i direction, with $i = 1, 2, 3$ representing the streamwise (x), spanwise (y) and vertical (z) directions. We denote $x = (x,y,z)$, $(u_1,u_2,u_3) = (u,v,w)$, and time as t. For a quantity, ϕ, $\langle\phi\rangle$ denotes a spatial average and $\overline{\phi}$ denotes a time average such that $\phi(x, t) = \langle\phi\rangle(t) + \phi''(x, t)$ and $\phi(\boldsymbol{x}, \ t) = \overline{\phi}(\boldsymbol{x}) + \phi'(\boldsymbol{x}, t)$. We refer to the quantities $\phi''(x, t)$ and $\phi'(x, t)$ as the "dispersive" and "turbulent" quantities, respectively, which reflect local departures from the space and time averages. The nth moment, where n is a positive integer, is given by $\overline{\phi'^n}$, when the time averaging operation is used. These moments can be similarly defined using other expectation operators, such as a spatial average. The standard deviations of the velocity components are $\sigma_{u_i} = (\overline{u_i'^2})^{1/2}$, the mean turbulence kinetic energy (TKE) $= 1/2\overline{u_i'u_i'}$, skewness $Sk_{u_i} = \overline{u_i'^3}/\sigma_{u_i}^3$, kurtosis $Kt_{u_i} = \overline{u_i'^4}/\sigma_{u_i}^4$, and the friction velocity, $u_* = (\overline{u'w'}^2 + \overline{v'w'}^2)^{1/4}$.

Forests are located in the atmospheric boundary layer (ABL), the layer of atmosphere that is directly influenced by the Earth's surface. Figure 1 presents a schematic of the structure of the daytime ABL. The top of the daytime ABL, at height z_i, caps the mixed layer, within which variables such as humidity and potential temperature are approximately constant with height. The lowest 10% or so of the ABL is known as the atmospheric surface layer (ASL), analogous to the "inner region" in wall boundary layers. Above rough surfaces, such as forests and urban areas, the ASL can be further divided into the inertial sublayer (ISL) and the roughness sublayer (RSL)

(Raupach et al., 1991). Within the ISL, the turbulent fluxes of momentum and scalar quantities are approximately constant with height. These constant fluxes are used as scaling parameters in a set of relationships known as Monin–Obukhov similarity theory (MOST) (Foken, 2006; Monin & Obukhov, 1954; Stull, 1988). MOST is widely used in surface-layer parametrizations for numerical weather prediction and climate modeling (Hari Prasad et al., 2016; Skamarock et al., 2008). The RSL extends from the ground up to around 1.5–5 times the mean height of the obstacles h_c, known as the blending height. The lowest part of the RSL, from the ground to $z = h_c$, is the canopy layer, in which obstacles and air are intimately intermingled. In neutral atmospheric conditions, turbulent structures that scale with the mean canopy height h_c control the exchange of momentum and scalar quantities between air and the surfaces of the obstacles. The friction velocity u_* is a scaling variable that is often used as a shorthand for ASL turbulence, with higher values indicating more turbulent conditions. The friction velocity is easiest to interpret when most of the turbulence is mechanically generated by friction with level ground, for example, in the ISL in statically neutral conditions. In conditions where u_* varies slowly in the x,y plane, u_* measured at the canopy top ($u_{*z=h_c}$) acts as a local velocity scale, a state known as "moving equilibrium" (Yaglom, 1979). This scaling allows landscapes, such as forest stands, to be represented as homogeneous patches, with each patch characterized by its own velocity (u_*) and length (h_c) scales (Katul et al., 1999). In these patches, the local turbulence statistics scaled by $u_{*z=h_c}$ become independent of their horizontal position. The moving equilibrium hypothesis approximately holds for flow over simplified vegetated hills in neutral conditions (B. Chen et al., 2019), although it has unfortunately not been widely tested. However, in terrain and atmospheric conditions where the turbulence structure varies strongly in the x,y plane—for example, around patchy forests, or in strongly stable or unstable conditions—then u_* alone provides limited information about the turbulence (Wharton et al., 2017).

2.2. The Double-Average Method

Early models of flow in vegetation canopies accounted for the presence of the plants through empirical drag terms based on spatially averaged velocity measurements (Cionco, 1965; Inoue, 1963). In the 1970s and 1980s, researchers developed a more formal basis for the plants' presence, often referred to as the "double-average method," which proceeds directly from the transport equations (Finnigan, 1985; Raupach & Shaw, 1982; Raupach et al., 1986; N. R. Wilson & Shaw, 1977). This is achieved using a volume average operation such that, for a quantity ϕ,

$$\langle\phi\rangle(\boldsymbol{x},t) = \frac{1}{V}\int\int\int \phi(\boldsymbol{x}+\boldsymbol{r},t)d\boldsymbol{r}. \tag{1}$$

The spatial average in Equation 1 is over a volume that (a) includes multiple trees and plants, but (b) is small compared to the distance over which the structure of the forest varies. The vertical resolution is high in order to properly resolve the flow gradients (Finnigan & Shaw, 2008). Around the same time, researchers applied similar procedures to investigate mass transfer in engineering applications (Howes & Whitaker, 1985; Whitaker, 1973). Because plant elements occupy a small proportion of the available volume, no distinction is typically made between the "superficial" averaging operation (including air and plant elements in the average) and the "intrinsic" average (within the body of fluid only). This distinction can be important in urban areas (Schmid et al., 2019) and probably also in dense monoculture plantations where the tree crowns overlap, although this has not been tested. The averaging operation is followed by a time average over a period sufficient to capture the dominant scales of motion but short enough for the flow to be approximately stationary. Applying the two operations to the continuity and momentum equations, ignoring the Coriolis force and the momentum transfer from viscosity, gives

$$\frac{\partial U_i}{\partial x_i} = 0, \tag{2a}$$

$$\frac{\partial U_i}{\partial t} + U_j\frac{\partial U_i}{\partial x_j} = -\frac{\partial P}{\partial x_i} + \frac{g}{\theta_0}\langle\bar{\theta}_v\rangle\delta_{i3} - \frac{\partial\langle\overline{u_i'u_j'}\rangle}{\partial x_j} - \frac{\partial\langle\overline{u_i}\varepsilon\overline{u_j}\varepsilon\rangle}{\partial x_j} + f_i, \tag{2b}$$

where P is the kinematic pressure, g is the gravitational acceleration, θ_0 is a reference temperature, θ_v is the virtual potential temperature, and δ_{ij} is the Kronecker delta (the second term on the right-hand side of Equation 2b is non-zero when $i = 3$). Capital letters denote the double-averaged quantities, which we refer to as the mean quantities—for example, the mean streamwise velocity component U. The term $-\partial\langle\bar{u}_i\varepsilon\bar{u}_i\varepsilon\rangle/\partial x_j$ is the dispersive flux of mean momentum, which accounts for spatial correlations in the time-averaged velocity field. The dispersive

flux is usually assumed to be low in homogeneous forests and is therefore typically disregarded in numerical models (Patton & Finnigan, 2012). However, recent evidence suggests that the dispersive fluxes of momentum and scalar quantities can be significant around patchy forests (see Section 6.4). See Finnigan (2000) and Finnigan and Shaw (2008) for more formal discussion of the double-average method.

2.3. The Double-Average Method in Numerical Models

In applications as complex as forest-atmosphere exchange, numerical models can only ever serve as incomplete models, rather than as mini versions of the real world, or even as computational wind tunnels. Nonetheless, numerical models have emerged as one of the most powerful tools to investigate forest-atmosphere exchange, supplementing experimental observations, theory, and physical models. Their main advantage is that the flow is defined at every cell within the simulated domain, allowing time series of interest to be extracted easily. With post-processing and visualization software, numerical models provide a picture of the flow that is impossible to replicate with observations or physical models. Researchers have adopted various approaches to approximate solutions to the double-averaged equations, including first-order analytical closure (Finnigan et al., 2015, and references therein), modified gradient-diffusion theory (Zeng & Takahashi, 2000), Reynolds-averaged Navier–Stokes (RANS) solvers (Boudreault et al., 2015; Brunet, 2020, and references therein; Katul & Albertson, 1998), and large-eddy simulation (LES; Shaw & Schumann, 1992). RANS methods span first-order closure, "1.5-order" closure based on the transport of the turbulence kinetic energy and its (specific) rate of dissipation, and second-order and higher closure schemes (Katul et al., 2004). For a variety of applications dealing with land-atmosphere exchange, second-order closure appears to be sufficient (Juang et al., 2008). Direct numerical simulation (DNS) has recently been used for small, idealized plant canopies (Sharma & García-Mayoral, 2020a, 2020b). However, the computational expense of DNS means it can still be employed only for relatively low Reynolds number (*Re*) flow and that it remains unsuitable for ecosystem-scale investigations around forests. LES has emerged as the most popular method for investigating ecosystem-scale exchange around forests, although analytical closure schemes and RANS remain popular for situations that do not require the turbulence to be resolved.

Using LES, a low-pass filter of kernel G is applied to the flow field variables,

$$\widetilde{\phi}(\boldsymbol{x}) = \int_{-\infty}^{\infty} G(x-y)\phi(y)dy, \tag{3}$$

where the overtilde denotes "resolved" field variables, whose prognostic equations are solved. The filter in Equation 3 directly resolves motion larger than the filter width Δ_f, which is greater than or equal to the grid resolution Δ_g, with ratios $\Delta_f/\Delta_g = 1$ or 2 common in practice (Basu & Porté-Agel, 2006; Geurts, 2003). The filtered equivalent of the averaged momentum equations in 2b are

$$\frac{\partial \widetilde{u}_i}{dt} + \widetilde{u}_j \frac{\partial \widetilde{u}_i}{dx_j} = -\frac{1}{\rho}\frac{\partial \widetilde{p}}{\partial x_i} + \frac{g}{\theta_0}\widetilde{\theta}_v \delta_{i3} - \frac{\partial \tau_{ij}}{\partial x_j} + \widetilde{D}_i, \tag{4}$$

where $\widetilde{D}_i$ accounts for forcings such as an imposed pressure gradient, the geostrophic wind, or distributed drag from vegetation and other obstacles smaller than the filter width, Δ_f. The sub-grid scale (SGS) stress term τ_{ij} accounts for unresolved scales, those smaller than Δ_f,

$$\tau_{ij} = \widetilde{u_i u_j} - \widetilde{u}_i \widetilde{u}_j. \tag{5}$$

The SGS stresses and fluxes must be parametrized, for which a variety of schemes have been developed (Section 6.5; Gadde et al., 2021; Kirkil et al., 2012; Moser et al., 2021; Rozema et al., 2015). Once the LES model has been "spun up"—that is, the flow reaches a statistical equilibrium—the statistics of the flow variables are generated by averaging the resolved quantities, usually in space and time (e.g., Cai et al., 2008; B. Chen et al., 2019). The turbulent perturbations are calculated as the departures from those averages (see Appendix A for an example). The main advantage of LES over RANS and analytical models is that LES expressly resolves the largest scales of turbulent motion in the simulated domain. Provided that Δ_f and the model's forcings are chosen carefully, LES also allows a visualization and term-by-term analysis of the turbulent flow of air that cannot be achieved using observations or physical models. To avoid distracting switches between notation, we use the double-average notation throughout this manuscript. References to LES results and models should be interpreted as referring to the resolved variables, unless otherwise stated.

2.4. Representing Forests Through Distributed Drag

The aerodynamic drag of the forest (per unit mass of air) is accounted for through the term f_i (m s^{-2}) on the right-hand side of Equation 2b. This term is the net sum of (a) the form drag from pressure differences either side of each plant element, and (b) the viscous boundary layers that develop over each plant element,

$$f_i = -\left\langle \frac{\partial \overline{P}''}{\partial x_i} \right\rangle + \nu \left\langle \frac{\partial^2 \overline{u}''}{\partial x_j \partial x_j} \right\rangle, \tag{6}$$

where ν is the kinematic viscosity of air. This term is typically parametrized by spatially averaging the localized drag from the individual plant elements as

$$f_i = -C_d a(z) |U| \langle u_i \rangle, \tag{7}$$

where $|U| = (U_j U_j)^{1/2}$ and C_d is a dimensionless drag coefficient. This parametrization is based on the aerodynamic drag equation, used in fluid mechanics and engineering applications. In the fluid mechanics literature, the drag equation (per unit mass) is usually written with a factor of 1/2, which originates from the formula for the kinetic energy of the fluid in front of the body. By meteorological convention, the factor of 1/2 is included in the drag coefficient and does not appear expressly here. This parametrization, which we refer to as the "distributed-drag parametrization," assumes the aerodynamic drag from the forest increases with the square of the velocity, as is the case around bluff bodies (Shaw & Schumann, 1992; N. R. Wilson & Shaw, 1977). The viscous component of the drag is usually neglected in the approximation of f_i because form drag dominates in high-Re flow through forests (Shaw & Patton, 2003; Thom, 1971). The local forest density $a(z)$ is typically assumed to be a function of the plant area density (PAD), the total one-sided plant area per unit layer volume (m^2/m^3). The plant area index (PAI) is the PAD integrated over the height of the forest h_c, that is, PAI $= \int_0^{h_c} a(z) dz$.

It is difficult to determine a robust approximation of the drag per unit volume, f_i, in real forests. The parametrization is based on the form drag imposed by the frontal area of the various tree and plant elements (N. R. Wilson & Shaw, 1977). In closed canopies such as forests, it is typically assumed that more of the plant material is sheltered from the flow than in clumps of leaves or isolated trees, resulting a lower value of the product $C_d a(z)$ for closed canopies (Queck et al., 2012; Sogachev & Panferov, 2006). Relatively low values of C_d are often used in modeling studies to accommodate this shelter effect, with values ranging from 0.1 to 0.5 (Table A1). These values are usually assumed to be constant and invariant with height. Although sheltering effects, and therefore low values of C_d, have been observed at moderate to high wind speeds (Amiro, 1990b; Koizumi et al., 2010), there is much more scatter at low wind speeds (Koizumi et al., 2010; Queck et al., 2012). This is probably because at low wind speeds, the leaves of the trees and plants are mostly relaxed, but will streamline temporarily in response to gusts, significantly altering the drag. At higher wind speeds, the plant elements spend more time in the streamlined position, so there is less scatter in the drag measurements during the passage of gusts. We discuss this reconfiguration in more detail in Section 5.

2.5. The Turbulence Structure Around Forests

As the air moves through a forest, momentum is transferred from the flow to the aerial parts of the plants and trees. This transfer reduces the streamwise wind speed throughout the depth of the canopy and a region of high wind shear forms around the crown top. The shear region is evidenced by an inflection in the mean streamwise wind-speed profile, which is approximately exponential within the canopy and logarithmic above it (Finnigan, 2000; Raupach et al., 1996). Below the main crown, a secondary wind-speed maximum may occur (Shaw, 1977), especially near edges and in forests with sparse understories (Dupont et al., 2011). The source of this secondary maximum is not certain, although it may result from the turbulent transport of momentum from the upper canopy (Shaw, 1977) or mesoscale pressure gradients (Holland, 1989). The high shear around the crown top generates Kelvin–Helmholtz-type instabilities, which in turn generate coherent large eddies around the tops of the trees, analogous to the dominant processes in a plane mixing layer (Raupach et al., 1996). Using this mixing-layer analogy, Raupach et al. (1996) reduce canopy turbulence to a single length scale, $L_s = U_{h_c}/(\partial U/\partial z)_{h_c}$, where U_{h_c} is the mean streamwise velocity component U at $z = h_c$. The shear length scale L_s, which equates to around $0.5h_c$ for medium density vegetation, provides a rough estimate of the diameter of the dominant turbulent eddies.

It is difficult to determine the value of L_s exactly for real forests because dU/dz varies quickly with height around the crown top (i.e., d^2U/dz^2 is not easily defined). However, L_s can be estimated from the spectral energy peaks in wavelet cospectra of momentum and scalar quantities (Katul et al., 1998).

The second-order moments $\langle \overline{u'^2} \rangle$, $\langle \overline{w'^2} \rangle$, $\langle \overline{u'w'} \rangle$, and the TKE increase with height within plant canopies, but are roughly constant above the canopy (Brunet, 2020; Raupach et al., 1996). The turbulent velocity components u' and w' are more correlated and skewed in the RSL than they are in the ISL above, where many velocity statistics display approximately Gaussian behavior. Streamwise and vertical skewness (Sk_u and Sk_w) are approximately zero in the ISL but take values $0.5 \leq Sk_u \leq 1$ and $-1 \leq Sk_w \leq 0$ in forests (Amiro, 1990a; Kruijt et al., 2000; Lee & Black, 1993; Raupach et al., 1996; Villani et al., 2003). The values of Sk_u and Sk_w may be higher, absolutely, at forest edges (Dupont & Brunet, 2008a). The association of positive Sk_u and negative Sk_w values indicates that turbulent transfer is dominated by strong but infrequent downward penetrations of air into the canopy, known as "sweep motions" ($u' > 0$ and $w' < 0$). Frequent upward motions of low-momentum air from within the canopy, known as "ejections" ($u' < 0$ and $w' > 0$), also account for a large proportion of the turbulent transfer (Shaw & Patton, 2003), although sweep motions contribute more to the total transfer of momentum around the crown top (Raupach et al., 1996; Shaw & Tavangar, 1983). Together sweep motions and ejections account for between 60% and 80% of the exchange of scalar quantities from homogeneous forest canopies to the atmosphere aloft (Gao et al., 1989). The greater magnitudes of the skewness statistics around forest edges reflect the significant differences in momentum and scalar exchange in patchy and gappy forests as compared to homogeneous canopies.

The mixing-layer analogy—where shear generated eddies around the crown top dominate turbulent exchange—has proved remarkably robust in forests and other vegetation. However, current understanding of canopy turbulence is far from complete. Further LES studies and targeted observations will help to reveal to what extent three-dimensional structures dominate the turbulence and the conditions under which the mixing-layer analogy breaks down when the canopy is patchy. Another knowledge gap concerns forest density. The vast majority of reported investigations have been on relatively dense tropical, Taiga, and northern temperate forests, usually in the growing season. In these forests, mixing-layer-type turbulence has been observed at low densities (Brunet, 2020). However, other sparse tree-dominated landscapes—say, the Guinea Savannah or temperate deciduous forests in winter—have similar mean densities (e.g., PAI 1–2; Xiao et al., 2017) but entirely different structural and meteorological drivers. These important landscapes remain poorly understood. For further discussion of plant-canopy turbulence see Finnigan (2000) for flow statistics and technical background, Finnigan et al. (2009) and Bailey and Stoll (2016) for the emergence of coherent fluid structures, Belcher et al. (2012) for scaling analysis in complex terrain, and Brunet (2020) for historical background and a review of recent studies in homogeneous plant canopies.

2.6. Atmospheric Stability and the Turbulence Structure

Air in the ASL is, on average, statically unstable during the day and stable at night, although the true dynamics are more complicated (Stull, 1991). The mixing-layer analogy of canopy turbulence assumes near-neutral conditions, with the dynamics controlled by the high shear in the mean wind velocity around the tops of the trees. However, in strongly stable or unstable conditions, the velocity shear can be much less influential (Brunet & Irvine, 2000; Lemone et al., 2019). As the ABL becomes more unstable, the turbulence structure around forests transitions from a shear-driven to a convection-driven regime, that is, thermal cells govern the flow dynamics, and the mixing-layer type turbulence becomes less prominent (Dupont & Patton, 2012; Lemone et al., 2019; Mahrt, 2000). Conversely, when the ABL is stable, the buoyancy of the air dampens vertical motion. Mixing-layer type coherent structures may still develop around a forest, but they are smaller and less energetic than those that form in near-neutral conditions (Dupont & Patton, 2012). ABL turbulence is generally more intermittent in space and time in stable conditions (Mahrt, 2014). In very stable conditions, fluxes of scalar quantities are driven by an interaction of mesoscale phenomena, such as gravity waves and nocturnal jets, and the local turbulence. This interaction is observed in the large, intermittent variations in temperature and CO_2 concentration around forest that occur when extended calm periods are interrupted by short bursts of intense turbulence (Aubinet, 2008; Heinesch et al., 2007; Wohlfahrt et al., 2005).

Simulations of flow around idealized forests in non-neutral conditions are beginning to add detail to this general picture. Patton et al. (2016) used LES to investigate the entire ABL over an interactive forest canopy, across five stability classes (near neutral to free convection). In strongly unstable conditions, thermal plumes may bubble

up from the forest floor or the canopy top, and the vertical profiles of the atmosphere in the RSL approach those predicted by MOST. As stability decreases from near neutral to free convection, the dominant turbulent structures around the forest change from shear layer vortices to thermal plumes, and momentum and scalar fluxes become less correlated. It is not clear whether this transition is gradual, with shear and thermally driven structures coexisting, or sudden, with a flip between regimes upon reaching a stability threshold. Nascent research indicates the transition may be sudden (Brunet, 2020). In unstable conditions, scalar quantities are transported predominantly by thermal plumes. The Canopy Horizontal Array Turbulence Study (CHATS) observations provide the strongest observational evidence as to the effect of atmospheric stability on exchange in a tree dominated landscape (Dupont & Patton, 2012; Patton et al., 2011). These measurements found the velocity variances, momentum stresses, and momentum transport efficiency decrease as the atmosphere becomes less stable, indicating that thermal plumes become increasingly influential.

In stable conditions, wind shear at the crown top is higher than in unstable or neutral conditions, and momentum penetrates less deeply into the forest (Chaudhari et al., 2016; Nebenführ & Davidson, 2015; Su et al., 2008). Within the forest, turbulence is much weaker and more intermittent than in neutral or unstable conditions, and the pressure transport term of the TKE budget becomes more significant with increasing stability (Nebenführ & Davidson, 2015). In open forests, intermittent turbulence, driven by shear in the air aloft, may penetrate into the canopy and dramatically alter the distribution of scalars (Wharton et al., 2017). These intermittent events in stable conditions are not well understood and are seldom resolved well by numerical models because they do not result from resolved shear generated turbulence at the microscale or the MOST parametrizations used in larger scale models. The events are thought to result from nonturbulent "submeso" motions, which fall between the scale of the largest turbulent ABL eddies (~O(100 m)) and the smallest γ–mesoscale (~O(2 km); Mahrt, 2014). There is some evidence that parametrizations of submeso motions may be possible by analogy with "self-organized criticality," the tendency of dynamical systems to organize their microscopic behavior to be scale independent (Cava et al., 2019). However, this remains an active area of future research, requiring careful comparison between numerical model results and observations (Sun et al., 2015).

The atmospheric stability within forests often differs to that of the surrounding atmosphere. For example, on a sunny day, warm convective thermals may form above a forest, while the air within it remains stable (Ramos et al., 2004; Stull, 2006). At night, the situation is reversed when the forest crown loses heat through radiative cooling, forming a capping layer of very stable air around the tops of the trees that can decouple the forest air space from its surroundings (Nebenführ & Davidson, 2015; Paul-Limoges et al., 2017; X. Xu et al., 2015). The decoupling is sensitive to site specific meteorological conditions, such as local temperature gradients (Alekseychik et al., 2013; Russell et al., 2016). When the ABL and forest air space decouple, eddy-covariance measurements are difficult to interpret because CO_2 and other scalars can accumulate within the canopy, and the measured turbulent flux is unrepresentative of the forest as a whole (Aubinet, 2008; Massman & Lee, 2002). In hilly terrain, the decoupling can trigger drainage flows, transporting CO_2, heat, and water vapor to and from forests (Finnigan et al., 2020; Sun et al., 2012; Wharton et al., 2017; X. Xu et al., 2015). Drainage flows and other below-canopy transport contribute a large proportion to the total scalar transport in certain meteorological conditions, such as during stable nights with weak winds (McHugh et al., 2017; Paul-Limoges et al., 2017).

3. Realistic Landscape Effects

3.1. Adaptation to Wind Loading

Wind affects all aerial parts of forests on time and space scales from those of the smallest eddy to those of climate variation and tree lifetimes. Many plants respond to wind by reducing their surface area to minimize drag, and therefore lower the likelihood of damage from wind loading. On longer timescales, plants may apportion biomass in such a way as to acclimate to the wind's prevailing direction and intensity, a process known as thigmomorphogenesis. Figure 2 presents examples of trees that show thigmomorphogenetic changes as a result of sustained wind loading. For example, trees at the upstream edge of a forest may have stiffer wood than those further inside the stand (Brüchert & Gardiner, 2006; Cucchi et al., 2004), and trees exposed to high winds develop lower crown densities, comprising a smaller number of smaller leaves (Telewski, 2009; Telewski & Pruyn, 1998). This adaptation is a trade-off for the trees, with increased resistance to wind loading and other environmental stresses coming

Figure 2. (a – left) A wind modified hawthorn (*Crataegus monogyna*) on the Isle of Wight, UK and (b – right) windswept trees at Slope Point, South Island, New Zealand (Aotearoa).

at the expense of slower growth (Hirons & Thomas, 2018). For further background on the permanent response of trees to wind loading, see, for example, Telewski and Pruyn (1998), Telewski (2009), Hirons and Thomas (2018).

Windbreaks, also known as shelter belts, exploit the ability of trees and shrubs to adapt to windy environments. Windbreaks have been used for centuries to shelter coastal buildings, to modify the microclimates around crops and grazing land, to protect woodland and wildlife, and, more recently, to modify pollutant transport around urban or industrial areas (Palmer et al., 1997; Pearce et al., 2021). Figure 3 shows a sketch of the streamlines around a windbreak for wind blowing left to right. The "quiet zone" is the region behind the barrier where the mean wind speeds are low and turbulence is dominated by recirculating eddies (Raine & Stevenson, 1977). The quiet zone extends $x/h_c \approx 8$–17 downstream of the windbreak, with higher values observed in conditions with low atmospheric turbulence. The "wake region" is above the quiet zone. The air in the wake region is highly turbulent because of the interaction of downward fluxes of momentum, and sharp velocity gradients as the flow adjusts around the barrier (Finnigan & Bradley, 1983). The sizes and energies of the vertical fluctuations are enhanced in the wake region compared to the incoming stream, whereas those of the vertical components are suppressed (McNaughton, 1989; H. Wang et al., 2001 and references therein).

3.2. Flow Adjustment Around Forest Edges

Compared to the flow around relatively isolated windbreaks, the flow around a forest is more complicated. Figure 4 presents a schematic of the statistical patterns in momentum transfer that emerge as the flow adjusts around a small forest in neutral atmospheric conditions (Belcher et al., 2003, 2012; Dupont & Brunet, 2008a, 2009).

In the *impact region*, (i) in Figure 4, the forest acts as a step-change in porosity, inducing a pressure gradient to slow the flow. Just downstream of the forest edge is the *adjustment region*, (ii) in Figure 4, in which the drag from the trees decelerates the flow over a distance x_A proportional to a canopy drag length scale $L_c = 1/C_d a(z)$. The length scale L_c emerges from quasi-inviscid solutions to the momentum equations in one-dimensional flow. It can be interpreted as a distance constant over which the velocity and drag adjust to balance the pressure gradient (Finnigan & Brunet, 1995). At the edge of homogeneous canopies, assuming constant shear and neutral atmospheric conditions, the canopy drag length scale L_c is related to the shear length scale L_s by

$$L_c \approx L_s/2\beta^2, \tag{8}$$

where $\beta = u_*/U$ measured at the canopy top ($z = h_c$) (Brunet, 2020; Ross & Vosper, 2005). Because L_c is inversely proportional to the plant density, the flow adjusts more quickly with increasing forest density, provided the density varies on scales greater than the volume averaging operation. (Planted forests are planted at a high density and then thinned repeatedly over the years to reach the final stocking density. It's not unusual for new forests to be planted at 1,000 stems per ha, or 3 m spacing (Forestry Commission, 2021; U.S. Department of Agriculture, 1982). Diameter at breast height measurements can then convert stand number density into basal area (i.e., m^2 (stem) ha^{-1}).

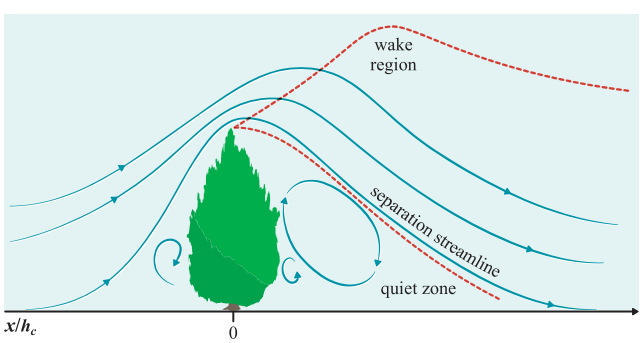

Figure 3. Flow streamlines around a shelter belt standing perpendicular to the flow of air from left to right. Strong turbulent mixing occurs in the wake region. Figure after McNaughton (1989).

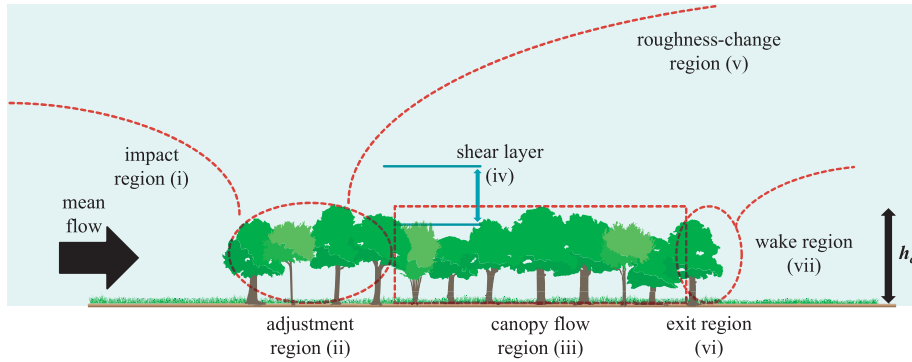

Figure 4. Dynamical flow patterns around a small forest in neutral atmospheric conditions. Each pictured tree represents approximately three trees in the streamwise direction. Figure after Belcher et al. (2003) and Dupont and Brunet (2009).

Converting basal area into PAD requires knowledge of the allometry (i.e., size and shape) of the trees in the stand from standard models or remote sensing (Section 5.2, below). Variations from the planted-and-thinned density arise from introduction of rides for timber extraction, topographic features, and mortality from disease and windthrow.) The length scale L_c is only an approximation for three-dimensional flow around real forests, for which the variables C_d and $a(z)$ may not be clearly defined (Section 5). Nonetheless, numerical simulations, field observations, and flume investigations of vegetation canopies show the adjustment distance x_A downstream of a forest edge is indeed proportional to L_c, with $x_A \approx 4{-}6L_c \approx 8{-}10h_c$ (Belcher et al., 2012; Morse et al., 2002; Rominger & Nepf, 2011; Yang, Raupach, et al., 2006). The canopy drag length scale permits an alternative expression for the PAI of a forest: $\mathrm{PAI}/h_c = a(z) \approx a$, so that $\mathrm{PAI} \approx h_c/C_d L_c$. This is only a rough approximation, because it assumes the plant area is evenly distributed in all directions. Modeling studies have used PAI values in the range 1–8, with most studies concentrating at the low-to-medium end of the range (Table A1). The relative scarcity of studies using PAI > 5 is surprising given that values in tropical and conifer forests often fall in the range 8–12 (Fleischbein et al., 2005; Lefsky et al., 1999). In the *canopy-flow region*, (iii) in Figure 4, the flow is fully adjusted to the presence of the forest. The *canopy-shear layer* (iv) is characterized by the shear-generated turbulent eddies that exchange most of the energy, mass and momentum between the forest and the atmosphere. These eddies are generated by processes analogous to those in a plane mixing layer (Section 2.5 above) (Raupach et al., 1996). Downstream of the adjustment region, an internal boundary layer may begin to develop above the trees, known as the *roughness-change region* (v).

If there is low vegetation or a large clearing in the lee of the forest, an *exit region* (vi) forms, within which mean wind speed increases, with a corresponding downwards flow, over a streamwise distance $1{-}4h_c$. The exit region may or may not contain a quiet zone of recirculating eddies, as behind windbreaks. Quiet zones are more likely to form in the lee of dense forests, especially those with an extensive understory, because the mean wind speed in the canopy flow region is typically low, meaning there is little exit flow at the leeward edge (Cassiani et al., 2008; Detto et al., 2008). However, because forest edges are typically more porous than purpose-built windbreaks, the recirculating eddies are more time intermittent than those behind windbreaks (Bergen, 1975; Cassiani et al., 2008). Recirculating eddies become increasingly common in forest lees as the forest density increases, although Cassiani et al. (2008) report a threshold $\mathrm{PAI} \approx 6$ after which further increases in density have little effect the turbulence structure in the lee. The formation and strength of the recirculating eddies appears to be relatively independent of a forest's foliage distribution (Ma et al., 2020), although the influence of edge morphology has not been carefully tested. A turbulent *wake region* (vii) occurs above the exit region. Because tree foliage creates substantial drag, the air above forests is typically more turbulent than that over the bare ground, sea, or fields typically found upstream of windbreaks. This higher turbulence decreases the distance over which the wake region reaches the ground behind forests as compared to windbreaks. The quiet zone is therefore relatively smaller behind forests ($x/h_c = 2$–5) than behind windbreaks ($x/h_c = 8$–17) and wake turbulence decays faster in the former. Banerjee and co-workers offer interesting arguments as to why the edge regions in Figure 4 appear to be so reproducible. Provided the forest is dense enough, the main features in Figure 4 are recovered from turbulently inviscid solutions of the momentum equations (Banerjee et al., 2013). This suggests that local forest structure and

corresponding turbulence modifies the details of the features in Figure 4 but not their existence. In other words, the turbulently inviscid solution determines the spatial patterns in the mean flow field and turbulence displaces them locally or smooths them.

3.3. The Edge Regions in Context

Only about half of the world's remaining forest area, mostly in the Amazon and the Congo Basin, lies more than 500 m from the nearest edge (Haddad et al., 2015). In much of the Northern Hemisphere, forests are small and patchy because they are located close to areas where large populations of humans have lived for centuries. As an extreme example, approximately three-quarters of English woodland lies less than 100 m from the nearest edge (Riutta et al., 2014). Simple geometric considerations indicate that the area of forest subject to edge effects, the "edge region," is surprisingly large. Among two-dimensional shapes with the same area, a circle has the shortest perimeter, that is, it is the most compact shape in terms of its edge to area ratio. By approximating the plan of a forest stand as a circle, we obtain a lower limit to the area of the edge region from the annulus of width x_A, where x_A is the flow's adjustment distance. The lower limit for the ratio R_0 of the area of the edge region to the total stand area is therefore

$$R_o = \frac{x_A(2r - x_A)}{r^2} = \frac{\pi \cdot x_A\left(2\sqrt{\frac{A}{\pi}} - x_A\right)}{A}; r \geq x_A > 0, \tag{9}$$

where A is the area of the forest stand and r is the radius of the equivalent-area circle. Taking $R_0 > 1/2$ in Equation 9 shows the edge region comprises over half the forest stand where $\sqrt{A/\pi} < (2 + \sqrt{2})x_A$, that is, where $A < (6 + 4\sqrt{2})\pi x_A^2$. Because most forest stands are not even approximately circular, the area subject to edge effects is substantially larger than this minimum. As a conservative heuristic for non-circular forests, we suggest edge effects dominate an area 25% greater than the area of the equivalent-area circle, therefore, where $A < 1.25 \times (6 + 4\sqrt{2})\pi x_A^2 \approx 46x_A^2$. Taking $x_A \approx 8h_c$—the lower end of reported values of x_A—provides a rule-of-thumb that edge effects dominate in forest stands where $A <\sim 3000h_c^2$. Since forested areas are usually reported in hectares and canopy heights in meters, a dimensional version of the rule-of-thumb is

$$A(\text{ha}) < 0.3[h_c(\text{m})]^2. \tag{10}$$

For example, for a mature forest with a canopy height of 20 m, edge effects dominate for patches whose area are less than 120 ha. In many parts of the world (Haddad et al., 2015), edge effects dominate most of the forested area.

3.4. Patches and Gaps

Most real forests contain openings of all shapes and sizes, some examples of which are shown in Figure 5. At which scale do these openings begin to influence forest-atmosphere exchange? As regards light penetration, Zhu et al. (2015) propose three categories of gap sizes in temperate forests: "small" $0.49 < R_{O_d/h_c} \leq 1$; "medium" $1 < R_{O_d/h_c} \leq 2$; and "large" gaps, $2 < R_{O_d/h_c} < 3.5$, where R_{O_d/h_c} is the ratio of the opening's diameter (O_d) to the mean height of the trees surrounding the gap. Openings with diameters such that $R_{O_d/h_c} \geq 3.5$ are considered clearings with their own edges. Small openings, such that $R_{O_d/h_c} \leq 0.49$ are not treated as gaps, because they remain in shade for much of the day. Regarding the flow of air, it is not clear at which size a canopy opening is a "pore," in that the filtering operations smooth out its effect on the flow, and at which size it is a "gap," in that it induces non-random dynamical effects. Determining a numerical threshold between pores and gaps is not possible using observations alone because of the difficulties inherent in obtaining spatially representative velocity observations in forests (Finnigan, 2000; Finnigan & Shaw, 2008), and is not straightforward even using idealized LES models, because the threshold likely to be around the scale of, or smaller than, the spatial filter. We propose, as a first approximation, that openings with horizontal diameter greater than the shear length scale ($O_d \geq L_s$) can be considered "gaps," because they are likely to induce fluid dynamical effects on the scale of the dominant turbulent eddies. Openings where $O_d \ll L_s$ can be considered "pores" in that they have only wake-scale effects on the flow and contribute little to the overall TKE budget (Finnigan, 2000; Raupach & Shaw, 1982; Raupach et al., 1996). The length scale L_s is most soundly defined in homogeneous, dense vegetation canopies, so this

Figure 5. Openings in various forest canopies. (a) In-canopy and (b) aerial views of the BIFoR FACE facility, situated in a mature deciduous woodland in the United Kingdom (Hart et al., 2020). The FACE infrastructure is sited in natural gaps in the forest canopy. Note the variation in foliage color and density in (b), which was caused by insect herbivory during an outbreak of the European winter moth; (c) canopy openings in the understory layer of a tropical rainforest in Suriname; (d) canopy openings in the understory layer of a boreal forest in British Columbia, Canada.

is only rough approximation for patchy forests. Because $L_s \approx 0.5h_c$, this dynamical definition of canopy gaps corresponds to the minimum size of the "small gaps" proposed by Zhu et al. (2015), which they determined with respect to light penetration rather than fluid dynamics.

Few studies have modeled the effects of patchiness on ecosystem-scale exchange. Bohrer et al. (2009) use a virtual canopy generator (Bohrer et al., 2007) to simulate three-dimensional deciduous canopies, including gaps smaller than a tree crown. The heterogeneity caused turbulent fluxes to become spatially correlated in some parts of the forests, such as stronger and more frequent ejection events occurring over shorter trees. Bohrer et al. (2009) also show that canopy gaps affect the flow differently depending on season. In winter, when deciduous forests are sparse, heterogeneity in the forest canopy causes the dominant turbulent eddies to penetrate less deeply into the canopy relative to the homogeneous case. This decreases the forest's roughness length z_0, a common measure of surface roughness, and the displacement height h_d, which reflects the height of the bulk sink of momentum. By the end of spring, however, when the PAI is higher, gaps in the forest canopy cause the dominant turbulent eddies to penetrate further into the canopy, and the values of z_0 and h_d to increase. In other words, in winter, the flow perceives a patchy forest as smoother than a homogeneous one but, after spring leaf-out, it perceives a patchy forest as rougher. This probably results from there being a smaller density contrast between the gaps (high eddy penetration) and full canopy cover (low eddy penetration) in winter, as well as lower wind speeds in spring. It is not clear why Bohrer et al. (2009) focused on spring rather than summer as their leaf-out season, since, for deciduous forests, spring is a time of rapid change in terms of weather and canopy structure. The changes to the values of z_0 and h_d induced by the transitions in canopy morphology are relevant to large-scale atmospheric mod-

els, which employ these parameters to represent forests' effect on the atmosphere. Bohrer et al. (2009) propose that variables such as the maximum PAI and the fractional area of gaps may be used in regional models to adjust the parameterized values of z_0, h_d and the eddy penetration depth, each of which may vary by around 25% in patchy forests relative to homogeneous forests of the same density. Maurer et al. (2015) find that varying z_0 and h_d seasonally, as a function of the canopy structure, produces more precise and less biased estimates of u_* than models taking constant values of those parameters. In Section 6.4, we discuss the dispersive fluxes arising from canopy gaps and patchiness.

4. Scalar Quantities in Realistic Landscapes

Scalar processes remain far less well understood than velocity adjustment and momentum transport, in terms of both the fundamental flow statistics (Shralman & Siggia, 2000) and in geophysical applications around forests (Bou-Zeid et al., 2020; Katul et al., 2013). However, the desire to understand forest-atmosphere scalar exchange is a major motivation for measuring and modeling forests in the first place. Important scalar quantities in forest ecology include energy; trace gases such as CO_2, water vapor, ozone, and volatile organic compounds (VOCs); ultrafine particles (UFP); litter fragments; soil particles; insect and animal detritus; and spores and pollen. In this section we focus on the numerical modeling of species that can be approximated as being passive and massless at the ecosystem scale. These include CO_2, as well as other gases and UFPs whose lifetimes are longer than the longest air parcel residence times (Bannister et al., 2021; Janhäll, 2015; Kanani-Sühring & Raasch, 2015; Petroff et al., 2008). Other scalars, such as litter, animal detritus, and certain pollens, are much larger and must be treated differently (Section 6 below). For a scalar quantity ϕ, the conservation equation (neglecting molecular diffusion) is

$$\frac{\partial \phi_i}{\partial t} + U_j \frac{\partial \phi_i}{\partial x_i} = -\frac{\partial \tau_{j\phi_i}}{\partial x_j} + S_{\phi_i}, \tag{11}$$

where $\tau_{j\phi_i}$ is the SGS scalar flux (this term is not present when the equation is not spatially filtered, see Section 2.2 above). The term S_{ϕ_i} is a source/sink accounting for the emission, deposition, and production or destruction of the scalar quantity. Equation 11 can be double filtered into mean, turbulent and dispersive components, as for Equation 2. We retain the forest edge terminology from Section 3 (Figure 4) in this section.

4.1. Scalar Transport at the Upstream Edges of Forests

Scalar quantities accumulate in the adjustment region at the upstream edge of the forest (region [ii] in Figure 4) over a streamwise distance $x \approx 9{-}12L_c \approx 2x_A \approx 16{-}20h_c$. Here, concentrations of the scalar quantity can be several times higher than in the air upstream of the forest. This pattern appears consistent across field observations of heat transport around forest edges (Klaassen et al., 2002), and in RANS (Sogachev et al., 2008) and LES (Kanani-Sühring & Raasch, 2015; Ma et al., 2020) models of flow around idealized forests. The turbulent fluxes of scalar quantities above the adjustment region are 1.2–3.8 times larger than the surface source rate, and are therefore compensated by horizontal fluxes from elsewhere in the forest (Kanani-Sühring & Raasch, 2015). The location of the peak scalar concentrations and turbulent fluxes is dictated by (a) the adjustment of the flow and (b) the streamwise turbulent scalar transport. The mean and turbulent fluxes are of the same order, with the turbulent component more influential in sparser forests. Strong turbulent fluxes occur above the end of the adjustment region at $x \approx x_A$, and $z \approx 1.5h_c$ (Kanani-Sühring & Raasch, 2015; Ma et al., 2020). Ma et al. (2020) attribute these fluxes to scalar-rich air being swept upwards by the mean and turbulent components of the flow (σ_w^2 is high in this region). Horizontal and vertical advection, which eddy covariance measurements do not usually account for (Aubinet et al., 2010), dominate CO_2 transport in the adjustment region (Ma et al., 2020).

Concentration peaks are more pronounced in forests with a higher mean density and are located closer to the upstream edge, for example, at $x \approx 9{-}12L_c \approx 8h_c$ for PAI $\approx h_c/C_dL_c = 8$ but $x \approx 5{-}6L_c \approx 14h_c$ for PAI = 2. Forest succession and management, both of which can change PAI will, therefore, greatly influence scalar concentration gradients close to edges. This is because denser forests impose more drag on the flow than sparser ones, which suppresses turbulent mixing and causes the flow to adjust more quickly, that is, the canopy drag length scale L_c is reduced. Turbulent scalar fluxes are greater in magnitude and located closer to the edge with increasing forest

density. The magnitude of the fluxes increases with increasing wind speed but, because the turbulent components w' and ϕ' vary inversely with increasing wind speed, the locations of the fluxes do not change. Higher concentrations and scalar fluxes occur at the upstream edges of forests in which the foliage is distributed uniformly than those in which the foliage is concentrated in the upper canopy (Ma et al., 2020). Forest management induces a step-change in the aerodynamics of the forest by substantially decreasing forest density. The subsequent flow pattern must then continuously adjust as the forest density increases steadily over the timescale of the management period (O(10 years)).

As to the vertical distribution of sources and sinks, scalar concentrations in the lower two-thirds of the canopy are generally higher for scalars with ground sources than for those with canopy sources (Edburg et al., 2012). The turbulent fluxes of scalar quantities are high throughout the depth of the canopy for ground sources, but their magnitudes decrease sharply toward the ground for scalars with canopy sources. Scalar quantities with canopy sources are stirred by the large turbulent eddies near the tops of the trees, whereas ground sources of scalars require intermittent turbulent motions to permeate the entire canopy depth. Scalars emitted from the canopy are therefore more evenly mixed vertically throughout the forest and have shorter residence times compared with those emitted from the ground (Edburg et al., 2012). With decreasing source height, there are larger variations in the concentrations and turbulent fluxes of scalar at the upstream edges of forests (Ma et al., 2020; Ross & Harman, 2015). This is primarily due to low wind speeds and thus less turbulent mixing within the lower canopy layers, resulting in local accumulation of scalar concentration and large gradients. The lowest scalar concentrations coincide with the vertical locations of the sinks, if one exists (e.g., for CO_2, in the upper canopy during the daytime in the growing season). The depth of the region of low concentration increases with distance from the upstream edge.

Around forest edges, the TKE and momentum transfer are much higher in unstable conditions than when the ABL is approximately neutral, and the flow takes longer to adjust upon meeting the canopy (Ma & Liu, 2019). In the adjustment region, the skewness of the streamwise Sk_u and vertical Sk_w velocity are smaller in magnitude in unstable conditions than in neutral conditions, indicating that sweep motions do not penetrate as easily into the forest canopy when the air is buoyant. In neutral conditions, CO_2 accumulates in the adjustment region at the upstream edge of the forest, and water vapor in the canopy flow region, but these patterns largely vanish in unstable conditions (Ma & Liu, 2019).

Scalar fluxes appear to adjust more slowly than momentum as the flow meets the forest, but the patterns in scalar transport are not always intuitive. Scalars are represented in models through the source term S in Equation 11 as either a concentration or flux boundary condition. In numerical models specifying flux boundary conditions, such as those discussed in the previous few paragraphs, one would expect scalar quantities to be slave to the flow because no additional length scales are introduced in the model. Based on Sogachev et al. (2008) and Belcher et al. (2012) suggest scalar concentrations and fluxes ought to reach equilibrium after a distance of $x \approx 2x_A$ downstream of the edge, where the value of x_A decreases with increasing forest density. Following this reasoning, we expect the fluxes of scalars to adjust more rapidly in denser forests. However, Kanani-Sühring and Raasch (2015) find the opposite: scalar fluxes adjust more slowly with increasing PAI, $x/x_A \approx 2$ for sparse forests, where PAI $\approx h_c/C_dL_c = 1$–2, and $x/x_A \approx 3$–4 for forests with PAI = 4.5–8. The relative size of sparse and dense patches of heterogeneity in forests may also affect scalar concentrations. For example, for flow through idealized porous media, maximum scalar concentrations occur in sparse patches where the patch size is less than the adjustment distance x_A, but in the dense patches where the patch size is greater than x_A (Bannister et al., 2021). The patterns in scalar transport are likely to be ecologically significant. For example, the simulations of Ma et al. (2020) indicate the air can be a few degrees warmer at the upstream edge of the forest. If this temperature variation is correct, a forest edge in the prevailing wind direction may provide very different habitats to forest only tens of meters away (Zellweger et al., 2020). Turbulent fluxes of scalar quantities adjust slowly around patchy forests and in other complex terrain. For example, turbulent fluxes of water vapor and CO_2 respectively adjust over distances $x \approx 30h_c \approx 38L_c$ and $x \approx 60h_c \approx 76L_c$ downstream of a forest edge (Ma et al., 2020). This amounts to some 500–1,000 m for mature forests which, given the abundance of edges in contemporary forested landscapes, indicates scalar concentrations and fluxes are out of equilibrium for much of the world's forested area.

4.2. Scalar Transport in the Lee of Forests

The area behind the leeward edges of forests shares some obvious similarities with that in the lee of windbreaks in that they are both sheltered from the flow of air. Because of the long history of windbreaks, their microme-

teorology is quite established, and gives some idea of what to expect in the lee of forests, for which little observational evidence exists. The turbulent transport of scalar quantities is generally enhanced in the wake region behind windbreaks but is suppressed in the quiet zone (McNaughton, 1989), that is, for a uniform ground source, we expect higher scalar concentrations in the quiet zone and lower concentrations in the wake region, compared to the landscape mean. LES studies of scalar transport in forest lees supports this assessment. Kanani-Sühring and Raasch (2017) show that scalars accumulate in the exit region over a distance $x/h_c \approx 2$ downstream of the trailing edge of the forest, with peak concentrations up to around twice as high as those at a reference point far downstream. Ma et al. (2020) obtained similar results using a coupled radiation-LES model, although the magnitudes of the concentration and fluxes depended on the specification of the sources and sinks. Turbulent transport accounts for around half the total scalar transport in the exit and wake regions. The locations of the highest concentrations and turbulent fluxes do not vary with wind speed. Higher concentrations in the exit region occur at lower wind speeds, but the magnitudes of the turbulent fluxes are not affected (Kanani-Sühring & Raasch, 2017). In the exit region, the magnitudes of both the concentrations and turbulent fluxes increase non-linearly with forest density. For example, the magnitude of the turbulent fluxes for forests of PAI $\approx h_c/C_d L_c = 8$ are around two and half times those of forests with PAI = 2.

4.3. Topographical Effects on Forest-Atmosphere Exchange

Topographical effects on forest-atmosphere exchange are not random and can introduce notable horizontal fluxes that are not captured by eddy covariance or smoothed out by time averaging. In heavily populated regions, forests are overwhelmingly confined to land of marginal agricultural value, which often means sloping land (Sabatini et al., 2018). The effect of topography on forest-atmosphere interactions is therefore of wide applicability. Finnigan et al. (2020) review boundary-layer flow in hilly terrain, including sections discussing flows around vegetated hills. We refer readers to their paper for a thorough overview of topographical effects on land-atmosphere exchange. Before moving on, however, we highlight notable results from recent studies that relate to ecosystem-scale forest-atmosphere exchange of scalar quantities.

4.3.1. Boundary-Layer Flow Over Hills and Forest-Atmosphere Exchange

A large proportion of the literature investigating land-atmosphere exchange over complex terrain studies the flow over simplified topography, such as two-dimensional Gaussian hills or sinusoidal ridges. These studies reveal phenomena around forested hills that appear remarkably robust, despite the studies' differing treatments of the physics (B. Chen et al., 2019; Finnigan et al., 2020; Katul et al., 2006; Ross & Harman, 2015). In the lee of a forested hill, an in-canopy recirculation region (ICR) may form within the forest, particularly when (a) the hills are steep, so there is a large pressure gradient at the upstream slope; and (b) in tall, dense forests, in which there is little mixing of high momentum air from above the forest with that near the forest floor. Another ICR may form at the foot of the slope at the upstream side of the hill. The ICRs result from a balancing act between the aerodynamic drag, the pressure perturbation induced by the hill, and the shear stress induced by the forests. A

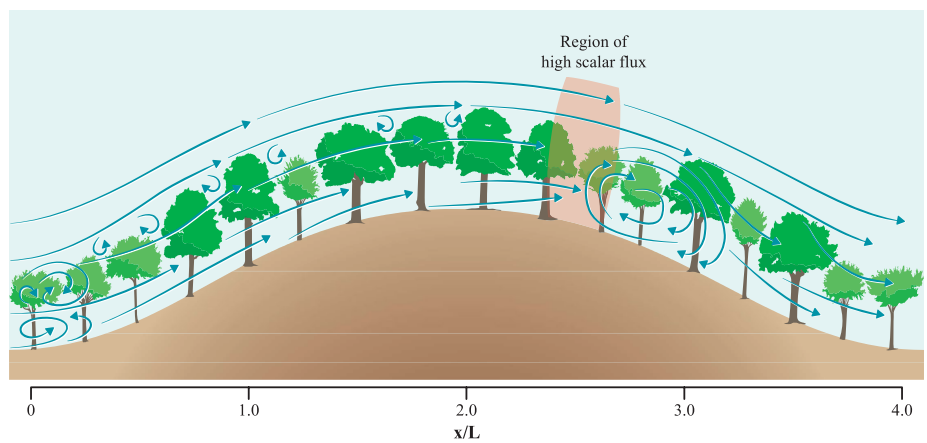

Figure 6. Schematic of the flow over a forested hill. A region of high scalar flux occurs around the in-canopy recirculation region in the lee of the hill. This region acts as a chimney for air parcels leaving the forest air space.

helpful scale to interpret flow in hilly terrain is the hill half length, L, defined in Finnigan and Belcher (2004) as a quarter of the wavelength of the topography. The ICR upstream of the hill occurs at $x/L \approx -1$ to 0, and another in the lee of the hill at $x/L \approx 2$–4 (Figure 6; B. Chen et al., 2019; Ross & Harman, 2015). The air in the wake of the lee ICR is often highly turbulent (Finnigan et al., 2020). Forests absorb lots of momentum, meaning ICRs are more common in forested landscapes than in those with low vegetation, and may form in the lee of even gentle hills (Finnigan & Belcher, 2004; Patton & Katul, 2009). Both the forest density, through its effect on the canopy drag length scale L_c, and the absolute height of the canopy influence the likelihood of ICRs forming. In "shallow" canopies, where $h_c / L_c < 2\beta^2 \approx 0.2$ (Poggi et al., 2008), not all of the momentum is absorbed by the foliage and ICRs are less likely to form than for "deep" canopies, where $h_c/L_c \gg 0.2$.

Figure 6 shows the region of strong vertical fluxes of scalar quantities forms between the crest of the hill and the upstream edge of the lee ICR. In this region, scalar fluxes may be up to nearly an order of magnitude larger than the mean landscape flux, depending on the emission location and sampling height (B. Chen et al., 2020; Ross & Harman, 2015). Scalar fluxes around the lee ICR are stronger for ground sources of scalars than for canopy sources, because the topography affects the flow and turbulent mixing more near the forest floor (Ross & Harman, 2015). In models for which multiple sources and sinks are specified, the net effect of the sources depends on the balance of the individual transport terms. B. Chen et al. (2019) propose two pathways by which air parcels leave the forest: (a) the "local" pathway, where ejection events transport air parcels out the forest, approximately vertically and (b) the "advection" pathway, where parcels are transported horizontally until they encounter and are entrained into the lee ICR, before turbulent fluxes eject them from the forest. The local and advection pathways are, respectively, the dominant passages for air parcels moving from the upper and lower parts of the forest air space. The whole forest air space contributes air parcels that leave via the advection pathway, although sources from the forest floor contribute a greater proportion of the total escape. The region of high flux acts as a chimney for air parcels leaving the forest. This behavior is amenable to observational testing but has not been verified by field measurements. Zeri et al. (2010) observed higher CO_2 concentrations around a forested hill when the wind blew from certain directions, which they attributed to CO_2 accumulating in the hill's lee. However, the accumulation region fell just outside of the observational area, so the authors could not investigate this behavior further. LES simulations over realistic topography show a region of enhanced fluxes develops downstream of hill crests, near the separation point, consistent with the chimney effect that has been observed for simplified two-dimensional terrain (B. Chen et al., 2020).

4.3.2. Looking Forward

It is not straightforward to interpret flux measurements in complex terrain, even when armed with theory and conceptual models. Measurement towers are typically sited on the tops of hills. When considering simplified topography, this decision is not controversial. The fluxes at the crest of the hill are similar to the landscape flux, although the terrain may induce biases that cause the flux measurements to be higher or lower than the landscape mean (B. Chen et al., 2020). However, over realistic topography, while the crest usually remains the best observational location, measurements consistently underestimate the landscape flux and there is a large variability in flux measurements at different hill locations (B. Chen et al., 2020). Further testing at other sites will reveal whether this tendency to underestimate flux measurements is a common problem. Chen et al. acknowledge that they performed their experiments in neutral conditions; mixing promoted by daytime buoyancy may alleviate some of the discrepancy between the crest measurements and the mean landscape flux.

Flows induced by gravity—as opposed to pressure perturbations in the flow, as in Figure 6—are an important topic of ongoing research in forest-atmosphere exchange. In mountainous regions, gravity flows often interact with one another across time and space scales larger than the focus of this review, so we do not discuss these flows in detail here (see Oke [1988] for an introduction to gravity flows, Mahrt [1982] and Belcher et al. [2012] for related scaling analysis, and Finnigan et al. [2020] for a review of recent studies and wider discussion). Downhill (katabatic) flows can occur at night when valley surfaces emit long-wave radiation, causing the air near the surface to cool and accelerate downslope under the influence of gravity. Katabatic flows tend to decouple soil CO_2 fluxes from eddy-covariance measurements above the canopy (Aubinet et al., 2003; Feigenwinter et al., 2008), which can introduce significant errors into diurnal carbon budgets (Van Gorsel et al., 2011). In stable conditions, even gentle slopes can generate strong gravity flows (Belcher et al., 2012), meaning that, at certain sites, advection complicates the interpretation of eddy-covariance measurements at night but not during the day (Leuning

et al., 2008). However, nighttime advection it is not easily addressed even with careful measurements within the forest (Aubinet et al., 2010). An interesting line of future research would be to compare low-wind nighttime eddy-covariance observations around forested hills to high-resolution LES simulations. This type of work may reveal much-needed scaling laws to determine the onset of gravity flows, the strength and even direction of which are sensitive to the balance of the inertial forces and the buoyancy (Belcher et al., 2012; Finnigan et al., 2020).

4.4. Air Parcel Residence Times

Once a molecule or particle enters a forest from outside, or is released from a leaf or the soil, it is mixed within the forest air space. This is easiest to visualize in terms of the stretching and dissipation of small air parcels. During the passage of these air parcels, the molecules or particles contained within may react, diffuse across leaf boundary layers, or deposit on surfaces. Air parcel residence times therefore affect forest ecology—for example, influencing chemical signaling (Szendrei & Rodriguez-Saona, 2010) and VOC chemical processes (e.g., Batista et al., 2019; Pugh et al., 2011), or varying the likelihood of nutrients (Fowler et al., 2009) or fungal spores (Norros et al., 2014; Pan, Chamecki, & Isard, 2014) being deposited. The lifetimes of some VOCs emitted by forests are in the order of tens of minutes (Wolfe et al., 2011), similar to the residence times parcels moving from close to the ground. Reactive scalar quantities emitted from the ground are therefore more likely to be chemically transformed within the forest than scalars emitted in the tree crowns.

The initial vertical position of an air parcel affects its residence time, with parcels "released" near the ground having much longer residence times than those released higher in the forest canopy (Edburg et al., 2012; Fuentes et al., 2007). (Numerical models allow the flow to be studied from an Eulerian or Lagrangian point of view. The Eulerian specification of the flow focuses on specific locations in space through which the air flows with time, whereas the Lagrangian specification follows an individual air parcel as it moves through space and time. Studies looking at particle residence times in plant canopies often adopt a Lagrangian point of view.) Estimates of parcel residence times vary from a few seconds for parcels moving from the crown, to around 30 min for parcels moving from the forest floor, with spatially averaged values in the order of a few minutes (Edburg et al., 2012; Fuentes et al., 2007; Gerken et al., 2017; Hart et al., 2020). The density and morphology of vegetation influences air parcel residence times. For example, in a short, trellis-trained crop, parcel residence time increases with canopy PAI, other than for parcels released high in the canopy (Bailey et al., 2014). Residence times increase with increasing PAI, because mixing-layer-type eddies and TKE do not penetrate as deeply into the canopy (Gerken et al., 2017). Air parcels remain in the canopy for longer when they are released from approximately the height at which most of the plant area is located. For example, for parcels released in the upper canopy, residence times are longer for top-heavy PAI profiles, such as pine plantations, than for forests with more plant area lower down. We expect longer residence times in stable atmospheric conditions, such as at night or on overcast days, because turbulent mixing is suppressed. We are not aware of any investigations into stability effects on parcel residence times in forests. Observations and RANS simulations in urban areas indicate parcel residence times generally increase with increasing atmospheric stability, although they also heavily influenced by the wind velocity and the geometry of local obstacles (Mavroidis et al., 2012).

The next challenge in this line of enquiry is to explain quantitatively how forest canopy turbulence affects air parcel residence times. As rough approximation in homogeneous forests, Gerken et al. (2017) propose that the parcel residence time (τ) is proportional to the reciprocal of the friction velocity, that is, $\tau \propto 1/u_*$. Unfortunately, this relationship is unlikely to hold even approximately in inhomogeneous landscapes. Around forest edges, and in other complex terrain, the flow is spatially variable (e.g., Figures 3 and 6). This variation means that we cannot infer residence times across the whole forest from single variables such as u_*, that is, we cannot assume a moving equilibrium (Yaglom, 1979). While there have been no investigations of the effect of forest heterogeneity on air parcel residence times, in vineyard-type canopies, heterogeneity generally decreases residence times (Bailey et al., 2014). Lagrangian investigations in urban settings show that heterogeneity induces spatial variations in the residence times of scalar quantities (Lo & Ngan, 2015, 2017) and this method may be applied to forested environments.

Part II: Improving ecosystem-scale models of forest-atmosphere exchange

In Part II we focus on recent attempts to improve numerical modeling techniques from developments in theory and experiments. Many of these topics, particularly those in Section 6, are important aspects of atmospheric science in their own right, which deserve their own reviews. However, certain techniques can be readily adapted to improve understanding of how forests and our atmosphere interact. We focus on the application of these topics in turbulence resolving models, rather than attempting to review each area exhaustively.

5. Canopy Structure

5.1. Drag and Plant Reconfiguration

The distributed-drag parametrization was introduced in the 1970s and remains the starting point for ecosystem-scale numerical investigations of forest-atmosphere exchange (see Table A1), usually through the approximation $f_i = -C_d a(z)|U|\langle u_i \rangle$ (Equation 7). The distributed-drag parametrization accounts for the average aerodynamic drag the plants impose over some spatial scale larger than individual twigs and leaves. For some applications, this averaging process is sufficient. Using this method, RANS and LES models can accurately resolve the mean flow through homogeneous forests and around bluff bodies (Yang, Raupach, et al., 2006; Yang, Morse, et al., 2006). However, the method poorly reproduces higher-order flow statistics around forests and in other vegetation canopies (Dupont & Brunet, 2008a; Ma & Liu, 2019; Pan, Chamecki, & Isard, 2014). The reason for this discrepancy may be lie in the fact that there is little in the formulation to account for the detailed morphology and mechanics of plants and trees. In this section, we look at numerically efficient ways to improve the drag parametrization to represent a more realistic range of forest structures.

Trees and other plants reconfigure elastically to reduce drag over short time scales, visible in the everyday observation of leaves curling and tree branches thrashing in high wind (e.g., Figure 7). The reconfiguration of large trees is less extreme than of many smaller plants, which can bend elastically throughout their whole body in strong wind, significantly reducing their mean height. However, even large hardwood trees are softer geometrically and mechanically than most human-made structures, and should not be approximated as being rigid. Measurements of isolated trees in wind tunnels show that streamlining reduces the trees' frontal area by up to 54%, depending on tree species and wind speed (Rudnicki et al., 2004; Vollsinger et al., 2005). Measuring the effect of reconfiguration is more difficult in a forest than on isolated trees. Trees deep inside forests are exposed to lower wind speeds than those around edges, but they are also usually more supple than edge trees (Gardiner et al., 2016). High-frequency velocity measurements in conifer forests show that trees reconfigure at the stand scale, especially around edges, large clearings, and in the region of high shear around the top of the canopy (Dellwik et al., 2014; Queck et al., 2012). The reconfiguration of dense forests and other plant canopies is also evident in coherent "honami" waves passing through a field of wheat (Inoue, 1955; Maitani, 1979), from wavelet analysis of pine plantations (Schindler et al., 2012), and in video footage of forests taken above the crowns (Harper, BIFoR FACE site, private communication 2021).

At low wind speeds, the movement of individual leaves dominates foliage reconfiguration (Tadrist et al., 2018), for example, curling up to form cones and cylinders (Vogel, 1989). This foliage-dominated configuration could account for the scatter observed in the measured values of coefficient C_d at low wind speeds. At low speeds, the

Figure 7. (a – left) Leaves of a cottonwood (*Populus deltoides*) curling in high wind. (b – right) Trees at the edge of a forest reconfiguring under wind loading.

total plant area exposed to the wind varies more than at higher speeds; at low speeds, some leaves will be sheltered only until a gust rolls though the forest. Measuring drag coefficients using instantaneous velocity measurements—that is, calculating the drag as being proportional to $|\bar{U}|u$ rather than U^2—reduces scatter in estimations of C_d and the wind-speed dependency of the product $C_d a(z)$ (Cescatti & Marcolla, 2004; Queck et al., 2012).

Plant reconfiguration is particularly relevant in patchy forests because the flow is constantly adjusting and readjusting as it moves across gaps and clearings. Capturing this reconfiguration directly in ecosystem-scale models is currently unworkable because of the computational expense of simulating the motion of flexible bodies in turbulent flow. However, it may be partly captured by modifying the drag parametrization in Equation 7. For example, one could consider the PAD, represented in $a(z)$ in Equation 7, as varying with velocity (Speck, 2003), or replace the drag coefficient C_d, with a shape factor that varies with the flow (Gaylord & Denny, 1997). However, these approaches require a detailed three-dimensional knowledge of the forest structure and its response to wind loading. A more empirical approach is to proceed from the observation that reconfiguration leads to a lower increase of drag with velocity than could be expected by assuming $a(z)$ and C_d both take constant values (Vogel, 1989). Therefore, instead of having the drag $f_i \propto U^2$, we have $f_i \propto U^{2+B}$, where B is known as the Vogel number (De Langre, 2008; Vogel, 2020). B therefore acts as an empirical modification to Equation 7 to account for the variation of $a(z)$ and C_d with velocity. Negative values of B imply that, because of reconfiguration, plant drag increases with velocity more slowly than the usual assumption of velocity squared. Where the plants do not reconfigure, $B \to 0$ and the drag increases approximately with the square of the velocity.

Pan, Chamecki, and Isard (2014) use LES to model the reconfiguration of a maize canopy. They maintain the quadratic dependence of drag on velocity in the drag parametrization in Equation 7, accounting for plant reconfiguration using a velocity-dependent drag coefficient $C_d = (|U|/A_v)^B$, where A_v is a velocity scale related to the shape and rigidity of the plants. Using the variable C_d, their LES model simulated flow with more accurate higher order statistics than the same model with a constant C_d value (with similar performance with respect to the mean velocities, momentum transfer and TKE). Using a variable C_d value also improved estimates of momentum transport by sweep motions penetrating the canopy. In similar work, Pan, Follett, et al. (2014) show plants reconfigure more at higher flow velocities, reflecting the results of lab investigations on isolated plants (Tadrist et al., 2018). In both Pan, Chamecki, and Isard (2014) and Pan, Follett, et al. (2014), the absolute values of Sk_u and Sk_w increase with a more negative Vogel number—that is, simulating more reconfiguration—as did the ratio of sweeps to ejections. To see why, taking $B = -0.74$ from Pan, Chamecki, and Isard (2014) gives $f_i \propto U^{1.26}$ in Equation 7 rather than $f_i \propto U^2$. The drag force therefore increases more slowly with increasing velocity, leading to a greater contrast of TKE inside and above the canopy. The decrease in the velocity exponent also increases the frequency and strength of sweep motions because strong events ($u' > 0$) penetrate further into the canopy. The canopy drag length scale L_c increases when the value of C_d is smaller because stronger events are able to penetrate further into the forest before drag halts their progress.

Field studies of plant reconfiguration typically focus on time-averaged adaptation over long time intervals, although measurements in poplar crowns show C_d values decrease with increasing wind speed across averaging periods as short as 1 s (Koizumi et al., 2010). Measurements in a patchy conifer canopy found $B \approx -0.8$, although this value varied with the wind direction (Queck et al., 2012). Pan, Follett, et al. (2014) ran simulations using $B = 0$, $-2/3$, -1, and $-4/3$, finding that a non-zero Vogel number improved the agreement of the simulations with flume observations, with the greatest fidelity obtained using $B = -1$. Other estimates for B include $-1 < B < -2/3$ from biomechanics theory (Gosselin et al., 2010). $B \approx -1$ appears to be a robust measurement for poroelastic structures, including forests and other vegetation canopies (Gosselin, 2019 and references therein). We suggest 0 and -1 as approximate upper and lower bounds for the Vogel number B.

5.2. Terrestrial Laser Scanning

Most studies assume that the local foliage density $a(z)$ varies only with height, if at all (Table A1). For example, Figure 8a shows $a(z)$ derived using the parametrization by Lalic and Mihailovic (2004), as employed by Yan et al. (2020), among many others. The forest is assumed to be horizontally homogeneous at each height, reducing the forest morphology to a single dimension (z), typically with most of the density confined to the tree crowns. This is a reasonable approximation for certain forests, such as unthinned conifer plantations (Figure 8c). However, it is a poor approximation for many forests, such as oak-dominated temperate forests (Figures 5 and 7b) and certain tropical forests (Figure 9), which have dense understory layers in which the PAD is similar to that of

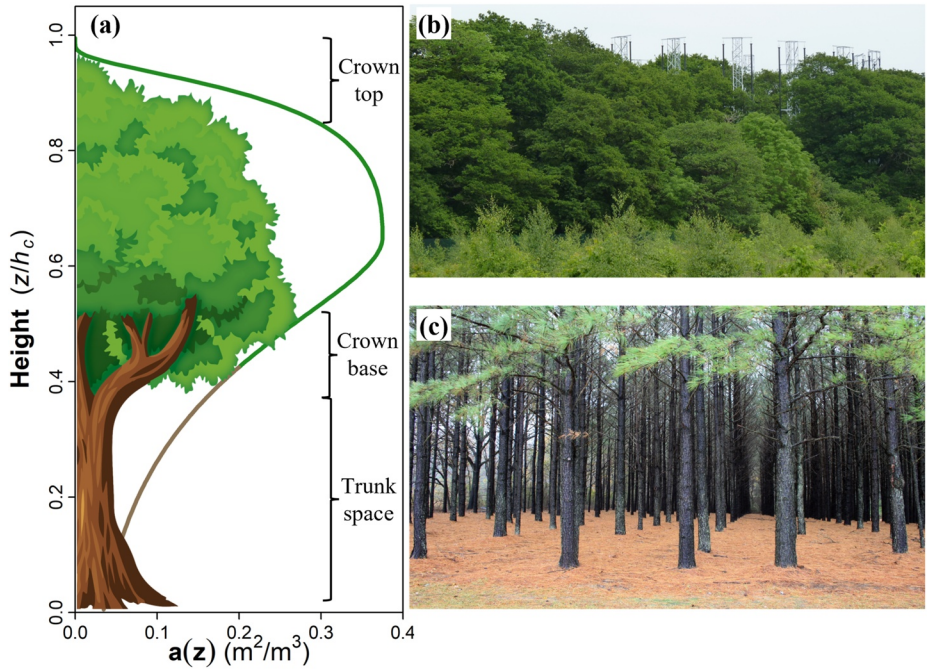

Figure 8. (a) Vertical profile of PAD, $a(z)$, calculated using the formula derived by Lalic and Mihailovic (2004), (b) the southern edge of the oak-dominated woodland at the Birmingham Institute of Forest Research (BIFoR) free-air carbon dioxide enrichment (FACE) facility belonging to the authors' institute, and (c) open trunk space of an even-aged *Pinus taeda* monoculture plantation.

the crown layer, or multiple modes of leaf density (Schneider et al., 2019; Zhao et al., 2011). Most models also assume that forest edges are structural continuations of the main body of the canopy (Dupont & Brunet, 2008a; Kanani-Sühring & Raasch, 2015; Ma et al., 2020). Unless the forest has been recently disturbed, this assumption is unrealistic because many trees and understory plants grow into the light to maximize the leaf area available for photosynthesis, thereby forming an almost closed edge (Figure 8b).

A major technological leap since the first LES investigation of forest-atmosphere interactions (Shaw & Schumann, 1992) has been the development of terrestrial laser scanning (TLS), also known as terrestrial LiDAR. TLS provides non-destructive, in situ information of the three-dimensional structure of trees and forests, down to a resolution of millimeters (Calders et al., 2020). See, for example, a captivating example of a TLS scan of an Australian notophyll vine forest in Figure 9 (Calders et al., 2020). Note the variety of plant forms, stem diameters, and leaf sizes for this uneven-aged, biodiverse, forest. Note also, in the right-hand panel of Figure 9, the pronounced increase in PAD at about 2 m, suggestive of a herbivore "browse line" (Hazeldine & Kirkpatrick, 2015), the rel-

Figure 9. 3D complexity of a Simple Notophyll Vine Forest (Robson Creek, Australia) captured using a time-of-flight RIEGL VZ-400 instrument. Left panel: The colors represent the distance from the scanner. Right panel: Derived plant area volume density as a function of canopy height derived for the same scan using (Calders et al., 2015). Figure and caption reproduced without modification from Calders et al. (2020) under Creative Commons License CC BY 4.0. "Plant area volume density" refers to PAD.

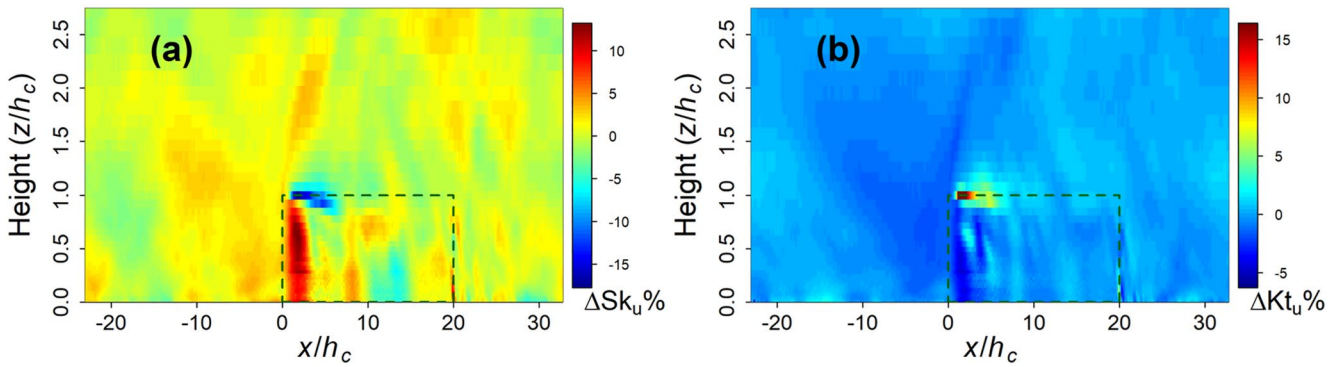

Figure 10. (a) Percentage difference in Sk_u; and (b) Kt_u between Case 1 and Case 2, as a total of the maxima for Case 1. The changes are induced by the stochastic variations in $C_d a(z)$ for Case 2. The green dashed line shows the presence of the forest. The x-axis is scaled so that 0 coincides with the upstream edge of the forest. ΔKt_u is around 25% for a few resolved cells in (b). These values are suppressed to 15% to aid presentation.

atively sparse canopy between 2 and 10 m, and the slow drop-off of PAD with height above about 28 m, typical of a biodiverse forest. TLS is currently used for a range of ecological applications (Ashcroft et al., 2014; Momo Takoudjou et al., 2018), but has yet to be adopted widely in models of forest-atmosphere exchange.

TLS combined with LES has the potential to revolutionize the realism of ecosystem-scale models of forest-atmosphere exchange. TLS allows real sites to be reconstructed numerically by splitting the forest volume into cells, each of which is assigned a plant density value calculated from TLS point clouds (Boudreault et al., 2015; Calders et al., 2015; Queck et al., 2012; Raumonen et al., 2015). The few studies that have used this approach in heterogeneous forests show important flow behavior may be missed by assuming heterogeneity. Schlegel et al. (2012, 2015) use TLS measurements in an LES model of flow around a large forest gap. They show that small-scale plant heterogeneity creates sustained upwards motion in denser patches of forest and downwards motion in clearings and large gaps. Failing to account for the true structure of forest edges strongly overestimates the penetration of air into the forest (Schlegel et al., 2012, 2015), and neglects the possibility of dispersive fluxes of momentum and scalar quantities (Boudreault et al., 2017; Li & Bou-Zeid, 2019). TKE and Reynolds stresses decay faster behind closed edges and strong cross flows may develop. Away from the edges, large gaps and clearings deflect the flow downwards, creating advective fluxes within the forest air space (Queck et al., 2016). Boudreault et al. (2017) use TLS measurements (outlined in Boudreault et al. [2015]) and LES to model air flow across a forest edge. Compared to a homogeneous edge, the gaps induce variations in the flow, for example, the streamwise (U) and vertical (W) velocity components respectively vary by around 20% and 5% of their spatial means at $z = 0.5h_c$. The turbulent momentum fluxes are likewise higher in the heterogeneous case, for example, σ_w varies by around 40% of its spatial mean, because air is forced through patches of low density.

5.3. Stochastic Drag Forcing

The product $C_d a(z)$ in Equation 7 is typically approximated as a smoothly varying function of height, with C_d taken as constant. However, Finnigan and Shaw (2008) raise the important point that the dominant large eddies around forests have diameters in the order of $L_s \propto h_c$ (Bailey & Stoll, 2016; Raupach et al., 1996). To resolve the structure of these eddies in numerical models, the vertical filter needs to be much smaller than h_c, for example, a filter of $h_c/25$ is taken in the model in Appendix A. At this resolution, we can no longer assume $a(z)$ is a smooth function—for example, notice the structural variation of the forest understories in Figures 5 and 8. Finnigan and Shaw (2008) propose representing $C_d a(z)$ through a stochastic variation overlaying a smooth background trend, thereby introducing a stochastic forcing into the resolved momentum equations.

To illustrate this argument, we consider a small, horizontally homogeneous forest patch, represented using the drag parametrization in Equation 7, with the transport equations solved using LES (see Appendix A for numerical details). We define two cases, with the same dimensions and mean density. For Case 1, $C_d a(z)$ is uniform throughout the domain. For Case 2, $C_d a(z)$ varies randomly in space throughout the forest by ±2% of the value for Case 1, a small variation in comparison to the natural variation of forests. The random spatial variation of

$C_d a(z)$ is almost imperceptible in the mean variables and second-order statistics such as the TKE and kinematic turbulent momentum flux. However, Figure 10a shows the streamwise velocity skewness Sk_u at the upstream edge of the forest ($x/h_c \approx 0$–5) is less negative for Case 2 than it is for Case 1. The value of Sk_u above the forest is more negative for Case 2 than it is for Case 1. The streamwise velocity kurtosis Kt_u at the upstream edge of the forest ($x/h_c \approx 0$–5) is smaller for Case 2 than it is for Case 1 within the forest, and larger for Case 2 than it is for Case 1 above the forest (Figure 10b). These statistics indicate the small stochastic forcing in Case 2 decreases the coherence of the flow at the upstream edge—that is, the upstream edge behaves less like a bluff body than the homogeneous Case 1—leading to fewer lulls in the streamwise velocity within the forest but more lulls just above the canopy. We do not generalize these results further because the cases are idealized. But they support the conclusions of Dupont and Brunet (2008a) and Pan, Chamecki, and Isard (2014), for example, that the probability distribution of gusts indicated by higher-order statistics are sensitive to the model setup, including any stochastic element. This sensitivity needs careful testing.

5.4. Waving Plants and Biological Backscatter

The velocity spectra of airflow around forests and other vegetation canopies often contain peaks that correspond to plant movement (Cava & Katul, 2008; Dupont et al., 2018; Finnigan, 1979a, 1979b). These peaks indicate energy is transferred in two directions—the flow perturbs the plants, but the plants also perturb the flow. The latter effect is usually ignored in models at the ecosystem scale and above on the assumption (usually implicit) that the turbulent structures generated by plant movement are much smaller and less energetic than the dominant mixing-layer eddies. However, this neglects the possibility of resonant effects occurring when the passage frequency of the dominant eddies approaches the natural frequency f_0 of the moving plants, as has been observed in crops (Py et al., 2006). Trees near the edges of forests, such as in patchy landscapes and around clearings, are more susceptible to resonance effects than those further inside forest stands (Dupont et al., 2018).

Accounting for this two-way transfer of energy is not straightforward at the ecosystem scale. Dupont et al. (2010) use LES to model a crop canopy as a poroelastic continuum, with plant movement incorporated into the momentum equations as small mechanical oscillations of rigid stems. Other researchers had previously developed models coupling wind flow and plant swaying in a similar way, but with analytical solutions obtained from simplified velocity statistics rather than through LES (Gosselin & de Langre, 2009; Webb & Rudnicki, 2009). Pivato et al. (2014) extend this approach, using LES to model the movement of pine trees as simplified flexible cantilever beams. Their model includes the possibility large tree deflections by strong gusts, which Dupont et al. (2010) did not account for in their crop model. Pivato et al.'s model performed well against field observations and more complex small-scale plant models in terms of the instantaneous tree response to gusts.

The direct approaches of Dupont et al. (2010) and Pivato et al. (2014) require the plant architectures to be heavily simplified to be computationally feasible. This is not a major problem for tall, slender trees such as maritime pine, the subject of Pivato et al. (2014). However, decurrent trees, which include many broadleaf species, are structurally more complex and can have modes of vibration across several scales, for example, $f_0 \approx 0.5$ Hz in the trunks and several Hz in the branches (Schindler et al., 2013). Capturing these interactions at the scale of an entire forest would be very demanding computationally. A possible workaround in patchy landscapes is to proceed from the observation that wind velocity spectra at forest edges contain peaks around f_0, the natural frequency of the trees (Dupont et al., 2018). This motion is especially visible in the spanwise direction because the turbulent velocity perturbations are smaller than those in the streamwise direction. From a modeling point of view, the trees' movement transfers energy from the SGS to the smallest resolved scales (Piomelli et al., 1991), a process known as "backscatter." In general, backscatter is most apparent where small but energetic eddies are present (Mason & Thomson, 1992), such as around forests and other complex structures. Studies of urban canopy flow provide a template of how backscatter could be incorporated into forest models. For example, O'Neill et al. represent the stochastic effects of backscatter in their LES simulations of the neutral surface layer (O'Neill et al., 2015) and street canyon flow (O'Neill et al., 2016) by incorporating random acceleration fields a_i in the momentum equations. This gives

$$\frac{\partial U_i}{\partial t} = \cdots + f_i + \underbrace{\frac{\partial}{\partial x_i}\left\{\nu_{SGS}\left(\frac{\partial U_i}{\partial x_j} + \frac{\partial U_j}{x_i}\right)\right\}}_{\text{SGS terms}} + a_i, \tag{12}$$

where ν_{SGS} is SGS eddy viscosity and the ellipsis represents the other terms carried over from Equation 2b. Here, the Smagorinsky SGS scheme is shown. In principle, this approach could be adopted for an LES of forest canopy flows, ideally with the acceleration terms a_i spaced at frequencies corresponding to the movement of tree parts, while ensuring zero divergence. Selino and Jones (2013) adopt a similar approach for a very different purpose, using synthetic SGS turbulence to improve video animations of trees moving in wind.

5.5. Resolved Trees

The difficulties involved in incorporating realistic structure into the distributed-drag parametrization, discussed above, raise the question of whether it is possible to model the forest elements directly. Poggi and coworkers approximate plants as rigid circular cylinders in water-flume experiments, finding the wakes in the lee of the vegetation stems perturbed the dominant mixing-layer type eddies at the crown top (Poggi & Katul, 2008a; Poggi et al., 2008; Poggi, Katul, & Albertson, 2004). Yue et al. (2007) model corn plants as stems surrounded by leaves, applying a distributed-drag parametrization at the leaf points and, at the stem points, a force calculated as drag around a cylinder. Chester et al. (2007) and Chester and Meneveau (2007) use LES to investigate the flow around isolated, solid tree-like fractals, finding that model's predictions of the drag imposed by the fractals were sensitive to the orientation of the branches. Böhm et al. (2013) modeled trees as cylindrical trunks below spherical crowns in a wind tunnel. They conclude similarly to Poggi, Porporato, et al. (2004) that the partially coherent wakes of the bluff canopy elements modify the dominant eddies at the crown top, and that the flow within the canopy divides into wake and non-wake regions, where the wake regions scale with the stem diameter (Ghannam et al., 2020). Yan et al. (2017) performed high-resolution LES studies of a regular array of bluff elements, specified similarly to the wind-tunnel model of Böhm et al. (2013). In a series of separate simulations, Yan et al. (2017) configure the trees as (a) entirely bluff bodies, (b) solid trunks with the crown represented as distributed drag, and (c) as entirely distributed drag. The spatially averaged flow statistics were similar across the three cases, with slightly higher turbulence in the shear layer using the bluff-body representations. As an interesting alternative, Schröttle and Dörnbrack (2013) use LES to simulate flow around 16 Pythagoras trees (A type of fractal constructed iteratively from a right-angled triangle with squares erected on each of its sides), treated as immersed boundary layers with the outer tree branches 3.35 K warmer than their surroundings. They show the thermally driven vortices from the trees, of diameter roughly h_c and turnover time of ~30 s, interfere with the shear-generated coherent structure at the tops of the trees. However, the study was a method prototype, and its results reveal little about real forests.

For the time being, because of the computational expense of simulating turbulent flow, resolving forest structure directly remains out of reach for ecosystem-scale investigations of forest-atmosphere exchange. For example, Yan et al. (2017) use an extremely high resolution model to discretize the trees ($dx = dy = 0.03h_c$), which severely constrains the number of trees that can be simulated. Further, treating the trees as bluff bodies does not account for plant reconfiguration, may overestimate the scales of vortical wakes behind tree crowns, and excludes the possibility of resolving the cooperative waving motion that occurs in real vegetation. There are no theoretical constraints on the number of trees that can be included in wind-tunnel models, although practical considerations to preserve scale relationships may of course impose limits. It is also difficult to include canopy exchange and other ecological processes in physical models of forests, and to maintain flow with sufficiently high *Re* values, because higher values are needed than in many buff-body engineering applications (Gromke, 2018). Results from bluff-body models may be useful to derive drag parametrization schemes for use in larger scale simulations. Böhm et al. (2013) motivate this approach by identifying that wake-scale TKE in bluff-body canopies is around 1/5 L_s rather than 1/100 to 1/10 L_s typical of vegetation canopies. This implies momentum is transferred more efficiently to vegetation than to canopies of bluff bodies. Further, information theoretical analysis of flume experiments suggests the von Kármán streets formed in the wake of stems can cause scalar variance to be transferred from small to large scales (Ghannam et al., 2020), that is, opposing the usual turbulent cascade characterized by constant fluxes of energy and scalar variance from the scales of production down to dissipation.

6. Atmospheric Physics and Chemistry

6.1. Modeling In-Canopy Chemistry

BVOCs are ecologically important in forests (Niinemets, 2010; Visakorpi et al., 2018) and influence air quality, meteorology, and the climate through their interactions with oxidants such as O_3 and OH (Lelieveld et al., 2008;

Peñuelas & Staudt, 2010; Rap et al., 2018). Plants release a wide variety of compounds from tissues above and below ground. Flowers and fruits release the widest variety of compounds, while leaves generally have the greatest mass emission rates (Laothawornkitkul et al., 2009). The most important class of BVOCs for air quality and climate is the terpenoid class of compounds, particularly the five-carbon (C5) hemi-terpene, isoprene, the C10 monoterpenes such as α- and β-pinene, and the C15 sesquiterpenes such as β-caryophyllene. Leaf-scale emissions of isoprene depend sensitively on temperature and light (and, hence, forest structure). Emissions of terpenoids vary exponentially with leaf temperature (Guenther et al., 2006). This class of compounds displays a great range of lifetimes with respect to reaction with OH and O_3, from several tens of minutes for isoprene for reaction with OH (Apel et al., 2002) to 2 min for the reaction of β-caryophyllene with O_3 (Shu & Atkinson, 1994). For reaction, BVOC molecules must be well mixed at the molecular scales. Because the source of oxidants (i.e., OH and O_3) for the degradation of BVOCs is outside the forest, imperfect mixing acts as an apparent brake on reaction rates, a process known as segregation (Butler et al., 2008; Krol et al., 2000; Pugh et al., 2011). Fluxes of unreacted terpenoids out of forest patches therefore depend sensitively air parcel residence times, which vary with position within the canopy, as discussed above in Section 4.4.

Studies investigating BVOC chemistry in forests are usually interested in time and space scales that are too large for the turbulent flow to be resolved by DNS, LES or RANS, requiring the turbulent exchange to be parametrized (Ashworth et al., 2015; Forkel et al., 2015; B. Wang et al., 2017). These parametrizations are typically based on K-theory, which should be used cautiously in forests and other vegetation canopies (Finnigan, 2000; Monteith & Unsworth, 2008). K-theory works well in situations where the sum of the flux transport and buoyancy terms of the scalar flux budget is small compared to the production term (Bash et al., 2010; Freire et al., 2017)—for example, in neutral conditions, where there is a strong vertical gradient in the scalar concentration, such as investigating isoprene released from leaves. However, the gradient diffusion assumptions in K-theory often fail in real forests—for example, in stable atmospheric conditions or when considering scalars with multiple and temporally varying sources and sinks. Model predictions of BVOCs and their oxidation products can be very sensitive to the turbulence parameterization used (Bryan et al., 2012; Makar et al., 2017). It is therefore important to make the parametrizations as robust as possible.

Ecosystem-scale LES models can simulate counter-gradient transport and are therefore likely to be indispensable tools in developing chemistry parametrizations that scale to large space and time resolutions. Due to the complexity of the task, there have been few attempts to investigate forest chemistry while resolving turbulence. However, the urban literature is an excellent source of relevant techniques (e.g., Bright et al., 2013; Buccolieri et al., 2018; Khan et al., 2020; Kwak et al., 2015; Liao et al., 2014; Zhong et al., 2016, and references in each). One possible path is to couple chemistry models to LES, a technique which has recently been used to investigate chemical transformation, transport, and deposition of air pollutants in realistically shaped urban areas (Khan et al., 2020). However, the computational expense of the coupled approach heavily restricts the resolution of the domain and the number of chemical species that can be investigated in each run. Another approach is to model chemistry inside a forest air space using "box models," which treat the air space as a fixed volume into which species are emitted and are able to react. Box models require the characteristics of the turbulence to be specified a priori, such as through an exchange velocity between the box and its surroundings. This simplification allows computing resources to be reallocated to more complex chemistry or particle microphysics than is possible when the turbulence is highly resolved using RANS or LES. Box models are widely used to model street canyon chemistry (Holmes & Morawska, 2006; Murena, 2012; Zhong et al., 2016) and have been used for one-dimensional investigations of forest-atmosphere exchange across large homogeneous canopies (Ashworth et al., 2015; Pugh et al., 2011). In patchy landscapes, multiple boxes would be required to account for the fluid dynamical regions that form around forest edges and clearings. The urban literature offers a precedent for dividing air spaces into dynamical regions. For example, models of street canyon chemistry have used multiple boxes to represent the "compartmentalization" of fluid dynamical phenomena such as counter-rotating vortices (Dai et al., 2021; Kwak & Baik, 2014; Murena, 2012; Zhong et al., 2016, 2018).

6.2. Modeling Particle Deposition

Ecosystem-scale investigations of forest-atmosphere interactions are often motivated by questions concerning trace gas exchange, usually representing the species of interest as passive scalars (see Section 4). However, the

behavior of many biologically important particles cannot be approximated in this way. For example, many pollens and spores have substantial mass and are subject to inertial forces different to those on a trace gas molecule (see, e.g., Hinds, 1999; Seinfeld & Pandis, 2016). Freshly nucleated UFPs, resulting from the oxidation of BVOCs (Kulmala et al., 2001, 2007), are produced in high number concentrations around forests and may coagulate (Kulmala et al., 2001; Pierce et al., 2012). These processes introduce physics requiring a different mathematical approach to that for fluid flow or particle growth/evaporation (Jacobson, 2005; Seinfeld & Pandis, 2016; Spracklen et al., 2006).

Many studies of scalar quantities (Poggi et al., 2006) and particles (Aylor & Flesch, 2001) in vegetation adopt a Lagrangian stochastic modeling (LSM) approach, which requires the vertical profiles of turbulence statistics to be specified a priori. However, around patchy forests, determining a priori vertical profiles is extremely difficult because the dynamics are so spatially varied. There have been a handful of attempts to incorporate non-Gaussian turbulence in an LSM framework, with varying success (e.g., Reynolds, 2012). More recently, several groups have adopted an Eulerian specification of the flow field to model particle deposition. Around patchy forests, Eulerian models offer the advantage of resolving the velocity statistics directly down to the scale of their grids. This does not necessarily affect the predictive ability of the models around vegetation. For example, Gleicher et al. (2014) simulated more accurate concentrations of spores in a homogeneous maize canopy using an Eulerian LES model than using their equivalent LSM. However, an inherent difficultly using LES is that canopy deposition occurs at spatial scales much finer than the spatial filter and therefore must be parametrized. One method is to include a sink term in the conservation equation,

$$S = E_\phi \alpha \phi_l |U|, \tag{13}$$

where α is the attenuation coefficient—which accounts for the flow's response to the forest density (Cionco, 1978)—ϕ_l the resolved local particle concentration, and E_ϕ the efficiency of particle deposition (Friedlander, 2000; M. Lin et al., 2012; X. Lin et al., 2018). Pan, Chamecki, and Isard (2014) use a similar approach, modifying the deposition model in Aylor and Flesch (2001) to generate a sink term linked to PAD,

$$S = E_\phi (P_x + P_y) a(z) \phi_l |U|. \tag{14}$$

This formulation considers the distribution of the forest density directly though the incorporation of PAD, as $a(z)$, and the projection coefficients P_x and P_y, which respectively account for the PAD facing the streamwise and spanwise directions. The ground deposition of particles can be modeled using a surface flux boundary condition. X. Lin et al. (2018) and Pan, Chamecki, and Isard (2014) use slightly different formulations for the deposition efficiency E_ϕ based, respectively, on a parametrization of molecular diffusion and on observations of particle impaction onto cylinders. The deposition efficiency term E_ϕ accounts for the momentum and size of the particles, so that Equations 13 and 14 are solved separately for each particle size, with the only difference between the solutions resulting from the approximation of the deposition efficiency. The same is true for the surface-flux parametrization representing ground deposition.

The mechanisms of particle deposition, and hence deposition velocities, are highly size-dependent for the size ranges of particles commonly encountered in forests (Litschike & Kuttler, 2008). X. Lin et al. (2018) found the deposition velocity decreased sharply with increasing particle size for the range of sizes they investigated (diameters 10–50 nm). Pan, Chamecki, and Isard (2014) investigate size indirectly through the ratio of the particle settling velocity w_s to the friction velocity u_*, with "light" particles having $w_s/u_* \approx 0.04 \ll 1$, and "heavy" particles $w_s/u_* \approx 0.2$. They show, for large values of w_s/u_* (heavy particles) and sources near the ground, few particles escape the canopy, reflecting their empirical observation that plant diseases initiated deep within a canopy move upward to the canopy top before spreading. Unsurprisingly, more particles are deposited in denser vegetation (Branford et al., 2004), particularly at $z \approx h_c$, and therefore lower concentrations of particles occur deep in the canopy. The rate of dry deposition generally increases with increasing turbulence because the thickness of the quasi-laminar boundary layers around plant elements is reduced, therefore increasing the probability of impaction (Fowler et al., 2009). However, the rate at which particles are deposited depends on the tree species. Studies of urban trees indicate that particles deposit onto conifers more efficiently than onto broadleaf trees (L. Chen et al., 2017; Pace & Grote, 2020). Beyond these general observations, there appears to be no clear dependence of fluxes or deposition of fine particles on broad-brush measures of the canopy morphology (Katul et al., 2011;

X. Lin et al., 2018). Deposition patterns appear to depend strongly on the complex arrangement of plant area in forests and other plant canopies (Fowler et al., 2009).

A future task, straddling in-canopy chemistry and trace-gas deposition, is to investigate how forest patchiness and more complicated weather conditions affect the rate of deposition and stomatal uptake of trace gases. For example, particle impaction can be several times higher in unstable conditions versus stable ones (Chiesa et al., 2019; Fowler et al., 2009; Pryor et al., 2008). This suggests leaf related removal by forests is likely much lower at night than measurements taken during the day would suggest; impaction is much lower in stable, nocturnal conditions and the stomata are mostly closed at night. Local atmospheric stability gradients, such as from patchy heating from sunlight, may produce apparent fluxes when particles and gases trapped in stable conditions are eventually released in convective plumes (Chiesa et al., 2019). Most models of spore dispersal in forests consider only dry deposition, which is a major simplification in many climates where forests are found, and pay little attention to the resuspension of deposited particles. However, the rates of particle removal by rain and resuspension by depend on species composition and the local meteorological conditions, such as the frequency and intensity of rainfall events (L. Chen et al., 2017). Airborne fungal spore concentrations in forests are generally higher in wet conditions (Crandall & Gilbert, 2017), which are physiologically favorable to certain fungal species such as *Ganoderma* spp. (Stępalska & Wołek, 2009). Air vortex rings, which can carry dry-dispersed spores away from the host plant, form around the impact site when raindrops hit plant surfaces, (Kim et al., 2019). This process, which is not accounted for in current models, is likely significant in the transmission of fungal spores because particles transported by the air vortices can reach beyond the laminar boundary layer around plant surfaces, enabling long-distance transport in the turbulent flow.

6.3. Heterogeneous Sources and Sinks of Scalar Quantities

Section 4 considered investigations where scalar quantities were approximated to have horizontally homogeneous sources and sinks. This approach provides a good conceptual template for certain processes around forests, such as the encroachment of pollutants from surrounding areas, or the release of isoprene, which is overwhelmingly from sunlit leaves in the canopy from a monoculture stand (Sharkey et al., 1996). However, in mature forests, most scalars have multiple sources and sinks, whose distribution varies temporally and spatially. This heterogeneity often requires dense networks of equipment to measure, and is therefore not widely reported, despite the known difficulties in generating spatially representative observations in forests (Aubinet, 2008; Finnigan, 2008; Massman & Lee, 2002). Visible examples of this heterogeneity include the water vapor plumes that form over forests after it has rained, for example, during periods of high convection but a low lifting condensation level height over tropical forests (Jiménez-Rodríguez et al., 2021). Less obvious examples include the steep temperature gradients that can form within forests on clear days. In direct sunlight, broad leaves may be 20°C warmer than their surroundings (Monteith & Unsworth, 2008; Schuepp, 1993; Vogel, 2009) and can therefore act as highly localized heat sources.

We are not aware of numerical investigations of how patchy sources and sinks affects scalar transport within forests. LES of unevenly heated generic surfaces suggests thermal heterogeneities drive the local mean flow in certain conditions, such as when the geostrophic wind is weak. In these conditions, the dispersive fluxes of heat account for more than 40% of the total sensible heat flux at $z = 100$ m and up to 10% near the surface (Margairaz et al., 2020). The effect of differential heating is not easy to constrain in models of forests because the locations of sunflecks (brief periods of high photon flux density) change quickly depending on branch movement (Way & Pearcy, 2012). The radiative properties of the leaves may even vary between the sun and shade sides of a tree (Vogel, 1968). One possible approach is to combine the modeling techniques of thermal transfer in urban areas (e.g., Martilli et al., 2002; Salamanca et al., 2010) and radiation transfer in vegetation (Ma & Liu, 2019). For example, the leaves of the forest may be represented using a probability density function (PDF) of small, flexible, surfaces with high absorptance, and the trunks through a PDF of vertically aligned cylinders of varying thickness and low absorptance. This type of testing is probably best carried out in uniform canopies to begin with, so as to differentiate between patterns in scalar transport resulting from terrain effects and those resulting from spatially heterogeneous sources and sinks. For uniform sources around forest edges, the patterns of scalar concentrations and fluxes are most complicated in the adjustment region where they are influenced by the strong turbulence, the inflow concentration from the surrounding environment, and the vertical distribution of the sources and sinks. Eventually, however, it may be possible to investigate the effect of heterogeneous source and sinks on scalar

transport in patchy Section 7.1 revisits this point again in the context of customized numerical models of real study sites.

6.4. Calculations of Dispersive Fluxes

Acknowledging the spatial heterogeneity of real forests raises the question of how to handle the dispersive fluxes of momentum and scalars that result from the double averaging of the momentum and transport equations. The dispersive fluxes are the spatial correlations in the time-averaged statistics; the dispersive flux of momentum, for example, is given by the term $-\partial\langle\bar{u}_i\varepsilon\bar{u}_i\varepsilon\rangle/\partial x_j$ in Equation 2b. The dispersive fluxes are usually excluded from analyses of forest-atmosphere exchange (Kaimal & Finnigan, 1994; Patton & Finnigan, 2012), which is a reasonable assumption in dense, homogeneous canopies in which the dispersive fluxes of momentum are usually small (Moltchanov et al., 2011; Poggi & Katul, 2008b; Poggi, Katul, & Albertson, 2004). However, in sparse canopies—roughly comparable to the densities found in savannahs—dispersive fluxes can be ≈ 30% of the conventional momentum flux, even when the canopy is homogeneous (Poggi & Katul, 2008b). Further, investigations in model canopies show structural inhomogeneities can generate large dispersive fluxes of momentum (Harman et al., 2016; Moltchanov et al., 2011, 2015). Boudreault et al. (2017) show that spatial variability in forest canopy structure induces dispersive fluxes that account for 10%–70% of the total variances of U and W at the upstream edge of the forest, across a streamwise distance of $x/h_c = 0–8 \approx 0–x_A$. Here, the dispersive momentum fluxes and skewness are greater than their turbulent counterparts, for example, with the dispersive flux of momentum accounting for >50% of the total momentum flux. Away from the edges, gaps and other patchiness decrease the efficiency of momentum transfer at the crown top. This suggests gap-induced flow phenomena interfere with the mixing-layer-type coherent structures that form around the tops of the trees. Bailey et al. (2014) observed a similar result in row-structured versus homogeneous trellis-trained crops. This interference is probably strongest when the structural inhomogeneities are of a size $\approx L_s$, so that the vortices shed around them are of a similar scale to the coherent structures that develop around the crown top. In a more idealized example, Li and Bou-Zeid (2019) use LES to show that rough, heterogeneous surfaces affect the dispersive fluxes of momentum and scalar quantities more than the turbulent components of the fluxes. As in Boudreault et al. (2017) and Li and Bou-Zeid (2019) show the dispersive components can comprise most of the total momentum flux.

Wind-tunnel measurements in homogeneous plant canopies found the dispersive scalar fluxes to be small (Legg et al., 1986). However, dispersive fluxes of scalar quantities generated by patchiness or spatially heterogeneous source/sinks have not been studied in real forests. Recent studies in urban areas and generalized porous media suggest the dispersive fluxes of scalar quantities should not be dismissed out of hand. Philips et al. (2013) use LES in an urban canopy to show that the dispersion of a scalar quantity is sensitive to the geometry of the obstacles surrounding the source (they observe a plume's evolution directly, rather than investigating time-averaged quantities). Li and Bou-Zeid (2019) show the dispersive fluxes of scalar quantities do not always follow the flow of momentum, with obstacle geometry typically affecting dispersive fluxes of momentum more than those of scalars. The authors attribute this difference to the physical mechanisms involved. The air's velocity decreases before it reaches the upstream face of an obstacle, and therefore pressure affects momentum transfer away from surfaces. However, the air must touch an obstacle's surface to deposit or take up scalars, so scalar transport is much more spatially confined. LES studies of ABL flow over homogeneous surfaces indicate dispersive fluxes of heat are modulated by two broad flow regimes. The first is where surface heterogeneities, such as unevenly heated ground, drive the dispersive fluxes. The second is where dispersive fluxes are driven by turbulent coherent structures in high-shear conditions (Inagaki et al., 2006; Margairaz et al., 2020). Numerical investigations of patchy forests should include calculations of the dispersive fluxes. Ignoring these fluxes may mean ignoring over half of the total momentum flux, for example, by focusing only on deviations from the time average and neglecting spatial deviations. Real forests channel air into gaps and patches, creating spatially coherent structures whose contributions can be as large as those induced by turbulence.

6.5. A Note on the Resolution and Domain Size in LES Models

Scientists continually face a trade-off between scale and resolution. This choice is particularly relevant to fluid modeling because of the extreme computational expense of simulating turbulence. LES of ecosystem-scale interactions around forests currently use around 10^6–10^7 cells (e.g., Ma et al., 2020), although Patton et al. (2016) deployed some 4×10^9 cells in an enormous computational effort. Researchers must decide how to deploy those

cells most effectively. Two competing demands must be balanced: (a) the LES domains should be large enough to simulate the largest boundary-layer eddies; but (b) should have a filter width fine enough to resolve the smallest eddies sufficiently (Wood, 2000). As to the first requirement, we denote the domain size (L_x, L_y, L_z), where L_i is the domain length in the *ith* direction, and z_i the boundary-layer depth. For neutrally stratified conditions, a domain size of at least ($\approx 3z_i$, $\approx 3z_i$, z_i) is probably sufficient (Mason & Thomson, 1987; Wurps et al., 2020). Larger horizontal domains—e.g. ($8z_i$, $8z_i$, z_i)—are needed to capture the largest eddies in free convection conditions. In stable conditions, smaller domains are required in an absolute sense, because the largest ABL eddies scale with z_i, which may be 100 m or less, compared with $z_i \approx 1$–2 km in highly unstable conditions (Basu & Porté-Agel, 2006; Wurps et al., 2020). However, using too small a value of L_z, particularly over obstacles, artificially negates any interaction of the boundary layer and the residual layer aloft (Grylls et al., 2020); $L_z \geq 3z_i$ appears to be a reasonable minimum for stable conditions (Basu & Porté-Agel, 2006; Wurps et al., 2020).

Determining an appropriate filter resolution for LES requires careful consideration of the atmospheric conditions, the forest structure, and the topography. A useful rule-of-thumb for ABL investigations is that a filter width $\Delta f < z_i/60$ is sufficient for the first- and second-order flow statistics to be well resolved (Sullivan & Patton, 2011). This equates to $\Delta_f \approx 2.5$, 10, and 20 m for stable, neutral, and convective conditions, respectively, over unvegetated ground (Wurps et al., 2020). However, for LES models of forests, we need to consider the dominant turbulent eddies in the shear layer at the top of the canopy. In neutral conditions, the length scale for these eddies is $L_s \approx 2\beta^2/C_d a(z)$ (by rearranging Equation 8), giving $L_s \approx 7$ m for $\beta = 0.35$, $C_d = 0.2$, and $a(z) \approx 0.18$ m^{2}m^{-3}, typical daytime values for mature forests. To resolve the eddies' structure, we need the vertical filter width to be significantly smaller than L_s, say $L_s/8$. A vertical filter width within the canopy of around a meter or less is a good first approximation. The dominant eddies have a mean streamwise spacing of around $8.1L_s \approx 50$ m (Finnigan, 2000; Raupach et al., 1996), requiring a horizontal filter width of around 5 m. Smaller filters may be required in the lee of hills, around which L_s can take smaller values (Finnigan, 2000; Ross, 2008). If gaps are to be simulated explicitly (i.e., openings with $O_d \geq L_s$), then a horizontal filter width of around $O_d/8$ or smaller is required to adequately resolve the turbulent structures in the gaps. Slightly coarser resolutions than those suggested may suffice for very unstable conditions, but finer filters may be required in very stable cases, because L_s decreases with increasing stability. In very stable and very unstable conditions around forests, mixing-layer-type eddies cease to dominate the turbulence structure. In very unstable conditions, the filter width should be chosen to scale with the dominant convective plumes, rather than L_s. It is not clear whether the distributed-drag parametrization is appropriate to model forest-atmosphere exchange in very stable conditions, during which the turbulent exchange can be dominated by intermittent bursts rather than mechanically generated eddies (Section 2.6; Mahrt, 2014).

Although LES resolution has increased more slowly than the general semiconductor capacity predicted by Moore's law (Bou-Zeid, 2014), computing capacity is expected to increase with time for the foreseeable future. This raises the question of whether the extra capacity should be applied toward increasing the resolution or the size of the simulated domain. In many fluid applications, the answer to this question is "both." However, the distributed-drag parametrization assumes the averaging volume—the filter width for LES—to be much larger than the individual tree and plant elements so that their presence is accounted for statistically. For mature forests, where the tree trunks can have diameters of a meter or more, decreasing the horizontal filter widths below a few meters makes little physical sense without a formal re-think of the averaging operations. In many cases, the increased computational capacity could be used more productively (a) to increase the simulated ABL height, thereby increasing the total amount of resolved TKE (Grylls et al., 2020), (b) to increase the size of the simulated domain, (c) to include a wider range of physical and chemical processes, or (iv) to account for plant movement. However, there may be instances for which a very fine filter is required, such as to investigate turbulent transfer in small gaps, in the lee of steep hills, or in stable conditions.

Outside of these specific applications, the workhorse spatial resolution of $\Delta_x = \Delta_y \approx 5$ m, and $\Delta_z \approx 1$ m, means a forest volume of up to tens of cubic meters is accounted for by a single grid cell, with the smallest resolved eddies $\approx$5 m in diameter. This implies a need for robust SGS schemes if LES simulations are to be useful. Although LES has become popular over the last few decades, the development of SGS schemes has been slow (Moser et al., 2021). The most widely used SGS parametrization is the Smagorinsky scheme, in which closure is achieved using empirical arguments and theory (Smagorinsky, 1963). This scheme assumes the turbulence is isotropic, which is not the case in forests (and in many other ASL applications). Recently, more suitable schemes have been developed by determining the minimum energy dissipation needed to balance the turbu-

lence production at SGS scales (Gadde et al., 2021; Rozema et al., 2015), but these schemes have not yet been widely adopted. Improving SGS schemes for forest applications is an important line of future research. Eddies larger than the plant elements lose TKE to heat and fine-scale TKE, which short cuts the usual eddy cascade that is assumed by Kolmogorov's −5/3 law (Finnigan, 2000). Shaw and Patton (2003) show this effect can be accounted for in LES using a TKE cascade term, without the need for extra modifications to account for wake-scale kinetic energy transfer. However, the effect of this short cut to fine scales has not been tested in patchy vegetation canopies, with moving plants, or with a view to determining its impact on scalar exchange across the boundary layers of leaves.

7. Future Challenges

It is an exciting time to investigate forest-atmosphere exchange. There is a growing body of high-quality observations from micrometeorological campaigns (e.g., Butterworth et al., 2021; Patton et al., 2011), long-term ecosystem monitoring sites (e.g., Hicks & Baldocchi, 2020; Oliphant, 2012), and ecosystem-scale FACE experiments (e.g., Drake et al., 2016; Hart et al., 2020; Norby et al., 2006). These observations allow researchers to investigate an increasingly diverse range of physical and biological phenomena in an increasingly diverse range of ecosystems. Numerical models, if deployed correctly, offer a fourth pillar in ecosystem-scale investigations, alongside measurements, theory, and physical models. However, fulfilling the potential of observational networks and new modeling techniques requires a concerted effort across scientific disciplines. Moving beyond idealized cases and moderate atmospheric conditions is not easy. First, the idealizations and simplifications are usually for good reason, for example, to reduce the dimensionality of investigations, or to attempt to reveal canonical processes rather than the idiosyncrasies of individual sites. Second, because many of the experimental and modeling techniques were developed from studies of idealized forests in moderate conditions, attempting to interpret results outside of these scenarios is not always straightforward because the techniques are not at their best (Baldocchi, 2008; Belcher et al., 2012; Brunet, 2020; Stoy et al., 2013; K. Wilson et al., 2002). Third, research into ecosystem-scale forest-atmosphere interactions is motivated by scientific questions across disciplines including forest ecology, fluid mechanics, plant physiology, meteorology and climatology, air and water quality, as well as policy and commercial need. The literature is therefore vast and widely dispersed. In a sense this dispersion is exciting because it suggests that progress may lie at the intersections of scientific disciplines. However, it is also a barrier to progress because results familiar to one scientific community may be unknown in another, even when they relate to important coupled phenomena. We conclude by framing progress and outstanding challenges under three overlapping headings.

7.1. Customized Numerical Models of Real Sites

Advances in non-destructive scanning techniques, computing power, and theory are poised to allow researchers to investigate forest-atmosphere exchange at real sites, using models capable of resolving turbulence. These models could be calibrated to study a variety of ecosystem-scale processes, including the wind dispersal of spores, turbulent fluxes of important scalar quantities, or the forest's microclimate. Regarding the structural element of this challenge, TLS allows researchers to include detailed, site-specific morphological detail in their models (Boudreault et al., 2015; Raumonen et al., 2015; D. Wang et al., 2020), and virtual canopy generators can be used to generate realistic forest canopies from a small number of structural variables (Bohrer et al., 2007). Researchers should include a careful description of the forest morphology in their numerical models, particularly when assessing simulated results against observations, or in forests with a high proportion of edge region. Ecosystem-scale exchange models should account for the streamlining of plants in high wind conditions. This can be accounted for efficiently in LES simulations by incorporating the Vogel number B into the parametrization of the aerodynamic drag f_i. Plant movement at an ecosystem scale can be incorporated through poroelastic and mechanical parametrizations (Dupont et al., 2010; Pivato et al., 2014) or by the inclusion of a stochastic forcing into the momentum equations at a frequency corresponding to plant movement.

However, two important knowledge gaps need to be narrowed before these customized models can be used to investigate the exchange of scalar quantities at real sites. The first is that there are few public datasets against which nascent models can be tested. The ability of turbulence-resolving models to simulate scalar transport in real landscapes therefore remains essentially unknown. The CHATS observations are the apogee of surface meas-

urements in a tree dominated landscape (Dupont & Patton, 2012; Patton et al., 2011) and a valuable resource for model developers (Ma & Liu, 2019). However, the CHATS measurements were made in a homogeneous orchard on level ground and are therefore unsuitable for testing models' ability to handle patchiness, species diversity, and undulating topography. More measurements are needed, especially of scalar quantities such as CO_2, water vapor, pollutants, and spores in patchy forests. For practical reasons, these measurements may not be on the scale of CHATS. However, existing eddy-covariance and FACE facilities have generated extensive timeseries that may be exploited, especially if combined with experiments of opportunity and targeted observational campaigns around edges, gaps, and hills. For example, further experimental testing will determine the extent to which scalar fluxes reach an approximate equilibrium in patchy landscapes, and whether the chimney effect in the lee of hills is observed in nature as well as in numerical models.

The second gap concerns the soil-forest-atmosphere coupling of scalar quantities. Researchers are beginning to incorporate multi-layer canopy exchange schemes in ecosystem-scale LES models (Ma & Liu, 2019; Patton et al., 2016) and in models designed for slightly larger space and time scales (Bonan et al., 2021; L. Xu et al., 2017; Yan et al., 2020). These schemes include parametrizations of phenomena such as evapotranspiration, soil fluxes, and the photosynthetic uptake of CO_2 that are designed to hold approximately across different ecosystems. A potentially fruitful area of research would be to modify these schemes to reflect observations at individual sites, for example, by adjusting the underlying parametrizations, or through some combination of Bayesian data assimilation and machine learning. A point of caution is that observations in forests tend to be sparse in space (e.g., wind measurements) and sometimes time (e.g., spore releases), and are often measured using proxies or with indirect techniques (e.g., photosynthetic capacity; Gardner et al., 2021). Machine learning techniques should therefore be carefully adapted to account for uncertainty in our knowledge of the underlying physical processes (Geer, 2021).

7.2. Connection to Larger Scales

Developments in theory and computing capacity are allowing researchers to begin incorporating ecosystem-scale phenomena into numerical weather prediction and earth system models (Arthur et al., 2019; Bonan et al., 2018, 2021; Shao et al., 2013; Yan et al., 2020). To be computationally feasible, these schemes rely on simplified versions of the forest canopy (Yan et al., 2020), a priori turbulence parameters (Y. Chen et al., 2016), or modifications of MOST with mixing-layer length scales (Bonan et al., 2018). These approximations perform best when the atmosphere is neutral and the surface homogeneous. Further work is needed to determine whether the length scales and approximations can be modified to account for patchy landscapes and a larger range of atmospheric conditions. Robust parametrizations for scalar quantities are especially difficult to find. Missing theoretical links may become apparent through further testing of customized LES models against high-quality field measurements, as outlined above. Another relatively unexplored approach is to reject the assumption that the scalar statistics should always relate to those of the velocity field. For example, understanding the movement of water vapor around at fragmented forest at dusk is a problem that may not yield to a deterministic, drag-based treatment or approximate vertical turbulence profiles. The geometries of velocity and scalar timeseries are often much less scale-dependent than their accompanying physics (Belušić & Mahrt, 2012; D. Chen et al., 2019; Kang, 2015). Turbulent events in these timeseries can also be clustered by their statistical properties, with no assumption of the underlying physical structures (Kang et al., 2015; Sun et al., 2015). The timeseries of well-chosen turbulence measurements may reveal scale-independent behaviors to parametrize forest-atmosphere exchange in terrain and conditions that are beyond the reach of current approaches. Spectral analysis of long-term eddy-covariance measurements over mixed hardwood forests showed smaller eddies are relatively more efficient in transporting sensible heat than momentum, while larger eddies are relatively more important in transporting momentum (Su et al., 2004). It would be fascinating if this type of analysis were conducted over even longer measurement periods, with a larger diversity of ecosystems.

7.3. Challenging Weather and Atmospheric Conditions

Numerical models permit low dimensionality experiments that are difficult to perform in the open atmosphere. A common simplification is that of an isolated forest in neutral atmospheric conditions. This removes all aspects of the atmosphere, other than a velocity field that is recycled using periodic boundary conditions. In nature,

however, forests are subject to all sorts of weather, climatic, atmospheric conditions. Atmospheric stability can change quickly in time, such as around dusk, and in space, such as when the forest air space decouples from the surrounding ABL. Simulations of the entire ABL will help explore these effects further (Ma & Liu, 2019; Patton et al., 2016; Yan et al., 2020). Local effects around gaps and areas of uneven heating should not be discounted and, with time, may be possible to resolve in site specific models. However, further research is needed into the effect of submeso motions on forest-atmosphere exchange. These motions are difficult to model because they often manifest as intermittent turbulent bursts, but do not result from mixing-layer-type eddies, and therefore must be generated using mesoscale coupling or synthetic turbulence. Submeso motions are common during the atmospheric conditions that tend to be most problematic for eddy-covariance measurements, such as stable nights, and discounting their effect from models introduces an unwelcome bias. Rainfall is a significant source of momentum into forests, affecting myriad ecological processes as well as the plants' mechanical response to the flow. Raindrop-induced vortices can carry small particles away from plant surfaces and into the turbulent flow. Wet conditions provide a major unexplored area for numerical investigations of forest-atmosphere exchange, especially given that much of the world's forested area is situated in climates where precipitation is common.

Appendix A: Numerical Details of LES Model

A1: Drag Parametrization and Simulated Cases

We simulate flow across small forests, with the presence of the aerial parts of the forests represented using the drag parametrization in Equation 7, $f_i = -C_d a(z)|\widetilde{U}| < \widetilde{u}_i >$ (the overtilde denotes the resolved variables, as in Section 2). We specified a height-averaged equational drag coefficient $\bar{C}_d = 0.2$, a value commonly used in previous studies (Table A1). Figure A1 shows the mean vertical profile of the LAD, $a(z)$, which was derived from terrestrial lidar surveys of the BIFoR FACE facility (Hart et al., 2020), using the method in Raumonen et al. (2015), giving PAI ≈ 5.

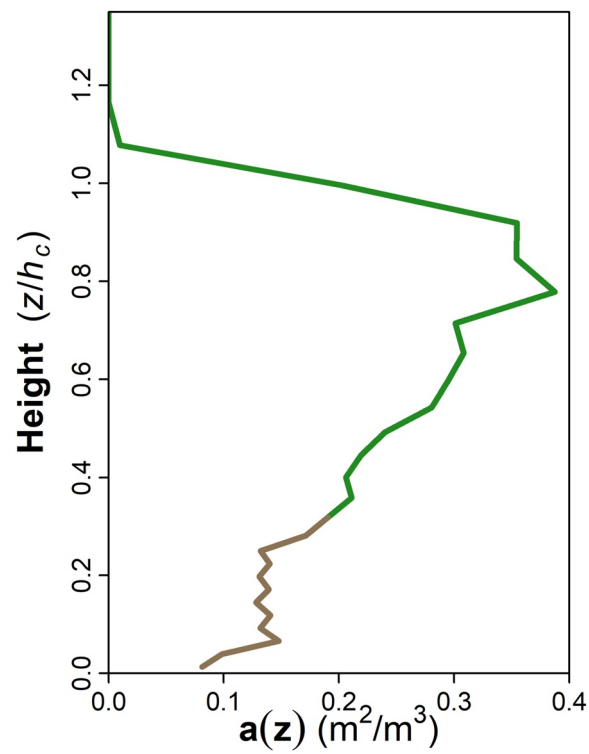

Figure A1. Vertical profile of PAD $a(z)$ (PAI ≈ 5) used in the LES model. Coloring indicates that the trunks account for much of the PAD in the lower part of the canopy, and the leaves account for much of the PAD in the upper part of the canopy. The coloring is illustrative only and does not reflect the detailed composition of the BIFoR FACE facility.

We specified two cases:

1. **Case 1**—We apply the distributed-drag parametrization over a patch extending 500 m in the streamwise direction, and across the entire domain in the spanwise direction, to simulate flow across a small, isolated forest.
2. **Case 2**—As for Case 1 but, for each forested cell, $\bar{C}_d a(z)$ taking a random number (uniformly distributed) within the range $\bar{C}_d a(z)$ (Case 1) $\pm 2\%$. This introduces a small spatial stochastic forcing into the momentum equations solved by the LES model via the drag term in Equation 7. The stochastic forcing does not directly vary with time using this formulation.

A2: Transport Equations

We solved the transport equations using the LES mode of WRF version 3.6.1 (Skamarock et al., 2008). The WRF model solves discretized forms of the spatially averaged momentum equations using the Runge–Kutta time-integration scheme (Wicker & Skamarock, 2002),

$$\frac{\partial \widetilde{u}_i}{\partial x_i} = 0, \tag{A1a}$$

$$\frac{\partial \widetilde{u}_i}{\partial t} + \frac{\partial \widetilde{u}_i \widetilde{u}_j}{\partial x_j} = -\frac{1}{\rho}\frac{\partial \widetilde{p}}{\partial x_i} + \frac{\partial \tau_{ij}}{\partial x_j} + B_i + f_c \epsilon_{ij3}(\widetilde{u}_j - U_{g,j}) + f_i, \tag{A1b}$$

where ρ is the air density; $\widetilde{p}$ is the resolved pressure; τ_{ij} is the kinematic mean stress tensor, which represents the SGS stresses; B_i is the buoyancy force: $B_i = -\delta_{i3} g\theta'/\bar{\theta}$, where $\bar{\theta}$ is the potential temperature for hydrostatic balance, and θ' is the temperature variations with respect to $\bar{\theta}$; f_c is the Coriolis parameter; ϵ_{ij3} is the alternating unit tensor; and U_{gj} is the geostrophic velocity. Equation A1b is closed by parametrizing the SGS stress tensor τ_{ij} as

$$\tau_{ij} = -2\nu_{\mathrm{SGS}} S_{ij}, \tag{A2}$$

$$S_{ij} = \frac{1}{2}\left(\frac{\partial \widetilde{u}_i}{\partial x_j} + \frac{\partial \widetilde{u}_j}{\partial x_i}\right), \tag{A3}$$

$$\nu_{\mathrm{SGS}} = c_k \sqrt{e_{\mathrm{SGS}}}(\Delta x \Delta y \Delta z)^{1/3}, \tag{A4}$$

where e_{SGS} is the SGS TKE and $c_k = 0.10$ is a modeling constant. The prognostic equation for the evolution of the term e_{SGS} is,

$$\frac{\partial e_{\mathrm{SGS}}}{\partial t} + \frac{\partial \widetilde{u}_j e_{\mathrm{SGS}}}{\partial x_j} = \nu_{\mathrm{SGS}} \frac{\partial}{\partial x_j}\left(\frac{\partial e_{\mathrm{SGS}}}{\partial x_j}\right) + P_r + F - \frac{C_\epsilon e_{\mathrm{SGS}}}{(\Delta x \Delta y \Delta z)^{1/3}}, \tag{A5}$$

where P_r represents the shear- and buoyancy-production terms (Skamarock et al., 2008), C_ϵ is the dissipation coefficient (Moeng et al., 2007). The term F is a cascade term, which accounts for additional dissipation of kinetic energy from air-forest interactions at scales smaller than the spatial filter (Shaw & Patton, 2003; Shaw & Schumann, 1992), with

$$F = -2\bar{C}_d a(z)|\widetilde{U}| e_{\mathrm{SGS}}. \tag{A6}$$

A3: Drag Parametrization and Simulated Cases

The simulated domain is 1,435 × 1,435 × 1,000 m in the streamwise, spanwise, and vertical directions, respectively, comprising 287 × 287 × 79 grid cells. The horizontal grid resolution is 5 m in each direction, and the vertical resolution is increased from around 0.67 m in the lower half of the forest to around 60 m at the top of the simulated domain. The mean height of the forest $h_c = 25$ m. The upstream edge of the forest is situated approximately 600 m from the inflow edge of the domain. We simulate flow under neutral conditions, with the initial profile of potential temperature θ specified as a constant at 283.15 K at the bottom of the domain (up to $z \approx 475$ m) followed by a linear increase to 291.7 K at the top of the domain. We include a dampening layer of $z \approx 300$ m at the top of the domain to minimize wave reflection (Nottrott et al., 2014). The geostrophic velocity components

above the boundary layer top are set to $U_g = -6$ m s^{-1} and $V_g = -9.3$ m s^{-1}, and this specification yields a mean wind speed of 1.6 m s^{-1} from a flow direction of 343° (approximately a northerly wind) at the crown top ($z = h_c$). We use the meteorological convention where the x-direction is aligned west–east and the y-direction south–north.

Spin-up was 5 hr, with cyclic boundary conditions for all dynamical variables in both horizontal directions. After the spin-up, we ran the simulations for a further 120 min, taking samples at intervals of 3 s. We time-averaged over the latter 100 min (denoted by T) of these samples (i.e., $t_0 = 20$ min to $t_0 + T = 120$ min). This process generates a three-dimensional time series of 2,000 resolved samples in the form $\widetilde{\phi}(x, y, z, t)$. We derived the resolved turbulent statistics using (a) time averages over the sampling period and (b) spatial averages along the y-direction ($L_y = 1{,}435$ m), over which the turbulent statistics are homogeneous. For each resolved variable, $\widetilde{\phi}$, the averaging process generates a two-dimensional function,

$$\bar{\Phi}(x, z) = \frac{1}{T L_y} \int_0^{L_y} \int_{t_0}^{t_0+T} \widetilde{\phi}(x, y, z, t)\ dt dy, \tag{A7}$$

from which we calculate the statistics presented in Figure 10. The resolved fluctuating component of $\widetilde{\phi}$ around $\bar{\Phi}$ is defined as $\phi'(x, y, z, t) = \widetilde{\phi}(x, y, z, t) - \bar{\Phi}(x, z)$, with the skewness $Sk_{u_i} = \overline{u_i'^3}/\sigma_{u_i}^3$ and kurtosis $t_{u_i} = \overline{u_i'^4}/\sigma_{u_i}^4$.

Appendix B: Summary of Modeling Investigations of Flow Around Forests

Table A1
Chronological Summary of Highly Cited Modeling Investigations of Flow Around Forests at the Ecosystem Scale

Study	Equations/model	Distribution of PAD as $a(z)$	C_d	PAI range (m^2/m^2)	Additional features
Shaw and Schumann (1992)	LES	Artificially generated vertical profile for a deciduous forest	0.15	2, 5	
Dwyer et al. (1997)	LES	Artificially generated vertical profile for a deciduous forest	0.15	2, 5	Numerical setup based on Shaw and Schumann (1992)
Su et al. (1998)	LES	Artificially generated vertical profile for a deciduous forest	0.15	2	Numerical setup based on Shaw and Schumann (1992)
Shaw and Patton (2003)	LES	Artificially generated vertical profile for a deciduous forest	0.15	2	
Watanabe (2004)	LES	Uniform vertical distribution	0.2	2	
Finnigan and Belcher (2004)	Mixing-length closure	Uniform vertical distribution	0.25	≈4	Drag parameters are approximations. Analysis is mostly expressed in dimensionless terms
Katul et al. (2006)	Mixing-length closure	Uniform vertical distribution	0.2	3	Investigated carbon dioxide exchange over forested hills
Yang, Morse, et al. (2006) and Yang, Raupach, et al. (2006)	LES	Artificially generated vertical profile for a deciduous forest	0.15	2	Numerical setup based on Shaw and Schumann (1992)
Dupont and Brunet (2008a)	LES	Four cases: (a) approximately vertically uniform, (b) sparse trunk space and dense crown, (c) very dense crown and very sparse trunk space, and (d) undergrowth in trunk space	≈0.5	2	PAI chosen so that the product $c_d a(z)$ was the same as in Raupach et al. (1987), where PAI ≈ 5
Dupont and Brunet (2008b)	LES	Uniform vertical distribution	0.2	2	Structure of the upstream edge of the forest was varied across seven shapes and densities
Dupont and Brunet (2008c)	LES	Three cases: (a) approximately vertically uniform, (b) sparse trunk space and dense crown, and (c) undergrowth in trunk space	0.2	1–5	

Table A1
Continued

Study	Equations/model	Distribution of PAD as $a(z)$	C_d	PAI range (m^2/m^2)	Additional features
Cassiani et al. (2008)	LES	Artificially generated vertical profile for a deciduous forest	0.2	2–8	Forest structure approximately based on that of Duke Forest (Katul & Albertson, 1998)
Sogachev et al. (2008)	RANS	Foliage distribution based on beta probability density function	0.2	0.5–3	Investigated scalar transport around a forest edge
Ross (2008)	LES	Uniform vertical distribution	0.15	5	Simulated flow over forested ridges
Bohrer et al. (2009)	LES	Randomly generated heterogeneous canopy	0.15	1.4–3	1,000 virtual canopies generated for each simulation, with randomized gaps of approximately crown width
Dupont and Brunet (2009)	LES	Artificially generated vertical profile for a deciduous forest	0.2	2, 5	Canopy structure approximately based on deciduous forest reported in Neumann et al. (1989)
Dupont et al. (2011)	LES	Dense canopy with sparse trunk space to approximate pine plantation	0.26	2	Includes five additional cases with the vertical profile gradually relaxed toward a uniform distribution
Edburg et al. (2012)	LES	Artificially generated vertical profile for a deciduous forest	0.5	1	
Schlegel et al. (2012)	LES	Forest dominated by *Picea abies*. PAD varied across simulated domain	0.15	≈7.1	PAD distribution derived from terrestrial Lidar
Mueller et al. (2014)	LES	Simplified vertical profiles estimates from observations in a pine plantation and a deciduous forest	0.26	2	Setup taken from Dupont et al. (2011) and Su et al. (1998)
Boudreault et al. (2015)	RANS	Forest dominated by *Picea abies*. Frontal area density varied across simulated domain	0.2	≈2.9	Vertical profile derived from aerial lidar scans of the forested area
X. Xu et al. (2015)	RANS	Vertical profile from measurements in a forest dominated by spruce and pine	≈0.3	3.3	Two-dimensional investigation of stably stratified flow around an idealized forested hill
Kanani-Sühring and Raasch (2015)	LES	Artificially generated vertical profile for a deciduous forest	0.2	1–8	Used LES to investigate scalar transport around a forest edge
Schlegel et al. (2015)	LES	Forest dominated by *Picea abies*. PAD varied across simulated domain	0.15	≈7.1	PAD distribution derived from terrestrial lidar. Developed preliminary work in Schlegel et al. (2012)
Ross and Harman (2015)	LES	Uniform vertical distribution	0.25	4	Simulated flow and scalar transport over forested hills
Kanani-Sühring and Raasch (2017)	LES	Artificially generated vertical profile for a deciduous forest	0.2	1–8	Investigated scalar transport in the lee of the forest, with multiple sources and sinks
Yan et al. (2017)	LES	Simplified deciduous trees. Three cases: (a) bluff objects, (b) bluff trunks and porous crowns, and (c) fully porous trees	≈0.2	≈5	Numerical details couched in terms of bluff objects (e.g., frontal area index) to be compared more easily to wind-tunnel observations in Böhm et al. (2013)
Boudreault et al. (2017)	LES	Two cases: (a) heterogeneous PAD derived from terrestrial lidar and (b) spatially homogeneous $a(z)$ from averaged data	0.2	6	Heterogeneous case included tapered upstream edge
B. Chen et al. (2019)	LES	Horizontally homogeneous. Profile derived from leaf area measurements in the Amazon rainforest	0.2	7	Simulated flow and scalar transport over forested hills. PAD profiles generated from observations reported in Tóta et al. (2012) and Fuentes et al. (2016)

Table A1
Continued

Study	Equations/model	Distribution of PAD as $a(z)$	C_d	PAI range (m^2/m^2)	Additional features
Ma and Liu (2019)	LES	Uniform vertical distribution	0.2	2.5	LES coupled with multiple-layer canopy exchange model
Watanabe et al. (2020)	LES (Lattice Boltzmann method)	Uniform vertical distribution	0.2	2	The equations of motion are resolved using the lattice Boltzmann method rather than solving the incompressible Navier–Stokes equations
Ma et al. (2020)	LES	Three cases: (a) vertically uniform, (b) sparse trunk space and dense crown, (c) very sparse trunk space and dense crown	0.25	4	LES coupled with a multiple-layer canopy exchange model used to investigate transport of different scalars across a forest edge
Yan et al. (2020)	LES	Profile generated using empirical relationship in Lalic and Mihailovic (2004)	0.15	4.3	LES coupled to the mesoscale Weather Research and Forecasting model. Grid resolution at the mesoscale
B. Chen et al. (2020)	LES	Horizontally homogeneous. Profile derived from measurements in the Amazon (as for B. Chen et al. [2019])	0.2	7	Simulated flow and scalar transport over forested hills, including realistic terrain

Note. PAD and PAI, respectively, refer to the plant area density/index, $a(z)$ is a height-dependent function of the PAD, and C_d is the drag coefficient.

Notation

ABL	Atmospheric boundary layer.
ASL	Atmospheric surface layer.
$a(z)$	Layer-wise plant area density.
B	Vogel number.
BIFoR	Birmingham Institute of Forest Research.
(B)VOCs	(Biogenic) volatile organic compounds.
C_d	Drag coefficient.
CHATS	Canopy Horizontal Array Turbulence Study
CLM	Community Land Model.
DNS	Direct numerical simulation.
E_ϕ	Efficiency of particle deposition.
FACE	Free-air carbon dioxide enrichment.
f_i	Aerodynamic drag.
f_0	Natural frequency of moving plants.
g	Gravitational acceleration.
h_c	Canopy height.
h_d	Displacement height.
ICR	In-canopy recirculation region.
ISL	Inertial sublayer.
Kt_{u_i}	Kurtosis of the velocity component u_i.
L	Hill half-length.
L_c	Canopy drag length scale.
LES	Large-eddy simulation.
L_s	Shear length scale.
LSM	Lagrangian stochastic modeling.

MOST	Monin–Obukhov similarity theory.
O_d	Diameter of opening.
P	Perturbation pressure.
PAD	Plant area density.
PAI	Plant area index.
Q_{h_c}	Specific flux at the crown top.
RANS	Reynolds-average Navier–Stokes.
Re	Reynolds number.
RSL	Roughness sublayer.
SGS	Sub-grid scale.
Sk_{u_i}	Skewness of the velocity component u_i.
S_{ϕ_i}	Source/sink of a scalar quantity ϕ_i.
TKE	Turbulence kinetic energy.
UFP	Ultrafine particles.
U_{h_c}	Mean streamwise wind speed at the crown top.
u_*	Friction velocity.
WRF	Weather Research and Forecasting model.
w_s	Particle settling velocity.
x_A	Adjustment distance.
z_i	Boundary-layer depth.
z_0	Roughness length.
α	Attenuation coefficient.
β	u_*/U, evaluated at $z = h_c$.
δ_{i3}	Kronecker delta.
θ_v	Virtual potential temperature.
θ_0	Reference temperature.
ν_{SGS}	Sub-grid scale eddy viscosity.
ν_ϕ	Dry deposition velocity.
σ_{u_i}	Standard deviation of the velocity component u_i.
τ	Air parcel residence time.
ϕ_l	Resolved local scalar concentration.

Conflict of Interest

The authors declare no conflicts of interest relevant to this study.

Data Availability Statement

The WRF-LES data used in this paper, and their supporting R scripts, are available at https://github.com/forested-dy/forest_exchange. Figure 2b seabirdnz on Flickr. "Slope Point". 18 February 2008. Online image with Creative Common License CC-BY-2.0. https://www.flickr.com/photos/seabirdnz/5460426633. Figure 5c -JvL- on Flickr. "Brownsberg jungle path". 22 October 2016. Online image with Creative Common License CC-BY-2.0. https://www.flickr.com/photos/-jvl-/33153976490/. Figure 5d R.V. on Flickr. "Forest, British Columbia, Canada". 6 July 2013. Online image with Creative Common License CC-BY-2.0. https://www.flickr.com/photos/bluegruen/9601965057. Figure 8c Soil-Science.info on Flickr. "*Pinus taeda* plantation". 21 May 2008. Online image with Creative Common License CC-BY-2.0. https://www.flickr.com/photos/22503286@N06/2512091836. Figure 9 and caption reproduced without modification from Calders et al. (2020) under Creative Commons License CC-BY-4.0.

Acknowledgments
The authors thank Jian Zhong for help and advice on LES simulations, Eric Casella for his terrestrial laser scans of BIFoR FACE, Chantal Jackson for her expertise in redrawing several figures in this paper, and the BIFoR FACE operations team for helpful discussions, photography, and drone footage. It is E. J. Bannister's pleasure to acknowledge the Natural Environment Research Council (NERC) for funding through a CENTA studentship (grant NE/L002493/1). A. R. MacKenzie gratefully acknowledges funding from the JABBS Foundation and NERC (grant NE/S015833/1) in support of this work.

References

Alekseychik, P., Mammarella, I., Launiainen, S., Rannik, Ü., & Vesala, T. (2013). Evolution of the nocturnal decoupled layer in a pine forest canopy. *Agricultural and Forest Meteorology*, *174–175*, 15–27. https://doi.org/10.1016/j.agrformet.2013.01.011

Amiro, B. D. (1990a). Comparison of turbulence statistics within three boreal forest canopies. *Boundary-Layer Meteorology*, *51*(1–2), 99–121. https://doi.org/10.1007/BF00120463

Amiro, B. D. (1990b). Drag coefficients and turbulence spectra within three boreal forest canopies. *Boundary-Layer Meteorology*, *52*(3), 227–246. https://doi.org/10.1007/BF00122088

Apel, E. C., Riemer, D. D., Hills, A., Baugh, W., Orlando, J., Faloona, I., et al. (2002). Measurement and interpretation of isoprene fluxes isoprene, methacrolein, and methyl vinyl ketone mixing ratios at the PROPHET site during the 1998 intensive. *Journal of Geophysical Research: Atmospheres*, *107*(3), 1–15. https://doi.org/10.1029/2000jd000225

Arthur, R. S., Mirocha, J. D., Lundquist, K. A., & Street, R. L. (2019). Using a canopy model framework to improve large-eddy simulations of the neutral atmospheric boundary layer in the weather research and forecasting model. *Monthly Weather Review*, *147*(1), 31–52. https://doi.org/10.1175/MWR-D-18-0204.1

Ashcroft, M. B., Gollan, J. R., & Ramp, D. (2014). Creating vegetation density profiles for a diverse range of ecological habitats using terrestrial laser scanning. *Methods in Ecology and Evolution*, *5*(3), 263–272. https://doi.org/10.1111/2041-210X.12157

Ashworth, K., Chung, S. H., Griffin, R. J., Chen, J., Forkel, R., Bryan, A. M., & Steiner, A. L. (2015). FOREst Canopy Atmosphere Transfer (FORCAsT) 1.0: A 1-D model of biosphere-atmosphere chemical exchange. *Geoscientific Model Development*, *8*(11), 3765–3784. https://doi.org/10.5194/gmd-8-3765-2015

Aubinet, M. (2008). Eddy covariance CO_2 flux measurements in nocturnal conditions: An analysis of the problem. *Ecological Applications*, *18*(6), 1368–1378. https://doi.org/10.1890/06-1336.1

Aubinet, M., Feigenwinter, C., Heinesch, B., Bernhofer, C., Canepa, E., Lindroth, A., et al. (2010). Direct advection measurements do not help to solve the night-time CO_2 closure problem: Evidence from three different forests. *Agricultural and Forest Meteorology*, *150*(5), 655–664. https://doi.org/10.1016/j.agrformet.2010.01.016

Aubinet, M., Heinesch, B., & Yernaux, M. (2003). Horizontal and vertical CO_2 advection in a sloping forest. *Boundary-Layer Meteorology*, *108*(3), 397–417. https://doi.org/10.1023/A:1024168428135

Aylor, D. E., & Flesch, T. K. (2001). Estimating spore release rates using a Lagrangian stochastic simulation model. *Journal of Applied Meteorology*, *40*(7), 1196–1208. https://doi.org/10.1175/1520-0450(2001)040<1196:ESRRUA>2.0.CO;2

Bailey, B. N., & Stoll, R. (2016). The creation and evolution of coherent structures in plant canopy flows and their role in turbulent transport. *Journal of Fluid Mechanics*, *789*, 425–460. https://doi.org/10.1017/jfm.2015.749

Bailey, B. N., Stoll, R., Pardyjak, E. R., & Mahaffee, W. F. (2014). Effect of vegetative canopy architecture on vertical transport of massless particles. *Atmospheric Environment*, *95*, 480–489. https://doi.org/10.1016/j.atmosenv.2014.06.058

Baldocchi, D. D. (2008). TURNER REVIEW No. 15. "Breathing" of the terrestrial biosphere: Lessons learned from a global network of carbon dioxide flux measurement systems. *Australian Journal of Botany*, *56*(1), 1–26. https://doi.org/10.1071/BT07151

Banerjee, T., Katul, G., Fontan, S., Poggi, D., & Kumar, M. (2013). Mean flow near edges and within cavities situated inside dense canopies. *Boundary-Layer Meteorology*, *149*(1), 19–41. https://doi.org/10.1007/s10546-013-9826-x

Bannister, E. J., Cai, X., Zhong, J., & Mackenzie, A. R. (2021). Neighbourhood-scale flow regimes and pollution transport in cities. *Boundary-Layer Meteorology*, *179*(2), 259–289. https://doi.org/10.1007/s10546-020-00593-y

Bash, J. O., Walker, J. T., Katul, G. G., Iones, M. R., Nemitz, E., & Robarge, W. P. (2010). Estimation of in-canopy ammonia sources and sinks in a fertilized Zea mays field. *Environmental Science and Technology*, *44*(5), 1683–1689. https://doi.org/10.1021/es9037269

Basu, S., & Porté-Agel, F. (2006). Large-eddy simulation of stably stratified atmospheric boundary layer turbulence: A scale-dependent dynamic modeling approach. *Journal of the Atmospheric Sciences*, *63*(8), 2074–2091. https://doi.org/10.1175/JAS3734.1

Batista, C. E., Ye, J., Ribeiro, I. O., Guimarães, P. C., Medeiros, A. S. S., Barbosa, R. G., et al. (2019). Intermediate-scale horizontal isoprene concentrations in the near-canopy forest atmosphere and implications for emission heterogeneity. *Proceedings of the National Academy of Sciences of the United States of America*, *116*(39), 19318–19323. https://doi.org/10.1073/pnas.1904154116

Belcher, S. E., Harman, I. N., & Finnigan, J. J. (2012). The wind in the willows: Flows in forest canopies in complex terrain. *Annual Review of Fluid Mechanics*, *44*(1), 479–504. https://doi.org/10.1146/annurev-fluid-120710-101036

Belcher, S. E., Jerram, N., & Hunt, J. C. R. (2003). Adjustment of a turbulent boundary layer to a canopy of roughness elements. *Journal of Fluid Mechanics*, *488*(488), 369–398. https://doi.org/10.1017/S0022112003005019

Belušić, D., & Mahrt, L. (2012). Is geometry more universal than physics in atmospheric boundary layer flow? *Journal of Geophysical Research: Atmospheres*, *117*(9). https://doi.org/10.1029/2011JD016987

Bergen, J. D. (1975). Air movement in a forest clearing as indicated by smoke drift. *Agricultural and Forest Meteorology*, *15*, 165–179. https://doi.org/10.1016/0002-1571(75)90002-3

Bogaert, J., Barima, Y., Mongo, L. I. W., Bamba, I., Mama, A., Toyi, M., & Lafortezza, R. (2011). Forest fragmentation: Causes, ecological impacts and implications for landscape management. In C. Li, R. Lafortezza, & J. Chen (Eds.), *Landscape ecology in forest management and conservation: Challenges and solutions for global change* (pp. 273–296). Springer. https://doi.org/10.1007/978-3-642-12754-0_12

Böhm, M., Finnigan, J. J., Raupach, M. R., & Hughes, D. (2013). Turbulence structure within and above a canopy of bluff elements. *Boundary-Layer Meteorology*, *146*(3), 393–419. https://doi.org/10.1007/s10546-012-9770-1

Bohrer, G., Katul, G. G., Walko, R. L., & Avissar, R. (2009). Exploring the effects of microscale structural heterogeneity of forest canopies using large-eddy simulations. *Boundary-Layer Meteorology*, *132*(3), 351–382. https://doi.org/10.1007/s10546-009-9404-4

Bohrer, G., Wolosin, M., Brady, R., & Avissar, R. (2007). A virtual canopy generator (V-CaGe) for modelling complex heterogeneous forest canopies at high resolution. In *Tellus B: Chemical and Physical Meteorology* (Vol. 59, pp. 566–576). Blackwell Munksgaard. https://doi.org/10.1111/j.1600-0889.2007.00253.x

Bonan, G. B., Patton, E. G., Finnigan, J. J., Baldocchi, D. D., & Harman, I. N. (2021). Moving beyond the incorrect but useful paradigm: Reevaluating big-leaf and multilayer plant canopies to model biosphere-atmosphere fluxes – A review. *Agricultural and Forest Meteorology*, *306*, 108435. https://doi.org/10.1016/j.agrformet.2021.108435

Bonan, G. B., Patton, E. G., Harman, I. N., Oleson, K. W., Finnigan, J. J., Lu, Y., & Burakowski, E. A. (2018). Modeling canopy-induced turbulence in the Earth system: A unified parameterization of turbulent exchange within plant canopies and the roughness sublayer (CLM-ml v0). *Geoscientific Model Development*, *11*(4), 1467–1496. https://doi.org/10.5194/gmd-11-1467-2018

Boudreault, L. É., Bechmann, A., Tarvainen, L., Klemedtsson, L., Shendryk, I., & Dellwik, E. (2015). A LiDAR method of canopy structure retrieval for wind modeling of heterogeneous forests. *Agricultural and Forest Meteorology*, *201*, 86–97. https://doi.org/10.1016/j.agrformet.2014.10.014

Boudreault, L. É., Dupont, S., Bechmann, A., & Dellwik, E. (2017). How forest inhomogeneities affect the edge flow. *Boundary-Layer Meteorology*, *162*(3), 375–400. https://doi.org/10.1007/s10546-016-0202-5

Bou-Zeid, E. (2014). Challenging the large eddy simulation technique with advanced a posteriori tests. *Journal of Fluid Mechanics*, *764*, 1–4. https://doi.org/10.1017/jfm.2014.616

Bou-Zeid, E., Anderson, W., Katul, G. G., & Mahrt, L. (2020). The persistent challenge of surface heterogeneity in boundary-layer meteorology: A review. *Boundary-Layer Meteorology*, *177*(2), 227–245. https://doi.org/10.1007/s10546-020-00551-8

Branford, D., Fowler, D., & Moghaddam, M. V. (2004). Study of aerosol deposition at a wind exposed forest edge using 210Pb and 137Cs soil inventories. *Water, Air, and Soil Pollution*, *157*(1–4), 107–116. https://doi.org/10.1023/B:WATE.0000038879.99600.69

Bright, V. B., Bloss, W. J., & Cai, X. (2013). Urban street canyons: Coupling dynamics, chemistry and within-canyon chemical processing of emissions. *Atmospheric Environment*, *68*, 127–142. https://doi.org/10.1016/j.atmosenv.2012.10.056

Brüchert, F., & Gardiner, B. A. (2006). The effect of wind exposure on the tree aerial architecture and biomechanics of Sitka spruce (*Picea sitchensis*, Pinaceae). *American Journal of Botany*, *93*(10), 1512–1521. https://doi.org/10.3732/ajb.93.10.1512

Brunet, Y. (2020). Turbulent flow in plant canopies: Historical perspective and overview. *Boundary-Layer Meteorology*, *177*(2–3), 315–364. https://doi.org/10.1007/s10546-020-00560-7

Brunet, Y., & Irvine, M. R. (2000). The control of coherent eddies in vegetation canopies: Streamwise structure spacing, canopy shear scale and atmospheric stability. *Boundary-Layer Meteorology*, *94*(1), 139–163. https://doi.org/10.1023/A:1002406616227

Bryan, A. M., Bertman, S. B., Carroll, M. A., Dusanter, S., Edwards, G. D., Forkel, R., et al. (2012). In-canopy gas-phase chemistry during CABINEX 2009: Sensitivity of a 1-D canopy model to vertical mixing and isoprene chemistry. *Atmospheric Chemistry and Physics*, *12*(18), 8829–8849. https://doi.org/10.5194/acp-12-8829-2012

Buccolieri, R., Santiago, J. L., Rivas, E., & Sanchez, B. (2018). Review on urban tree modelling in CFD simulations: Aerodynamic, deposition and thermal effects. *Urban Forestry and Urban Greening*, *31*, 212–220. https://doi.org/10.1016/j.ufug.2018.03.003

Butler, T. M., Taraborrelli, D., Brühl, C., Fischer, H., Harder, H., Martinez, M., et al. (2008). Improved simulation of isoprene oxidation chemistry with the ECHAM5/MESSy chemistry-climate model: Lessons from the GABRIEL airborne field campaign. *Atmospheric Chemistry and Physics*, *8*(16), 4529–4546. https://doi.org/10.5194/acp-8-4529-2008

Butterworth, B. J., Desai, A. R., Metzger, S., Townsend, P. A., Schwartz, M. D., Petty, G. W., et al. (2021). Connecting land–atmosphere interactions to surface heterogeneity in CHEESEHEAD19. *Bulletin of the American Meteorological Society*, *102*(2), E421–E445. https://doi.org/10.1175/BAMS-D-19-0346.1

Cai, X., Barlow, J. F., & Belcher, S. E. (2008). Dispersion and transfer of passive scalars in and above street canyons—Large-eddy simulations. *Atmospheric Environment*, *42*(23), 5885–5895. https://doi.org/10.1016/j.atmosenv.2008.03.040

Calders, K., Adams, J., Armston, J., Bartholomeus, H., Bauwens, S., Bentley, L. P., et al. (2020). Terrestrial laser scanning in forest ecology: Expanding the horizon. *Remote Sensing of Environment*, *251*, 112102. https://doi.org/10.1016/j.rse.2020.112102

Calders, K., Schenkels, T., Bartholomeus, H., Armston, J., Verbesselt, J., & Herold, M. (2015). Monitoring spring phenology with high temporal resolution terrestrial LiDAR measurements. *Agricultural and Forest Meteorology*, *203*, 158–168. https://doi.org/10.1016/j.agrformet.2015.01.009

Cassiani, M., Katul, G. G., & Albertson, J. D. (2008). The effects of canopy leaf area index on airflow across forest edges: Large-eddy simulation and analytical results. *Boundary-Layer Meteorology*, *126*, 433–460. https://doi.org/10.1007/s10546-007-9242-1

Cava, D., & Katul, G. G. (2008). Spectral short-circuiting and wake production within the canopy trunk space of an alpine hardwood forest. *Boundary-Layer Meteorology*, *126*(3), 415–431. https://doi.org/10.1007/s10546-007-9246-x

Cava, D., Mortarini, L., Giostra, U., Acevedo, O. C., & Katul, G. G. (2019). Submeso motions and intermittent turbulence across a nocturnal low-level jet: A self-organized criticality analogy. *Boundary-Layer Meteorology*, *172*(1), 17–43. https://doi.org/10.1007/s10546-019-00441-8

Cescatti, A., & Marcolla, B. (2004). Drag coefficient and turbulence intensity in conifer canopies. *Agricultural and Forest Meteorology*, *121*(3–4), 197–206. https://doi.org/10.1016/j.agrformet.2003.08.028

Chaudhari, A., Conan, B., Aubrun, S., & Hellsten, A. (2016). Numerical study of how stable stratification affects turbulence instabilities above a forest cover: Application to wind energy. *Journal of Physics: Conference Series*, *753*(3), 032037. https://doi.org/10.1088/1742-6596/753/3/032037

Chen, B., Chamecki, M., & Katul, G. G. (2019). Effects of topography on in-canopy transport of gases emitted within dense forests. *Quarterly Journal of the Royal Meteorological Society*, *145*(722), 2101–2114. https://doi.org/10.1002/qj.3546

Chen, B., Chamecki, M., & Katul, G. G. (2020). Effects of gentle topography on forest-atmosphere gas exchanges and implications for eddy-covariance measurements. *Journal of Geophysical Research: Atmospheres*, *125*(11), 1–15. https://doi.org/10.1029/2020JD032581

Chen, D., Hu, F., Xu, J., & Liu, L. (2019). Long-range correlation analysis among non-stationary passive scalar series in the turbulent boundary layer. *Physica A: Statistical Mechanics and Its Applications*, *517*, 290–296. https://doi.org/10.1016/j.physa.2018.09.094

Chen, L., Liu, C., Zhang, L., Zou, R., & Zhang, Z. (2017). Variation in tree species ability to capture and retain airborne fine particulate matter (PM2.5). *Scientific Reports*, *7*(1), 1–11. https://doi.org/10.1038/s41598-017-03360-1

Chen, Y., Ryder, J., Bastrikov, V., McGrath, M. J., Naudts, K., Otto, J., et al. (2016). Evaluating the performance of land surface model ORCHIDEE-CAN v1.0 on water and energy flux estimation with a single-and multi-layer energy budget scheme. *Geoscientific Model Development*, *9*(9), 2951–2972. https://doi.org/10.5194/gmd-9-2951-2016

Chester, S., & Meneveau, C. (2007). Renormalized numerical simulation of flow over planar and non-planar fractal trees. *Environmental Fluid Mechanics*, *7*(4), 289–301. https://doi.org/10.1007/s10652-007-9026-7

Chester, S., Meneveau, C., & Parlange, M. B. (2007). Modeling turbulent flow over fractal trees with renormalized numerical simulation. *Journal of Computational Physics*, *225*(1), 427–448. https://doi.org/10.1016/j.jcp.2006.12.009

Chiesa, M., Bignotti, L., Finco, A., Marzuoli, R., & Gerosa, G. (2019). Size-resolved aerosol fluxes above a broadleaved deciduous forest. *Agricultural and Forest Meteorology*, *279*, 107757. https://doi.org/10.1016/j.agrformet.2019.107757

Cionco, R. M. (1965). A mathematical model for air flow in a vegetative canopy. *Journal of Applied Meteorology*, *4*(4), 517–522. https://doi.org/10.1175/1520-0450(1965)004<0517:ammfaf>2.0.co;2

Cionco, R. M. (1978). Analysis of canopy index values for various canopy densities. *Boundary-Layer Meteorology*, *15*(1), 81–93. https://doi.org/10.1007/BF00165507

Crandall, S. G., & Gilbert, G. S. (2017). Meteorological factors associated with abundance of airborne fungal spores over natural vegetation. *Atmospheric Environment*, *162*, 87–99. https://doi.org/10.1016/j.atmosenv.2017.05.018

Cucchi, V., Meredieu, C., Stokes, A., Berthier, S., Bert, D., Najar, M., et al. (2004). Root anchorage of inner and edge trees in stands of Maritime pine (Pinus pinaster Ait.) growing in different podzolic soil conditions. *Trees - Structure and Function*, *18*(4), 460–466. https://doi.org/10.1007/s00468-004-0330-2

Dai, Y., Cai, X., Zhong, J., & MacKenzie, A. R. (2021). Modelling chemistry and transport in urban street canyons: Comparing offline multi-box models with large-eddy simulation. *Atmospheric Environment*, *264*, 118709. https://doi.org/10.1016/j.atmosenv.2021.118709

De Langre, E. (2008). Effects of wind on plants. *Annual Review of Fluid Mechanics*, *40*, 141–168. https://doi.org/10.1146/annurev.fluid.40.111406.102135
De Langre, E. (2019). Plant vibrations at all scales: A review. *Journal of Experimental Botany*, *70*(14), 3521–3531. https://doi.org/10.1093/jxb/erz209
Dellwik, E., Bingöl, F., & Mann, J. (2014). Flow distortion at a dense forest edge. *Quarterly Journal of the Royal Meteorological Society*, *140*(679), 676–686. https://doi.org/10.1002/qj.2155
Detto, M., Katul, G. G., Siqueira, M., Juang, J. Y., & Stoy, P. C. (2008). The structure of turbulence near a tall forest edge: The backward-facing step flow analogy revisited. *Ecological Applications*, *18*(6), 1420–1435. https://doi.org/10.1890/06-0920.1
Drake, J. E., Macdonald, C. A., Tjoelker, M. G., Crous, K. Y., Gimeno, T. E., Singh, B. K., et al. (2016). Short-term carbon cycling responses of a mature eucalypt woodland to gradual stepwise enrichment of atmospheric CO_2 concentration. *Global Change Biology*, *22*(1), 380–390. https://doi.org/10.1111/gcb.13109
Dupont, S., Bonnefond, J. M., Irvine, M. R., Lamaud, E., & Brunet, Y. (2011). Long-distance edge effects in a pine forest with a deep and sparse trunk space: In situ and numerical experiments. *Agricultural and Forest Meteorology*, *151*(3), 328–344. https://doi.org/10.1016/j.agrformet.2010.11.007
Dupont, S., & Brunet, Y. (2008a). Edge flow and canopy structure: A large-eddy simulation study. *Boundary-Layer Meteorology*, *126*(1), 51–71. https://doi.org/10.1007/s10546-007-9216-3
Dupont, S., & Brunet, Y. (2008b). Impact of forest edge shape on tree stability: A large-eddy simulation study. *Forestry*, *81*(3), 299–315. https://doi.org/10.1093/forestry/cpn006
Dupont, S., & Brunet, Y. (2008c). Influence of foliar density profile on canopy flow: A large-eddy simulation study. *Agricultural and Forest Meteorology*, *148*(6–7), 976–990. https://doi.org/10.1016/j.agrformet.2008.01.014
Dupont, S., & Brunet, Y. (2009). Coherent structures in canopy edge flow: A large-eddy simulation study. *Technical Reports*, *630*, 93–128. https://doi.org/10.1017/S0022112009006739
Dupont, S., Défossez, P., Bonnefond, J. M., Irvine, M. R., & Garrigou, D. (2018). How stand tree motion impacts wind dynamics during windstorms. *Agricultural and Forest Meteorology*, *262*, 42–58. https://doi.org/10.1016/j.agrformet.2018.06.022
Dupont, S., Gosselin, F. P., Py, C., De Langre, E., Hemon, P., & Brunet, Y. (2010). Modelling waving crops using large-eddy simulation: Comparison with experiments and a linear stability analysis. *Journal of Fluid Mechanics*, *652*, 5–44. https://doi.org/10.1017/S0022112010000686
Dupont, S., & Patton, E. G. (2012). Influence of stability and seasonal canopy changes on micrometeorology within and above an orchard canopy: The CHATS experiment. *Agricultural and Forest Meteorology*, *157*, 11–29. https://doi.org/10.1016/j.agrformet.2012.01.011
Dwyer, M. J., Patton, E. G., & Shaw, R. H. (1997). Turbulent kinetic energy budgets from a large-eddy simulation of airflow above and within a forest canopy. *Boundary-Layer Meteorology*, *84*(1), 23–43. https://doi.org/10.1023/A:1000301303543
Edburg, S. L., Stock, D., Lamb, B. K., & Patton, E. G. (2012). The effect of the vertical source distribution on scalar statistics within and above a forest canopy. *Boundary-Layer Meteorology*, *142*(3), 365–382. https://doi.org/10.1007/s10546-011-9686-1
Fahrig, L. (2003). Effects of habitat fragmentation on biodiversity. *Annual Review of Ecology, Evolution and Systematics*, *34*, 487–515. https://doi.org/10.1146/annurev.ecolsys.34.011802.132419
Feigenwinter, C., Bernhofer, C., Eichelmann, U., Heinesch, B., Hertel, M., Janous, D., et al. (2008). Comparison of horizontal and vertical advective CO_2 fluxes at three forest sites. *Agricultural and Forest Meteorology*, *148*, 12–24. https://doi.org/10.1016/j.agrformet.2007.08.013
Finnigan, J. J. (1979a). Turbulence in waving wheat: I. Mean statistics and honami. *Boundary-Layer Meteorology*, *16*(3), 181–211. https://doi.org/10.1007/BF03335366
Finnigan, J. J. (1979b). Turbulence in waving wheat: II. Structure of momentum transfer. *Boundary-Layer Meteorology*, *16*(2), 213–236. https://doi.org/10.1007/bf02350512
Finnigan, J. J. (1985). Turbulent transport in flexible plant canopies. In B. B. Hicks, & B. A. Hutchinson (Eds.), *The forest-atmosphere interaction* (pp. 443–480). Reidel. https://doi.org/10.1007/978-94-009-5305-5_28
Finnigan, J. J. (2000). Turbulence in plant canopies. *Annual Review of Fluid Mechanics*, *32*, 519–571. https://doi.org/10.1146/annurev.fluid.32.1.519
Finnigan, J. J. (2008). An introduction to flux measurements in difficult conditions. *Ecological Applications*, *18*(6), 1340–1350. https://doi.org/10.1890/07-2105.1
Finnigan, J. J., Ayotte, K., Harman, I. N., Katul, G. G., Oldroyd, H., Patton, E. G., et al. (2020). Boundary-layer flow over complex topography. *Boundary-Layer Meteorology*, *177*(2–3), 247–313. https://doi.org/10.1007/s10546-020-00564-3
Finnigan, J. J., & Belcher, S. E. (2004). Flow over a hill covered with a plant canopy. *Quarterly Journal of the Royal Meteorological Society*, *130*(596), 1–29. https://doi.org/10.1256/qj.02.177
Finnigan, J. J., & Bradley, E. F. (1983). The turbulent kinetic energy budget behind a porous barrier: An analysis in streamline co-ordinates. *Journal of Wind Engineering and Industrial Aerodynamics*, *15*(1–3), 157–168. https://doi.org/10.1016/0167-6105(83)90186-1
Finnigan, J. J., & Brunet, Y. (1995). Turbulent airflow in forests on flat and hilly terrain. In M. P. Coutts, & J. Grace (Eds.), *Wind and trees* (pp. 3–40). Cambridge University Press. https://doi.org/10.1017/cbo9780511600425.002
Finnigan, J. J., Harman, I. N., Ross, A. N., & Belcher, S. E. (2015). First-order turbulence closure for modelling complex canopy flows. *Quarterly Journal of the Royal Meteorological Society*, *141*(692), 2907–2916. https://doi.org/10.1002/qj.2577
Finnigan, J. J., & Shaw, R. H. (2008). Double-averaging methodology and its application to turbulent flow in and above vegetation canopies. *Acta Geophysica*, *56*(3), 534–561. https://doi.org/10.2478/s11600-008-0034-x
Finnigan, J. J., Shaw, R. H., & Patton, E. G. (2009). Turbulence structure above a vegetation canopy. *Journal of Fluid Mechanics*, *637*, 387–424. https://doi.org/10.1017/S0022112009990589
Fisher, R. A., & Koven, C. D. (2020). Perspectives on the future of land surface models and the challenges of representing complex terrestrial systems. *Journal of Advances in Modeling Earth Systems*, *12*(4). https://doi.org/10.1029/2018MS001453
Fleischbein, K., Wilcke, W., Goller, R., Boy, J., Valarezo, C., Zech, W., & Knoblich, K. (2005). Rainfall interception in a lower montane forest in Ecuador: Effects of canopy properties. *Hydrological Processes*, *19*(7), 1355–1371. https://doi.org/10.1002/hyp.5562
Foken, T. (2006). 50 years of the Monin-Obukhov similarity theory. *Boundary-Layer Meteorology*, *119*(3), 431–447. https://doi.org/10.1007/s10546-006-9048-6
Forestry Commission. (2021). *Woodland carbon code*.
Forkel, R., Guenther, A. B., Ashworth, K., Bedos, C., Delon, C., Lathiere, J., et al. (2015). *Review and integration of biosphere-atmosphere modelling of reactive trace gases and volatile aerosols* (pp. 169–179). Springer. https://doi.org/10.1007/978-94-017-7285-3_8
Fowler, D., Pilegaard, K., Sutton, M. A., Ambus, P., Raivonen, M., Duyzer, J., et al. (2009). Atmospheric composition change: Ecosystems-atmosphere interactions. *Atmospheric Environment*, *43*(33), 5193–5267. https://doi.org/10.1016/j.atmosenv.2009.07.068
Fox, J. (1977). Alternation and coexistence of tree species. *The American Naturalist*, *111*(977), 69–89. https://doi.org/10.1086/283138

Freire, L. S., Gerken, T., Ruiz-Plancarte, J., Wei, D., Fuentes, J. D., Katul, G. G., et al. (2017). Turbulent mixing and removal of ozone within an Amazon rainforest canopy. *Journal of Geophysical Research*, *122*(5), 2791–2811. https://doi.org/10.1002/2016JD026009

Friedlander, S. K. (2000). *Smoke, dust and haze: Fundamentals of aerosol dynamics*. Oxford University Press.

Fuentes, J. D., Chamecki, M., Dos Santos, R. M. N., Von Randow, C., Stoy, P. C., Katul, G. G., et al. (2016). Linking meteorology, turbulence, and air chemistry in the amazon rain forest. *Bulletin of the American Meteorological Society*, *97*(12), 2329–2342. https://doi.org/10.1175/BAMS-D-15-00152.1

Fuentes, J. D., Wang, D., Bowling, D. R., Potosnak, M., Monson, R. K., Goliff, W. S., & Stockwell, W. R. (2007). Biogenic hydrocarbon chemistry within and above a mixed deciduous forest. *Journal of Atmospheric Chemistry*, *56*(2), 165–185. https://doi.org/10.1007/s10874-006-9048-4

Gadde, S. N., Stieren, A., & Stevens, R. J. A. M. (2021). Large-eddy simulations of stratified atmospheric boundary layers: Comparison of different subgrid models. *Boundary-Layer Meteorology*, *178*(3), 363–382. https://doi.org/10.1007/s10546-020-00570-5

Gao, W., Shaw, R. H., & Paw U, K. T. (1989). Observation of organized structure in turbulent flow within and above a forest canopy. In *Boundary layer studies and applications* (pp. 349–377). Springer Netherlands. https://doi.org/10.1007/978-94-009-0975-5_22

Gardiner, B. A., Berry, P., & Moulia, B. (2016). Review: Wind impacts on plant growth, mechanics and damage. *Plant Science*, *245*, 94–118. https://doi.org/10.1016/j.plantsci.2016.01.006

Gardner, A., Ellsworth, D. S., Crous, K. Y., Pritchard, J., & Mackenzie, A. R. (2021). Is photosynthetic enhancement sustained through three years of elevated CO_2 exposure in 175-year old Quercus robur? *Tree Physiology*, tpab090. https://doi.org/10.1093/treephys/tpab090

Gaylord, B. P., & Denny, M. W. (1997). Flow and flexibility. *Journal of Experimental Biology*, *200*, 3141–3164. https://doi.org/10.1242/jeb.200.24.3141

Geer, A. J. (2021). Learning earth system models from observations: Machine learning or data assimilation? *Philosophical Transactions of the Royal Society A: Mathematical, Physical and Engineering Sciences*, *379*(2194), 20200089. https://doi.org/10.1098/rsta.2020.0089

Gerken, T., Chamecki, M., & Fuentes, J. D. (2017). Air-parcel residence times within forest canopies. *Boundary-Layer Meteorology*, *165*(1), 29–54. https://doi.org/10.1007/s10546-017-0269-7

Geurts, B. J. (2003). *Elements of direct and large eddy simulation*. RT Edwards, Inc.

Ghannam, K., Poggi, D., Bou-Zeid, E., & Katul, G. G. (2020). Inverse cascade evidenced by information entropy of passive scalars in submerged canopy flows. *Geophysical Research Letters*, *47*(9), 1–10. https://doi.org/10.1029/2020GL087486

Gleicher, S. C., Chamecki, M., Isard, S. A., Pan, Y., & Katul, G. G. (2014). Interpreting three-dimensional spore concentration measurements and escape fraction in a crop canopy using a coupled Eulerian-Lagrangian stochastic model. *Agricultural and Forest Meteorology*, *194*, 118–131. https://doi.org/10.1016/j.agrformet.2014.03.020

Gosselin, F. P. (2019). Mechanics of a plant in fluid flow. *Journal of Experimental Botany*, *70*(14), 3533–3548. https://doi.org/10.1093/jxb/erz288

Gosselin, F. P., & de Langre, E. (2009). Destabilising effects of plant flexibility in air and aquatic vegetation canopy flows. *European Journal of Mechanics-B/Fluids*, *28*(2), 271–282. https://doi.org/10.1016/j.euromechflu.2008.06.003

Gosselin, F. P., de Langre, E., & MacHado-Almeida, B. A. (2010). Drag reduction of flexible plates by reconfiguration. *Journal of Fluid Mechanics*, *650*, 319–341. https://doi.org/10.1017/S0022112009993673

Gromke, C. (2018). Wind tunnel model of the forest and its Reynolds number sensitivity. *Journal of Wind Engineering and Industrial Aerodynamics*, *175*, 53–64. https://doi.org/10.1016/j.jweia.2018.01.036

Grylls, T., Suter, I., & van Reeuwijk, M. (2020). Steady-state large-eddy simulations of convective and stable urban boundary layers. *Boundary-Layer Meteorology*, *175*, 309–341. https://doi.org/10.1007/s10546-020-00508-x

Guenther, A. B., Karl, T., Harley, P., Weidinmyer, C., Palmer, P. I., & Geron, C. (2006). Estimates of global terrestrial isoprene emissions using MEGAN (Model of Emissions of Gases and Aerosols from Nature). *Atmospheric Chemistry and Physics*, *6*(11), 3181–3210. https://doi.org/10.5194/acp-6-3181-2006

Haddad, N. M., Brudvig, L. A., Clobert, J., Davies, K. F., Gonzalez, A., Holt, R. D., et al. (2015). Habitat fragmentation and its lasting impact on Earth's ecosystems. *Science Advances*, *1*(2). https://doi.org/10.1126/sciadv.1500052

Hari Prasad, K. B. R. R., Venkata Srinivas, C., Venkateswara Naidu, C., Baskaran, R., & Venkatraman, B. (2016). Assessment of surface layer parameterizations in ARW using micro-meteorological observations from a tropical station. *Meteorological Applications*, *23*(2), 191–208. https://doi.org/10.1002/met.1545

Harman, I. N., Böhm, M., Finnigan, J. J., & Hughes, D. (2016). Spatial variability of the flow and turbulence within a model canopy. *Boundary-Layer Meteorology*, *160*(3), 375–396. https://doi.org/10.1007/s10546-016-0150-0

Hart, K. M., Curioni, G., Blaen, P., Harper, N. J., Miles, P., Lewin, K. F., et al. (2020). Characteristics of free air carbon dioxide enrichment of a northern temperate mature forest. *Global Change Biology*, *26*(2), 1023–1037. https://doi.org/10.1111/gcb.14786

Hazeldine, A., & Kirkpatrick, J. B. (2015). Practical and theoretical implications of a browsing cascade in Tasmanian forest and woodland. *Australian Journal of Botany*, *63*(5), 435–443. https://doi.org/10.1071/BT14334

Heinesch, B., Yernaux, M., & Aubinet, M. (2007). Some methodological questions concerning advection measurements: A case study. *Boundary-Layer Meteorology*, *122*(2), 457–478. https://doi.org/10.1007/s10546-006-9102-4

Hicks, B. B., & Baldocchi, D. D. (2020). Measurement of fluxes over land: Capabilities, origins, and remaining challenges. *Boundary-Layer Meteorology*, *177*(2–3), 365–394. https://doi.org/10.1007/s10546-020-00531-y

Hinds, W. C. (1999). *Aerosol technology: Properties, behavior, and measurement of airborne particles* (2nd ed.). John Wiley & Sons.

Hirons, A. D., & Thomas, P. A. (2018). *Applied tree biology*. Wiley Blackwell.

Holland, J. Z. (1989). On pressure-driven wind in deep forests. *Journal of Applied Meteorology*, *28*(12), 1349–1355. https://doi.org/10.1175/1520-0450(1989)028<1349:OPDWID>2.0.CO;2

Holmes, N. S., & Morawska, L. (2006). A review of dispersion modelling and its application to the dispersion of particles: An overview of different dispersion models available. *Atmospheric Environment*, *40*(30), 5902–5928. https://doi.org/10.1016/j.atmosenv.2006.06.003

Howes, F. A., & Whitaker, S. (1985). The spatial averaging theorem revisited. *Chemical Engineering Science*, *40*(8), 1387–1392. https://doi.org/10.1016/0009-2509(85)80078-6

Inagaki, A., Letzel, M. O., Raasch, S., & Kanda, M. (2006). The impact of the surface heterogeneity on the energy imbalance problem using LES. *Journal of the Meteorological Society of Japan*, *84*(1), 187–198. https://doi.org/10.2208/prohe.49.343

Inoue, E. (1955). Studies of phenomena of waving plants ("Honami") caused by wind. Part 1. Mechanism and characteristics of waving plants phenomena. *Journal of Agricultural Meteorology*, *11*, 18–22. (in Japanese). https://doi.org/10.2480/agrmet.11.18

Inoue, E. (1963). On the turbulent structure of airflow within crop canopies. *Journal of the Meteorological Society of Japan. Ser. II*, *41*(6), 317–326. https://doi.org/10.2151/jmsj1923.41.6_317

Jacobson, M. Z. (2005). *Fundamentals of atmospheric modeling* (2nd ed.). Cambridge University Press. https://doi.org/10.1017/CBO9781139165389

Janhäll, S. (2015). Review on urban vegetation and particle air pollution – Deposition and dispersion. *Atmospheric Environment*, *105*, 130–137. https://doi.org/10.1016/j.atmosenv.2015.01.052

Jiménez-Rodríguez, C. D., Coenders-Gerrits, M., Schilperoort, B., González-Angarita, A. D. P., & Savenije, H. (2021). Vapor plumes in a tropical wet forest: Spotting the invisible evaporation. *Hydrology and Earth System Sciences*, *25*(2), 619–635. https://doi.org/10.5194/hess-25-619-2021

Juang, J. Y., Katul, G. G., Siqueira, M. B., Stoy, P. C., & McCarthy, H. R. (2008). Investigating a hierarchy of Eulerian closure models for scalar transfer inside forested canopies. *Boundary-Layer Meteorology*, *128*(1), 1–32. https://doi.org/10.1007/s10546-008-9273-2

Kaimal, J. C., & Finnigan, J. J. (1994). *Atmospheric boundary layer flows: Their structure and measurement*. Oxford University Press. https://doi.org/10.16085/j.issn.1000-6613.2012.02.016

Kanani-Sühring, F., & Raasch, S. (2015). Spatial variability of scalar concentrations and fluxes downstream of a clearing-to-forest transition: A large-eddy simulation study. *Boundary-Layer Meteorology*, *155*, 1–27. https://doi.org/10.1007/s10546-014-9986-3

Kanani-Sühring, F., & Raasch, S. (2017). Enhanced scalar concentrations and fluxes in the lee of forest patches: A large-eddy simulation study. *Boundary-Layer Meteorology*, *164*(1), 1–17. https://doi.org/10.1007/s10546-017-0239-0

Kang, Y. (2015). Detection, classification and analysis of events in turbulence time series. *Bulletin of the Australian Mathematical Society*, *91*(3), 521–522. https://doi.org/10.1017/S0004972715000106

Kang, Y., Belušić, D., & Smith-Miles, K. (2015). Classes of structures in the stable atmospheric boundary layer. *Quarterly Journal of the Royal Meteorological Society*, *141*(691), 2057–2069. https://doi.org/10.1002/qj.2501

Katul, G. G., & Albertson, J. D. (1998). An investigation of higher-order closure models for a forested canopy. *Boundary-Layer Meteorology*, *89*(1), 47–74. https://doi.org/10.1023/A:1001509106381

Katul, G. G., Cava, D., Siqueira, M., & Poggi, D. (2013). Scalar turbulence within the canopy sublayer. In J. G. Venditti, J. L. Best, M. Church, & R. J. Hardy (Eds.), *Coherent flow structures at Earth's surface* (pp. 73–95). https://doi.org/10.1002/9781118527221.ch6

Katul, G. G., Finnigan, J. J., Poggi, D., Leuning, R., & Belcher, S. E. (2006). The influence of hilly terrain on canopy-atmosphere carbon dioxide exchange. *Boundary-Layer Meteorology*, *118*(1), 189–216. https://doi.org/10.1007/s10546-005-6436-2

Katul, G. G., Geron, C. D., Hsieh, C. I., Vidakovic, B., & Guenther, A. B. (1998). Active turbulence and scalar transport near the forest-atmosphere interface. *Journal of Applied Meteorology*, *37*(12), 1533–1546. https://doi.org/10.1175/1520-0450(1998)037<1533:ATASTN>2.0.CO;2

Katul, G. G., Grönholm, T., Launiainen, S., & Vesala, T. (2011). The effects of the canopy medium on dry deposition velocities of aerosol particles in the canopy sub-layer above forested ecosystems. *Atmospheric Environment*, *45*(5), 1203–1212. https://doi.org/10.1016/j.atmosenv.2010.06.032

Katul, G. G., Hsieh, C. I., Bowling, D., Clark, K., Shurpali, N., Turnipseed, A., et al. (1999). Spatial variability of turbulent fluxes in the roughness sublayer of an even-aged pine forest. *Boundary-Layer Meteorology*, *93*(1), 1–28. https://doi.org/10.1023/A:1002079602069

Katul, G. G., Mahrt, L., Poggi, D., & Sanz, C. (2004). One- and two-equation models for canopy turbulence. *Boundary-Layer Meteorology*, *113*(1), 81–109. https://doi.org/10.1023/B:BOUN.0000037333.48760.e5

Katul, G. G., Oren, R., Manzoni, S., Higgins, C., & Parlange, M. B. (2012). Evapotranspiration: A process driving mass transport and energy exchange in the soil-plant-atmosphere-climate system. *Reviews of Geophysics*, *50*(3). https://doi.org/10.1029/2011RG000366

Khan, B., Banzhaf, S., Chan, E., Forkel, R., Kanani-Sühring, F., Ketelsen, K., et al. (2020). Development of an atmospheric chemistry model coupled to the PALM model system 6.0: Implementation and first applications. *Geoscientific Model Development Discussions*, 1–34. https://doi.org/10.5194/gmd-2020-286

Kim, S., Park, H., Gruszewski, H. A., Schmale, D. G., & Jung, S. (2019). Vortex-induced dispersal of a plant pathogen by raindrop impact. *Proceedings of the National Academy of Sciences of the United States of America*, *116*(11), 4917–4922. https://doi.org/10.1073/pnas.1820318116

Kirkil, G., Mirocha, J. D., Bou-Zeid, E., Chow, F. K., & Kosović, B. (2012). Implementation and evaluation of dynamic subfilter-scale stress models for large-eddy simulation using WRF. *Monthly Weather Review*, *140*(1), 266–284. https://doi.org/10.1175/MWR-D-11-00037.1

Klaassen, W., Van Breugel, P. B., Moors, E. J., & Nieveen, J. P. (2002). Increased heat fluxes near a forest edge. *Theoretical and Applied Climatology*, *72*(3–4), 231–243. https://doi.org/10.1007/s00704-002-0682-8

Koizumi, A., Motoyama, J.-I., Sawata, K., Sasaki, Y., & Hirai, T. (2010). Evaluation of drag coefficients of poplar-tree crowns by a field test method. *Journal of Wood Science*, *56*(3), 189–193. https://doi.org/10.1007/s10086-009-1091-8

Krol, M. C., Molemaker, M. J., & Vilà-Guerau de Arellano, J. (2000). Effects of turbulence and heterogeneous emissions on photochemically active species in the convective boundary layer. *Journal of Geophysical Research*, *105*(D5), 6871–6884. https://doi.org/10.1029/1999jd900958

Kruijt, B., Malhi, Y., Lloyd, J., Nobre, A. D., Miranda, A. C., Pereira, M. G. P., et al. (2000). Turbulence statistics above and within two Amazon rain forest canopies. *Boundary-Layer Meteorology*, *94*(2), 297–331. https://doi.org/10.1023/A:1002401829007

Kulmala, M., Dal Maso, M., Mäkelä, J. M., Pirjola, L., Väkevä, M., Aalto, P., et al. (2001). On the formation, growth and composition of nucleation mode particles. *Tellus, Series B: Chemical and Physical Meteorology*, *53*(4), 479–490. https://doi.org/10.3402/tellusb.v53i4.16622

Kulmala, M., Riipinen, I., Sipilä, M., Manninen, H. E., Petäjä, T., Junninen, H., et al. (2007). Toward direct measurement of atmospheric nucleation. *Science*, *318*(5847), 89–92. https://doi.org/10.1126/science.1144124

Kwak, K. H., & Baik, J. J. (2014). Diurnal variation of NOx and ozone exchange between a street canyon and the overlying air. *Atmospheric Environment*, *86*, 120–128. https://doi.org/10.1016/j.atmosenv.2013.12.029

Kwak, K. H., Baik, J. J., Ryu, Y. H., & Lee, S. H. (2015). Urban air quality simulation in a high-rise building area using a CFD model coupled with mesoscale meteorological and chemistry-transport models. *Atmospheric Environment*, *100*, 167–177. https://doi.org/10.1016/j.atmosenv.2014.10.059

Lalic, B., & Mihailovic, D. T. (2004). An empirical relation describing leaf-area density inside the forest for environmental modeling. *Journal of Applied Meteorology*, *43*(4), 641–645. https://doi.org/10.1175/1520-0450(2004)043<0641:aerdld>2.0.co;2

Laothawornkitkul, J., Taylor, J. E., Paul, N. D., & Hewitt, C. N. (2009). Biogenic volatile organic compounds in the Earth system: Tansley review. *New Phytologist*, *183*(1), 27–51. https://doi.org/10.1111/j.1469-8137.2009.02859.x

Lee, X., & Black, T. A. (1993). Atmospheric turbulence within and above a Douglas-fir stand. Part I: Statistical properties of the velocity field. *Boundary-Layer Meteorology*, *64*(1–2), 149–174. https://doi.org/10.1007/BF00705666

Lefsky, M. A., Cohen, W. B., Acker, S. A., Parker, G. G., Spies, T. A., & Harding, D. (1999). Lidar remote sensing of the canopy structure and biophysical properties of Douglas-fir western hemlock forests. *Remote Sensing of Environment*, *70*(3), 339–361. https://doi.org/10.1016/S0034-4257(99)00052-8

Legg, B. J., Raupach, M. R., & Coppin, P. A. (1986). Experiments on scalar dispersion within a model plant canopy, Part III: An elevated line source. *Boundary-Layer Meteorology*, *35*(3), 277–302. https://doi.org/10.1007/BF00123645

Lelieveld, J., Butler, T. M., Crowley, J. N., Dillon, T. J., Fischer, H., Ganzeveld, L., et al. (2008). Atmospheric oxidation capacity sustained by a tropical forest. *Nature*, *452*(7188), 737–740. https://doi.org/10.1038/nature06870

Lemone, M. A., Angevine, W. M., Bretherton, C. S., Chen, F., Dudhia, J., Fedorovich, E., et al. (2019). 100 Years of progress in boundary layer meteorology. *Meteorological Monographs*, *59*(1), 9.1–9.85. https://doi.org/10.1175/AMSMONOGRAPHS-D-18-0013.1

Leuning, R., Zegelin, S. J., Jones, K., Keith, H., & Hughes, D. (2008). Measurement of horizontal and vertical advection of CO_2 within a forest canopy. *Agricultural and Forest Meteorology*, *148*(11), 1777–1797. https://doi.org/10.1016/j.agrformet.2008.06.006

Li, Q., & Bou-Zeid, E. (2019). Contrasts between momentum and scalar transport over very rough surfaces. *Journal of Fluid Mechanics*, *880*, 32–58. https://doi.org/10.1017/jfm.2019.687

Liao, J., Wang, T., Wang, X., Xie, M., Jiang, Z., Huang, X., & Zhu, J. (2014). Impacts of different urban canopy schemes in WRF/Chem on regional climate and air quality in Yangtze River Delta, China. *Atmospheric Research*, *145–146*, 226–243. https://doi.org/10.1016/j.atmosres.2014.04.005

Lin, M., Katul, G. G., & Khlystov, A. (2012). A branch scale analytical model for predicting the vegetation collection efficiency of ultrafine particles. *Atmospheric Environment*, *51*, 293–302. https://doi.org/10.1016/j.atmosenv.2012.01.004

Lin, X., Chamecki, M., Katul, G. G., & Yu, X. (2018). Effects of leaf area index and density on ultrafine particle deposition onto forest canopies: A LES study. *Atmospheric Environment*, *189*, 153–163. https://doi.org/10.1016/j.atmosenv.2018.06.048

Litschike, T., & Kuttler, W. (2008). On the reduction of urban particle concentration by vegetation - A review. *Meteorologische Zeitschrift*, *17*(3), 229–240. https://doi.org/10.1127/0941-2948/2008/0284

Lo, K. W., & Ngan, K. (2015). Characterising the pollutant ventilation characteristics of street canyons using the tracer age and age spectrum. *Atmospheric Environment*, *122*, 611–621. https://doi.org/10.1016/j.atmosenv.2015.10.023

Lo, K. W., & Ngan, K. (2017). Characterizing ventilation and exposure in street canyons using Lagrangian particles. *Journal of Applied Meteorology and Climatology*, *56*(5), 1177–1194. https://doi.org/10.1175/JAMC-D-16-0168.1

Ma, Y., & Liu, H. (2019). An advanced multiple-layer canopy model in the WRF model with large-eddy simulations to simulate canopy flows and scalar transport under different stability conditions. *Journal of Advances in Modeling Earth Systems*, *11*, 2330–2351. https://doi.org/10.1029/2018MS001347

Ma, Y., Liu, H., Liu, Z., Yi, C., & Lamb, B. K. (2020). Influence of forest-edge flows on scalar transport with different vertical distributions of foliage and scalar sources. *Boundary-Layer Meteorology*, *174*(1), 99–117. https://doi.org/10.1007/s10546-019-00475-y

Magnago, L. F. S., Rocha, M. F., Meyer, L., Martins, S. V., & Meira-Neto, J. A. A. (2015). Microclimatic conditions at forest edges have significant impacts on vegetation structure in large Atlantic forest fragments. *Biodiversity and Conservation*, *24*(9), 2305–2318. https://doi.org/10.1007/s10531-015-0961-1

Mahrt, L. (1982). Momentum balance of gravity flows. *Journal of the Atmospheric Sciences*, *39*(12), 2701–2711. https://doi.org/10.1175/1520-0469(1982)039<2701:MBOGF>2.0.CO;2

Mahrt, L. (2000). Surface heterogeneity and vertical structure of the boundary layer. *Boundary-Layer Meteorology*, *96*(1–2), 33–62. https://doi.org/10.1023/A:1002482332477

Mahrt, L. (2014). Stably stratified atmospheric boundary layers. *Annual Review of Fluid Mechanics*, *46*, 23–45. https://doi.org/10.1146/annurev-fluid-010313-141354

Maitani, T. (1979). An observational study of wind-induced waving of plants. *Boundary-Layer Meteorology*, *16*(3), 49–65. https://doi.org/10.1007/BF03335354

Makar, P. A., Staebler, R. M., Akingunola, A., Zhang, J., McLinden, C., Kharol, S. K., et al. (2017). The effects of forest canopy shading and turbulence on boundary layer ozone. *Nature Communications*, *8*, 1–14. https://doi.org/10.1038/ncomms15243

Margairaz, F., Pardyjak, E. R., & Calaf, M. (2020). Surface thermal heterogeneities and the atmospheric boundary layer: The relevance of dispersive fluxes. *Boundary-Layer Meteorology*, *175*(3), 369–395. https://doi.org/10.1007/s10546-020-00509-w

Martilli, A., Clappier, A., & Rotach, M. W. (2002). An urban surface exchange parameterisation for mesoscale models. *Boundary-Layer Meteorology*, *104*(2), 261–304. https://doi.org/10.1023/A:1016099921195

Mason, P. J., & Thomson, D. J. (1987). Large-eddy simulations of the neutral-static-stability planetary boundary layer. *Quarterly Journal of the Royal Meteorological Society*, *113*(476), 413–443. https://doi.org/10.1002/qj.49711347602

Mason, P. J., & Thomson, D. J. (1992). Stochastic backscatter in large-eddy simulations of boundary layers. *Journal of Fluid Mechanics*, *242*(28), 51–78. https://doi.org/10.1017/S0022112092002271

Massman, W. J., & Lee, X. (2002). Eddy covariance flux corrections and uncertainties in long-term studies of carbon and energy exchanges. *Agricultural and Forest Meteorology*, *113*, 121–144. https://doi.org/10.1016/s0168-1923(02)00105-3

Maurer, K. D., Bohrer, G., Kenny, W. T., & Ivanov, V. Y. (2015). Large-eddy simulations of surface roughness parameter sensitivity to canopy-structure characteristics. *Biogeosciences*, *12*(8), 2533–2548. https://doi.org/10.5194/bg-12-2533-2015

Mavroidis, I., Andronopoulos, S., & Bartzis, J. G. (2012). Computational simulation of the residence of air pollutants in the wake of a 3-dimensional cubical building. The effect of atmospheric stability. *Atmospheric Environment*, *63*, 189–202. https://doi.org/10.1016/j.atmosenv.2012.09.032

McHugh, I. D., Beringer, J., Cunningham, S. C., Baker, P. J., Cavagnaro, T. R., MacNally, R., & Thompson, R. M. (2017). Interactions between nocturnal turbulent flux, storage and advection at an "ideal" eucalypt woodland site. *Biogeosciences*, *14*(12), 3027–3050. https://doi.org/10.5194/bg-14-3027-2017

McNaughton, K. G. (1989). Micrometeorology of shelter belts and forest edges. *Philosophical Transactions of the Royal Society of London - B*, *324*(1223), 351–368. https://doi.org/10.1098/rstb.1989.0052

Moeng, C. H., Dudhia, J., Klemp, J., & Sullivan, P. P. (2007). Examining two-way grid nesting for large eddy simulation of the PBL using the WRF model, *135*, 2295, 2311. https://doi.org/10.1175/MWR3406.1

Moltchanov, S., Bohbot-Raviv, Y., Duman, T., & Shavit, U. (2015). Canopy edge flow: A momentum balance analysis. *Water Resources Research*, *51*(4), 2081–2095. https://doi.org/10.1002/2014WR015397

Moltchanov, S., Bohbot-Raviv, Y., & Shavit, U. (2011). Dispersive stresses at the canopy upstream edge. *Boundary-Layer Meteorology*, *139*(2), 333–351. https://doi.org/10.1007/s10546-010-9582-0

Momo Takoudjou, S., Ploton, P., Sonké, B., Hackenberg, J., Griffon, S., de Coligny, F., et al. (2018). Using terrestrial laser scanning data to estimate large tropical trees biomass and calibrate allometric models: A comparison with traditional destructive approach. *Methods in Ecology and Evolution*, *9*(4), 905–916. https://doi.org/10.1111/2041-210X.12933

Monin, A. S., & Obukhov, A. M. (1954). Osnovnye zakonomernosti turbulentnogo peremeshivanija v prizemnom sloe atmosfery (Basic laws of turbulent mixing in the atmosphere near the ground). *Akademii Nauk SSSR Geofizicheskii Institut Trudy*, *24*(151), 163–187.

Monteith, J. L., & Unsworth, M. H. (2008). *Principles of environmental physics* (4th ed.). Academic Press. Retrieved from http://elsevier.com/locate/permissions

Morse, A. P., Gardiner, B. A., & Marshall, B. J. (2002). Mechanics controlling turbulence development across a forest edge. *Boundary-Layer Meteorology*, *103*(103), 227–251. https://doi.org/10.1023/a:1014507727784

Moser, R. D., Haering, S. W., & Yalla, G. R. (2021). Statistical properties of subgrid-scale turbulence models. *Annual Review of Fluid Mechanics*, *53*(1), 255–286. https://doi.org/10.1146/annurev-fluid-060420-023735

Mueller, E., Mell, W., & Simeoni, A. (2014). Large eddy simulation of forest canopy flow for wildland fire modeling. *Canadian Journal of Forest Research*, *44*(12), 1534–1544. https://doi.org/10.1139/cjfr-2014-0184

Murena, F. (2012). Monitoring and modelling carbon monoxide concentrations in a deep street canyon: Application of a two-box model. *Atmospheric Pollution Research*, *3*(3), 311–316. https://doi.org/10.5094/APR.2012.034

Nebenführ, B., & Davidson, L. (2015). Large-eddy simulation study of thermally stratified canopy flow. *Boundary-Layer Meteorology*, *156*(2), 253–276. https://doi.org/10.1007/s10546-015-0025-9

Neumann, H. H., Den Hartog, G., & Shaw, R. H. (1989). Leaf area measurements based on hemispheric photographs and leaf-litter collection in a deciduous forest during autumn leaf-fall. *Agricultural and Forest Meteorology*, *45*(3–4), 325–345. https://doi.org/10.1016/0168-1923(89)90052-X

Niinemets, Ü. (2010). Mild versus severe stress and BVOCs: Thresholds, priming and consequences. *Trends in Plant Science*, *15*(3), 145–153. https://doi.org/10.1016/j.tplants.2009.11.008

Norby, R. J., Wullschleger, S. D., Hanson, P. J., Gunderson, C. A., Tschaplinski, T. J., & Jastrow, J. D. (2006). CO_2 enrichment of a deciduous forest: The Oak Ridge FACE experiment. In J. Nösberger, S. P. Long, R. J. Norby, M. Stitt, G. R. Hendrey, & H. Blum (Eds.), *Managed ecosystems and CO_2. Ecological studies (analysis and synthesis)* (Vol. 187, pp. 231–251). Springer. https://doi.org/10.1007/3-540-31237-4_13

Norros, V., Rannik, Ü., Hussein, T., Petäjä, T., Vesala, T., & Ovaskainen, O. (2014). Do small spores disperse further than large spores? *Ecology*, *95*(6), 1612–1621. https://doi.org/10.1890/13-0877.1

Nottrott, A., Kleissl, J., & Keeling, R. (2014). Modeling passive scalar dispersion in the atmospheric boundary layer with WRF large-eddy simulation. *Atmospheric Environment*, *82*, 172–182. https://doi.org/10.1016/j.atmosenv.2013.10.026

Oke, T. R. (1988). The urban energy balance. *Progress in Physical Geography*, *12*(4), 471–508. https://doi.org/10.1177/030913338801200401

Oliphant, A. J. (2012). Terrestrial ecosystem-atmosphere exchange of CO_2, water and energy from FLUXNET; review and meta-analysis of a global in-situ observatory. *Geography Compass*, *6*(12), 689–705. https://doi.org/10.1111/gec3.12009

O'Neill, J. J., Cai, X., & Kinnersley, R. (2015). A generalised stochastic backscatter model: Large-eddy simulation of the neutral surface layer. *Quarterly Journal of the Royal Meteorological Society*, *141*(692), 2617–2629. https://doi.org/10.1002/qj.2548

O'Neill, J. J., Cai, X., & Kinnersley, R. (2016). Stochastic backscatter modelling for the prediction of pollutant removal from an urban street canyon: A large-eddy simulation. *Atmospheric Environment*, *142*, 9–18. https://doi.org/10.1016/j.atmosenv.2016.07.024

Pace, R., & Grote, R. (2020). Deposition and resuspension mechanisms into and from tree canopies: A study modeling particle removal of conifers and broadleaves in different cities. *Frontiers in Forests and Global Change*, *3*, 1–12. https://doi.org/10.3389/ffgc.2020.00026

Palmer, H., Gardiner, B. A., Hislop, M., Sibbald, A., & Duncan, A. (1997). *Forestry Commission Technical Paper 21: Trees for shelter*. Retrieved from https://www.forestry.gov.uk/pdf/FCTP021.pdf/$file/FCTP021.pdf

Pan, Y., Chamecki, M., & Isard, S. A. (2014). Large-eddy simulation of turbulence and particle dispersion inside the canopy roughness sublayer. *Journal of Fluid Mechanics*, *753*, 499–534. https://doi.org/10.1017/jfm.2014.379

Pan, Y., Follett, E., Chamecki, M., & Nepf, H. M. (2014). Strong and weak, unsteady reconfiguration and its impact on turbulence structure within plant canopies. *Physics of Fluids*, *26*(10), 105102. https://doi.org/10.1063/1.4898395

Patton, E. G., & Finnigan, J. J. (2012). Canopy turbulence. In *Handbook of environmental fluid dynamics*. (Vol. 1, pp. 311–280). CRC Press. https://doi.org/10.1201/b14241-28

Patton, E. G., Horst, T. W., Sullivan, P. P., Lenschow, D. H., Oncley, S. P., Brown, W. O. J., et al. (2011). The canopy horizontal array turbulence study. *Bulletin of the American Meteorological Society*, *92*(5), 593–611. https://doi.org/10.1175/2010BAMS2614.1

Patton, E. G., & Katul, G. G. (2009). Turbulent pressure and velocity perturbations induced by gentle hills covered with sparse and dense canopies. *Boundary-Layer Meteorology*, *133*(2), 189–217. https://doi.org/10.1007/s10546-009-9427-x

Patton, E. G., Sullivan, P. P., Shaw, R. H., Finnigan, J. J., & Weil, J. C. (2016). Atmospheric stability influences on coupled boundary layer and canopy turbulence. *Journal of the Atmospheric Sciences*, *73*(4), 1621–1647. https://doi.org/10.1175/JAS-D-15-0068.1

Paul-Limoges, E., Wolf, S., Eugster, W., Hörtnagl, L., & Buchmann, N. (2017). Below-canopy contributions to ecosystem CO_2 fluxes in a temperate mixed forest in Switzerland. *Agricultural and Forest Meteorology*, *247*, 582–596. https://doi.org/10.1016/j.agrformet.2017.08.011

Pearce, H., Levine, J. G., Cai, X., & Rob Mackenzie, A. (2021). Introducing the green infrastructure for roadside air quality (Gi4raq) platform: Estimating site-specific changes in the dispersion of vehicular pollution close to source. *Forests*, *12*(6), 769. https://doi.org/10.3390/f12060769

Peñuelas, J., & Staudt, M. (2010). BVOCs and global change. *Trends in Plant Science*, *15*(3), 133–144. https://doi.org/10.1016/j.tplants.2009.12.005

Petroff, A., Mailliat, A., Amielh, M., & Anselmet, F. (2008). Aerosol dry deposition on vegetative canopies. Part I: Review of present knowledge. *Atmospheric Environment*, *42*(16), 3625–3653. https://doi.org/10.1016/j.atmosenv.2007.09.043

Philips, D. A., Rossi, R., & Iaccarino, G. (2013). Large-eddy simulation of passive scalar dispersion in an urban-like canopy. *Journal of Fluid Mechanics*, *723*, 404–428. https://doi.org/10.1017/jfm.2013.135

Pierce, J. R., Leaitch, W. R., Liggio, J., Westervelt, D. M., Wainwright, C. D., Abbatt, J. P. D., et al. (2012). Nucleation and condensational growth to CCN sizes during a sustained pristine biogenic SOA event in a forested mountain valley. *Atmospheric Chemistry and Physics*, *12*(7), 3147–3163. https://doi.org/10.5194/acp-12-3147-2012

Piomelli, U., Cabot, W. H., Moin, P., & Lee, S. (1991). Subgrid-scale backscatter in turbulent and transitional flows. *Physics of Fluids A*, *3*(7), 1766–1771. https://doi.org/10.1063/1.857956

Pivato, D., Dupont, S., & Brunet, Y. (2014). A simple tree swaying model for forest motion in windstorm conditions. *Trees - Structure and Function*, *28*(1), 281–293. https://doi.org/10.1007/s00468-013-0948-z

Poggi, D., & Katul, G. G. (2008a). Micro- and macro-dispersive fluxes in canopy flows. *Acta Geophysica*, *56*(3), 778–799. https://doi.org/10.2478/s11600-008-0029-7

Poggi, D., & Katul, G. G. (2008b). The effect of canopy roughness density on the constitutive components of the dispersive stresses. *Experiments in Fluids*, *45*(1), 111–121. https://doi.org/10.1007/s00348-008-0467-7

Poggi, D., Katul, G. G., & Albertson, J. D. (2004). A note on the contribution of dispersive fluxes to momentum transfer within canopies. *Boundary-Layer Meteorology*, *111*(3), 615–621. https://doi.org/10.1023/B:BOUN.0000016563.76874.47

Poggi, D., Katul, G. G., & Albertson, J. D. (2006). Scalar dispersion within a model canopy: Measurements and three-dimensional Lagrangian models. *Advances in Water Resources*, *29*(2), 326–335. https://doi.org/10.1016/j.advwatres.2004.12.017

Poggi, D., Katul, G. G., Finnigan, J. J., & Belcher, S. E. (2008). Analytical models for the mean flow inside dense canopies on gentle hilly terrain. *Quarterly Journal of the Royal Meteorological Society*, *134*(634), 1095–1112. https://doi.org/10.1002/qj.276

Poggi, D., Porporato, A., Ridolfi, L., Albertson, J. D., & Katul, G. G. (2004). The effect of vegetation density on canopy sub-layer turbulence. *Boundary-Layer Meteorology*, *111*(3), 565–587. https://doi.org/10.1023/B:BOUN.0000016576.05621.73

Pryor, S. C., Barthelmie, R. J., Sørensen, L. L., Larsen, S. E., Sempreviva, A. M., Grönholm, T., et al. (2008). Upward fluxes of particles over forests: When, where, why? *Tellus, Series B: Chemical and Physical Meteorology*, *60*(3), 372–380. https://doi.org/10.1111/j.1600-0889.2008.00341.x

Pugh, T. A. M., Mackenzie, A. R., Langford, B., Nemitz, E., Misztal, P. K., & Hewitt, C. N. (2011). The influence of small-scale variations in isoprene concentrations on atmospheric chemistry over a tropical rainforest. *Atmospheric Chemistry and Physics*, *11*(9), 4121–4134. https://doi.org/10.5194/acp-11-4121-2011

Py, C., De Langre, E., & Moulia, B. (2006). A frequency lock-in mechanism in the interaction between wind and crop canopies. *Journal of Fluid Mechanics*, *568*, 425–449. https://doi.org/10.1017/S0022112006002667

Queck, R., Bernhofer, C., Bienert, A., & Schlegel, F. (2016). The TurbEFA field experiment—Measuring the influence of a forest clearing on the turbulent wind field. *Boundary-Layer Meteorology*, *160*(3), 397–423. https://doi.org/10.1007/s10546-016-0151-z

Queck, R., Bienert, A., Maas, H. G., Harmansa, S., Goldberg, V., & Bernhofer, C. (2012). Wind fields in heterogeneous conifer canopies: Parameterisation of momentum absorption using high-resolution 3D vegetation scans. *European Journal of Forest Research*, *131*(1), 165–176. https://doi.org/10.1007/s10342-011-0550-0

Raine, J. K., & Stevenson, D. C. (1977). Wind protection by model fences in a simulated atmospheric boundary layer. *Journal of Industrial Aerodynamics*, *2*, 159–180. https://doi.org/10.1016/0167-6105(77)90015-0

Ramos, F. M., Bolzan, M. J. A., Sá, L. D. A., & Rosa, R. R. (2004). Atmospheric turbulence within and above an Amazon forest. *Physica D: Nonlinear Phenomena*, *193*(1–4), 278–291. https://doi.org/10.1016/j.physd.2004.01.026

Rap, A., Scott, C. E., Reddington, C. L., Mercado, L., Ellis, R. J., Garraway, S., et al. (2018). Enhanced global primary production by biogenic aerosol via diffuse radiation fertilization. *Nature Geoscience*, *11*(9), 640–644. https://doi.org/10.1038/s41561-018-0208-3

Raumonen, P., Casella, E., Calders, K., Murphy, S., Åkerblom, M., & Kaasalainen, M. (2015). Massive-scale tree modelling from TLS data. *ISPRS Annals of the Photogrammetry, Remote Sensing and Spatial Information Sciences*, *2*(3W4), 189–196. https://doi.org/10.5194/isprsannals-II-3-W4-189-2015

Raupach, M. R., Antonia, R. A., & Rajagopalan, S. (1991). Rough-wall turbulent boundary layers. *Applied Mechanics Reviews*, *44*(1). https://doi.org/10.1115/1.3119492

Raupach, M. R., Bradley, E. F., & Ghadiri, H. (1987). *A wind tunnel investigation into the aerodynamic effect of forest clearings on the nesting of Abbott's Booby on Christmas Island* (Vol. 2). CSIRO Division of Environmental Mechanics. https://doi.org/10.4225/08/587521fe26b7f

Raupach, M. R., Coppin, P. A., & Legg, B. J. (1986). Experiments on scalar dispersion within a model plant canopy part I: The turbulence structure. *Boundary-Layer Meteorology*, *35*(1–2), 21–52. https://doi.org/10.1007/BF00117300

Raupach, M. R., Finnigan, J. J., & Brunet, Y. (1996). Coherent eddies and turbulence in vegetation canopies: The mixing-layer analogy. *Boundary-Layer Meteorology 25th Anniversary Volume, 1970–1995*, 351–382. https://doi.org/10.1007/978-94-017-0944-6_15

Raupach, M. R., & Shaw, R. H. (1982). Averaging procedures for flow within vegetation canopies. *Boundary-Layer Meteorology*, *22*(1), 79–90. https://doi.org/10.1007/BF00128057

Raupach, M. R., & Thom, A. S. (1981). Turbulence in and above plant canopies. *Annual Review of Fluid Mechanics*, *13*(1), 97–129. https://doi.org/10.1146/annurev.fl.13.010181.000525

Reynolds, A. M. (2012). Incorporating sweeps and ejections into Lagrangian stochastic models of spore trajectories within plant canopy turbulence: Modeled contact distributions are heavy-tailed. *Phytopathology*, *102*(11), 1026–1033. https://doi.org/10.1094/PHYTO-01-12-0002

Riutta, T., Slade, E. M., Morecroft, M. D., Bebber, D. P., & Malhi, Y. (2014). Living on the edge: Quantifying the structure of a fragmented forest landscape in England. *Landscape Ecology*, *29*(6), 949–961. https://doi.org/10.1007/s10980-014-0025-z

Rominger, J. T., & Nepf, H. M. (2011). Flow adjustment and interior flow associated with a rectangular porous obstruction. *Journal of Fluid Mechanics*, *680*, 636–659. https://doi.org/10.1017/jfm.2011.199

Ross, A. N. (2008). Large-eddy simulations of flow over forested ridges. *Boundary-Layer Meteorology*, *128*(1), 59–76. https://doi.org/10.1007/s10546-008-9278-x

Ross, A. N., & Harman, I. N. (2015). The impact of source distribution on scalar transport over forested hills. *Boundary-Layer Meteorology*, *156*(2), 211–230. https://doi.org/10.1007/s10546-015-0029-5

Ross, A. N., & Vosper, S. B. (2005). Neutral turbulent flow over forested hills. *Quarterly Journal of the Royal Meteorological Society*, *131*(609), 1841–1862. https://doi.org/10.1256/qj.04.129

Rozema, W., Bae, H. J., Moin, P., & Verstappen, R. (2015). Minimum-dissipation models for large-eddy simulation. *Physics of Fluids*, *27*(8), 085107. https://doi.org/10.1063/1.4928700

Rudnicki, M., Mitchell, S. J., & Novak, M. D. (2004). Wind tunnel measurements of crown streamlining for drag relationships for three conifer species. *Canadian Journal of Forest Research*, *34*(3), 666–676. https://doi.org/10.1139/x03-233

Russell, E. S., Liu, H., Gao, Z., Lamb, B., & Wagenbrenner, N. (2016). Turbulence dependence on winds and stability in a weak-wind canopy sublayer over complex terrain. *Journal of Geophysical Research*, *121*(19), 11502–11511. https://doi.org/10.1002/2016JD025057

Ruth, R. H., & Yoder, R. A. (1953). *Reducing wind damage in the forests of the Oregon Coast Range*. U.S. Deparment of Agriculture: Forest Service. https://doi.org/10.5962/bhl.title.81527

Sabatini, F. M., Burrascano, S., Keeton, W. S., Levers, C., Lindner, M., Pötzschner, F., et al. (2018). Where are Europe's last primary forests? *Diversity and Distributions*, *24*(10), 1426–1439. https://doi.org/10.1111/ddi.12778

Salamanca, F., Krpo, A., Martilli, A., & Clappier, A. (2010). A new building energy model coupled with an urban canopy parameterization for urban climate simulations—Part I. Formulation, verification, and sensitivity analysis of the model. *Theoretical and Applied Climatology*, *99*(3–4), 331–344. https://doi.org/10.1007/s00704-009-0142-9

Schindler, D., Fugmann, H., Schönborn, J., & Mayer, H. (2012). Coherent response of a group of plantation-grown Scots pine trees to wind loading. *European Journal of Forest Research*, *131*(1), 191–202. https://doi.org/10.1007/s10342-010-0474-0

Schindler, D., Schönborn, J., Fugmann, H., & Mayer, H. (2013). Responses of an individual deciduous broadleaved tree to wind excitation. *Agricultural and Forest Meteorology*, *177*, 69–82. https://doi.org/10.1016/j.agrformet.2013.04.001

Schlegel, F., Stiller, J., Bienert, A., Maas, H. G., Queck, R., & Bernhofer, C. (2012). Large-eddy simulation of inhomogeneous canopy flows using high resolution terrestrial laser scanning data. *Boundary-Layer Meteorology*, *142*(2), 223–243. https://doi.org/10.1007/s10546-011-9678-1

Schlegel, F., Stiller, J., Bienert, A., Maas, H. G., Queck, R., & Bernhofer, C. (2015). Large-eddy simulation study of the effects on flow of a heterogeneous forest at sub-tree resolution. *Boundary-Layer Meteorology*, *154*(1), 27–56. https://doi.org/10.1007/s10546-014-9962-y

Schmid, M. F., Lawrence, G. A., Parlange, M. B., & Giometto, M. G. (2019). Volume averaging for urban canopies. *Boundary-Layer Meteorology*, *173*(3), 349–372. https://doi.org/10.1007/s10546-019-00470-3

Schneider, F. D., Kükenbrink, D., Schaepman, M. E., Schimel, D. S., & Morsdorf, F. (2019). Quantifying 3D structure and occlusion in dense tropical and temperate forests using close-range LiDAR. *Agricultural and Forest Meteorology*, *268*, 249–257. https://doi.org/10.1016/j.agrformet.2019.01.033

Scholes, R. J. (2017). Taking the mumbo out of the jumbo: Progress towards a robust basis for ecological scaling. *Ecosystems*, *20*(1), 4–13. https://doi.org/10.1007/s10021-016-0047-2

Schröttle, J., & Dörnbrack, A. (2013). Turbulence structure in a diabatically heated forest canopy composed of fractal Pythagoras trees. *Theoretical and Computational Fluid Dynamics*, *27*(3–4), 337–359. https://doi.org/10.1007/s00162-012-0284-8

Schuepp, P. H. (1993). Tansley Review No. 59 Leaf boundary layers. *New Phytologist*, *125*(3), 477–507. https://doi.org/10.1111/j.1469-8137.1993.tb03898.x

Schymanski, S. J., & Or, D. (2016). Wind increases leaf water use efficiency. *Plant, Cell and Environment*, *39*(7), 1448–1459. https://doi.org/10.1111/pce.12700

Seinfeld, J. H., & Pandis, S. N. (2016). *Atmospheric chemistry and physics: From air pollution to climate change* (3rd ed.). John Wiley & Sons.

Selino, A., & Jones, M. D. (2013). Large and small eddies matter: Animating trees in wind using coarse fluid simulation and synthetic turbulence. *Computer Graphics Forum*, *32*(1), 75–84. https://doi.org/10.1111/j.1467-8659.2012.03232.x

Shao, Y., Liu, S., Schween, J. H., & Crewell, S. (2013). Large-eddy atmosphere-land-surface modelling over heterogeneous surfaces: Model development and comparison with measurements. *Boundary-Layer Meteorology*, *148*(2), 333–356. https://doi.org/10.1007/s10546-013-9823-0

Sharkey, T. D., Singsaas, E. L., Vanderveer, P. J., & Geron, C. (1996). Field measurements of isoprene emission from trees in response to temperature and light. *Tree Physiology*, *16*(7), 649–654. https://doi.org/10.1093/treephys/16.7.649

Sharma, A., & García-Mayoral, R. (2020a). Scaling and dynamics of turbulence over sparse canopies. *Journal of Fluid Mechanics*, *888*. https://doi.org/10.1017/jfm.2019.999

Sharma, A., & García-Mayoral, R. (2020b). Turbulent flows over dense filament canopies. *Journal of Fluid Mechanics*, *888*. https://doi.org/10.1017/jfm.2020.27

Shaw, R. H. (1977). Secondary wind speed maxima inside plant canopies. *Journal of Applied Meteorology*, *16*, 514–521. https://doi.org/10.1175/1520-0450(1977)016<0514:swsmip>2.0.co;2

Shaw, R. H., & Patton, E. G. (2003). Canopy element influences on resolved- and subgrid-scale energy within a large-eddy simulation. *Agricultural and Forest Meteorology*, *115*, 5–17. https://doi.org/10.1016/S0168-1923(02)00165-X

Shaw, R. H., & Schumann, U. (1992). Large-eddy simulation of turbulent flow above and within a forest. *Boundary-Layer Meteorology*, *61*(1–2), 47–64. https://doi.org/10.1007/BF02033994

Shaw, R. H., Tavangar, J., & Ward, D. P. (1983). Structure of the Reynolds stress in the canopy layer. *Journal of Climate and Applied Meteorology*, *22*, 1922–1931. https://doi.org/10.1175/1520-0450(1983)022<1922:sotrsi>2.0.co;2

Shralman, B. I., & Siggia, E. D. (2000). Scalar turbulence. *Nature*, *405*(6787), 639–646. https://doi.org/10.1038/35015000

Shu, Y., & Atkinson, R. (1994). Rate constants for the gas-phase reactions of O_3 with a series of Terpenes and OH radical formation from the O_3 reactions with Sesquiterpenes at 296 ± 2 K. *International Journal of Chemical Kinetics*, *26*(12), 1193–1205. https://doi.org/10.1002/kin.550261207

Skamarock, W. C., Klemp, J. B., Dudhia, J. B., Gill, D. O., Barker, D. M., Duda, M. G., et al. (2008). *A description of the Advanced Research WRF Version 3, NCAR Technical Note TN-475+STR. Technical Report*. https://doi.org/10.5065/D68S4MVH

Smagorinsky, J. (1963). General circulation experiments with the primitive equations: 1. The basic experiment. *Monthly Weather Review*, *91*(3), 99–164. https://doi.org/10.1175/1520-0493(1963)091<0099:gcewtp>2.3.co;2

Sogachev, A., Leclerc, M. Y., Zhang, G., Rannik, Ü., & Vesala, T. (2008). CO_2 fluxes near a forest edge: A numerical study. *Ecological Applications*, *18*(6), 1454–1469. https://doi.org/10.1890/06-1119.1

Sogachev, A., & Panferov, O. (2006). Modification of two-equation models to account for plant drag. *Boundary-Layer Meteorology*, *121*(2), 229–266. https://doi.org/10.1007/s10546-006-9073-5

Speck, O. (2003). Field measurements of wind speed and reconfiguration in Arundo donax (Poaceae) with estimates of drag forces. *American Journal of Botany*, *90*(8), 1253–1256. https://doi.org/10.3732/ajb.90.8.1253

Spracklen, D. V., Carslaw, K. S., Kulmala, M., Kerminen, V. M., Mann, G. W., & Sihto, S. L. (2006). The contribution of boundary layer nucleation events to total particle concentrations on regional and global scales. *Atmospheric Chemistry and Physics*, *6*(12), 5631–5648. https://doi.org/10.5194/acp-6-5631-2006

Stępalska, D., & Wołek, J. (2009). Intradiurnal periodicity of fungal spore concentrations (Alternaria, Botrytis, Cladosporium, Didymella, Ganoderma) in Cracow, Poland. *Aerobiologia*, *25*(4), 333–340. https://doi.org/10.1007/s10453-009-9137-3

Stoy, P. C., Mauder, M., Foken, T., Marcolla, B., Boegh, E., Ibrom, A., et al. (2013). A data-driven analysis of energy balance closure across FLUXNET research sites: The role of landscape scale heterogeneity. *Agricultural and Forest Meteorology*, *171–172*, 137–152. https://doi.org/10.1016/j.agrformet.2012.11.004

Stull, R. B. (1988). *An introduction to boundary layer meteorology*. Kluwer Academic Publishers. https://doi.org/10.1007/978-94-009-3027-8

Stull, R. B. (1991). Static stability—An update. *Bulletin of the American Meteorological Society*, *72*(10), 1521–1529. https://doi.org/10.1175/1520-0477(1991)072<1521:ssu>2.0.co;2

Stull, R. B. (2006). The atmospheric boundary layer. In J. M. Wallace, & P. V Hobbs (Eds.), *Atmospheric science: An introductory survey* (2nd ed., Vol. 92, pp. 375–418). Elsevier.

Su, H. B., Schmid, H. P., Grimmond, C. S. B., Vogel, C. S., & Oliphant, A. J. (2004). Spectral characteristics and correction of long-term eddy-covariance measurements over two mixed hardwood forests in non-flat terrain. *Boundary-Layer Meteorology*, *110*, 213–253. https://doi.org/10.1023/a:1026099523505

Su, H. B., Schmid, H. P., Vogel, C. S., & Curtis, P. S. (2008). Effects of canopy morphology and thermal stability on mean flow and turbulence statistics observed inside a mixed hardwood forest. *Agricultural and Forest Meteorology*, *148*(6–7), 862–882. https://doi.org/10.1016/j.agrformet.2007.12.002

Su, H. B., Shaw, R. H., Pawu, K. T., Moeng, C. H., & Sullivan, P. P. (1998). Turbulent statistics of neutrally stratified flow within and above a sparse forest from large-eddy simulation and field observations. *Boundary-Layer Meteorology*, *88*(3), 363–397. https://doi.org/10.1023/A:1001108411184

Sullivan, P. P., & Patton, E. G. (2011). The effect of mesh resolution on convective boundary layer statistics and structures generated by large-eddy simulation. *Journal of the Atmospheric Sciences*, *68*(10), 2395–2415. https://doi.org/10.1175/JAS-D-10-05010.1

Sun, J., Mahrt, L., Banta, R. M., & Pichugina, Y. L. (2012). Turbulence regimes and turbulence intermittency in the stable boundary layer: During CASES-99. *Journal of the Atmospheric Sciences*, *69*(1), 338–351. https://doi.org/10.1175/JAS-D-11-082.1

Sun, J., Nappo, C. J., Mahrt, L., Belušic, D., Grisogono, B., Stauffer, D. R., et al. (2015). Review of wave-turbulence interactions in the stable atmospheric boundary layer. *Reviews of Geophysics*, *53*(3), 956–993. https://doi.org/10.1002/2015RG000487

Szendrei, Z., & Rodriguez-Saona, C. (2010). A meta-analysis of insect pest behavioral manipulation with plant volatiles. *Entomologia Experimentalis et Applicata*, *134*(3), 201–210. https://doi.org/10.1111/j.1570-7458.2009.00954.x

Tadrist, L., Saudreau, M., Hémon, P., Amandolese, X., Marquier, A., Leclercq, T., & de Langre, E. (2018). Foliage motion under wind, from leaf flutter to branch buffeting. *Journal of The Royal Society Interface*, *15*(142), 20180010. https://doi.org/10.1098/rsif.2018.0010

Taubert, F., Fischer, R., Groeneveld, J., Lehmann, S., Müller, M. S., Rödig, E., et al. (2018). Global patterns of tropical forest fragmentation. *Nature*, *554*(7693), 519–522. https://doi.org/10.1038/nature25508

Telewski, F. W. (2009). Wind-induced physiological and developmental responses in trees. In *Wind and trees* (pp. 237–263). Cambridge University Press. https://doi.org/10.1017/cbo9780511600425.015

Telewski, F. W., & Pruyn, M. L. (1998). Thigmomorphogenesis: A dose response to flexing in *Ulmus americana* seedlings. *Tree Physiology*, *18*(1), 65–68. https://doi.org/10.1093/treephys/18.1.65

Thom, A. S. (1971). Momentum absorption by vegetation. *Quarterly Journal of the Royal Meteorological Society*, *97*(414), 414–428. https://doi.org/10.1002/qj.49709741404

Tinya, F., Márialigeti, S., Király, I., Németh, B., & Ódor, P. (2009). The effect of light conditions on herbs, bryophytes and seedlings of temperate mixed forests in Őrség, Western Hungary. *Plant Ecology*, *204*(1), 69–81. https://doi.org/10.1007/s11258-008-9566-z

Tóta, J., Roy Fitzjarrald, D., & Da Silva Dias, M. A. F. (2012). Amazon rainforest exchange of carbon and subcanopy air flow: Manaus LBA site—A complex terrain condition. *The Scientific World Journal*, *2012*, 165067. https://doi.org/10.1100/2012/165067

U.S. Department of Agriculture. (1982). *Forest stand density guide. Technical Notes*. https://doi.org/10.1300/J184v06n02_06

Van Gardingen, P., & Grace, J. (1991). Plants and wind. *Advances in Botanical Research*, *18*, 189–253. https://doi.org/10.1016/S0065-2296(08)60023-3

Van Gorsel, E., Harman, I. N., Finnigan, J. J., & Leuning, R. (2011). Decoupling of air flow above and in plant canopies and gravity waves affect micrometeorological estimates of net scalar exchange. *Agricultural and Forest Meteorology*, *151*(7), 927–933. https://doi.org/10.1016/j.agrformet.2011.02.012

Villani, M. G., Schmid, H. P., Su, H. B., Hutton, J. L., & Vogel, C. S. (2003). Turbulence statistics measurements in a northern hardwood forest. *Boundary-Layer Meteorology*, *108*(3), 343–364. https://doi.org/10.1023/A:1024118808670

Visakorpi, K., Gripenberg, S., Malhi, Y., Bolas, C., Oliveras, I., Harris, N., et al. (2018). Small-scale indirect plant responses to insect herbivory could have major impacts on canopy photosynthesis and isoprene emission. *New Phytologist*, *220*(3), 799–810. https://doi.org/10.1111/nph.15338

Vogel, C. S. (1968). "Sun leaves" and "shade leaves": Differences in convective heat dissipation. *Ecology*, *49*(6), 1203–1204. https://doi.org/10.2307/1934517

Vogel, C. S. (1989). Drag and reconfiguration of broad leaves in high winds. *Journal of Experimental Botany*, *40*. https://doi.org/10.1093/jxb/40.8.941

Vogel, C. S. (2009). Leaves in the lowest and highest winds: Temperature, force and shape: Tansley review. *New Phytologist*, *183*(1), 13–26. https://doi.org/10.1111/j.1469-8137.2009.02854.x

Vogel, C. S. (2020). *Life in moving fluids: The physical biology of flow-revised and expanded* (2nd ed.). Princeton University Press.

Vollsinger, S., Mitchell, S. J., Byrne, K. E., Novak, M. D., & Rudnicki, M. (2005). Wind tunnel measurements of crown streamlining and drag relationships for several hardwood species. *Canadian Journal of Forest Research*, *35*(5), 1238–1249. https://doi.org/10.1139/x05-051

Wang, B., Shugart, H. H., & Lerdau, M. T. (2017). An individual-based model of forest volatile organic compound emissions—UVAFME-VOC v1.0. *Ecological Modelling*, *350*, 69–78. https://doi.org/10.1016/j.ecolmodel.2017.02.006

Wang, D., Momo Takoudjou, S., & Casella, E. (2020). LeWoS: A universal leaf-wood classification method to facilitate the 3D modelling of large tropical trees using terrestrial LiDAR. *Methods in Ecology and Evolution*, *11*(3), 376–389. https://doi.org/10.1111/2041-210X.13342

Wang, H., Takle, E. S., & Shen, J. (2001). Shelterbelts and windbreaks: Mathematical modeling and computer simulations of turbulent flows. *Annual Review of Fluid Mechanics*, *33*(1), 549–586. https://doi.org/10.1146/annurev.fluid.33.1.549

Watanabe, T. (2004). Large-eddy simulation of coherent turbulence structures associated with scalar ramps over plant canopies. *Boundary-Layer Meteorology*, *112*(2), 307–341. https://doi.org/10.1023/B:BOUN.0000027912.84492.54

Watanabe, T., Shimoyama, K., Kawashima, M., Mizoguchi, Y., & Inagaki, A. (2020). Large-eddy simulation of neutrally-stratified turbulent flow within and above plant canopy using the central-moments-based lattice Boltzmann method. *Boundary-Layer Meteorology*, *176*(1), 35–60. https://doi.org/10.1007/s10546-020-00519-8

Way, D. A., & Pearcy, R. W. (2012). Sunflecks in trees and forests: From photosynthetic physiology to global change biology. *Tree Physiology*, *32*(9), 1066–1081. https://doi.org/10.1093/treephys/tps064

Webb, V. A., & Rudnicki, M. (2009). A linear analysis of the interaction between the atmosphere and an underlying compliant plant canopy. *Boundary-Layer Meteorology*, *133*(1), 93–111. https://doi.org/10.1007/s10546-009-9417-z

Wharton, S., Ma, S., Baldocchi, D. D., Falk, M., Newman, J. F., Osuna, J. L., & Bible, K. (2017). Influence of regional nighttime atmospheric regimes on canopy turbulence and gradients at a closed and open forest in mountain-valley terrain. *Agricultural and Forest Meteorology*, *237–238*, 18–29. https://doi.org/10.1016/j.agrformet.2017.01.020

Whitaker, S. (1973). The transport equations for multi-phase systems. *Chemical Engineering Science*, *28*(1), 139–147. https://doi.org/10.1016/0009-2509(73)85094-8

Whitmore, T. C. (1989). Canopy gaps and the two major groups of forest trees. *Ecology*, *70*(3), 536–538. https://doi.org/10.2307/1940195

Wicker, L. J., & Skamarock, W. C. (2002). Time-splitting methods for elastic models using forward time schemes. *Monthly Weather Review*, *130*(8), 2088–2097. https://doi.org/10.1175/1520-0493(2002)130<2088:TSMFEM>2.0.CO;2

Wilson, K., Goldstein, A., Falge, E., Aubinet, M., Baldocchi, D. D., Berbigier, P., et al. (2002). Energy balance closure at FLUXNET sites. *Agricultural and Forest Meteorology*, *113*(1–4), 223–243. https://doi.org/10.1016/S0168-1923(02)00109-0

Wilson, N. R., & Shaw, R. H. (1977). A higher order closure model for canopy flow. *Journal of Applied Meteorology*, *16*(11), 1197–1205. https://doi.org/10.1175/1520-0450(1977)016<1197:ahocmf>2.0.co;2

Wohlfahrt, G., Anfang, C., Bahn, M., Haslwanter, A., Newesely, C., Schmitt, M., et al. (2005). Quantifying nighttime ecosystem respiration of a meadow using eddy covariance, chambers and modelling. *Agricultural and Forest Meteorology*, *128*(3–4), 141–162. https://doi.org/10.1016/j.agrformet.2004.11.003

Wolfe, G. M., Thornton, J. A., Mckay, M., & Goldstein, A. (2011). Forest-atmosphere exchange of ozone: Sensitivity to very reactive biogenic VOC emissions and implications for in-canopy photochemistry. *Atmospheric Chemistry and Physics*, *11*, 7875–7891. https://doi.org/10.5194/acp-11-7875-2011

Wood, N. (2000). Wind flow over complex terrain: A historical perspective and the prospect for large-eddy modelling. *Boundary-Layer Meteorology*, *96*(1–2), 11–32. https://doi.org/10.1023/A:1002017732694

Wurps, H., Steinfeld, G., & Heinz, S. (2020). Grid-resolution requirements for large-eddy simulations of the atmospheric boundary layer. *Boundary-Layer Meteorology*, *175*(2), 179–201. https://doi.org/10.1007/s10546-020-00504-1

Xiao, Z., Liang, S., & Jiang, B. (2017). Evaluation of four long time-series global leaf area index products. *Agricultural and Forest Meteorology*, *246*, 218–230. https://doi.org/10.1016/j.agrformet.2017.06.016

Xu, L., Pyles, R. D., Paw U, K. T., Snyder, R., Monier, E., Falk, M., & Chen, S. H. (2017). Impact of canopy representations on regional modeling of evapotranspiration using the WRF-ACASA coupled model. *Agricultural and Forest Meteorology*, *247*, 79–92. https://doi.org/10.1016/j.agrformet.2017.07.003

Xu, X., Yi, C., & Kutter, E. (2015). Stably stratified canopy flow in complex terrain. *Atmospheric Chemistry and Physics*, *15*(13), 7457–7470. https://doi.org/10.5194/acp-15-7457-2015

Yaglom, M. (1979). Similarity laws for constant-pressure and pressure-gradient turbulent wall flows. *Annual Review of Fluid Mechanics*, *11*, 505–540. https://doi.org/10.1146/annurev.fl.11.010179.002445

Yan, C., Huang, W. X., Miao, S., Cui, G., & Zhang, Z.-S. (2017). Large-eddy simulation of flow over a vegetation-like canopy modelled as arrays of bluff-body elements. *Boundary-Layer Meteorology*, *165*, 233–249. https://doi.org/10.1007/s10546-017-0274-x

Yan, C., Miao, S., Liu, Y., & Cui, G. (2020). Multiscale modeling of the atmospheric environment over a forest canopy. *Science China Earth Sciences*, *63*, 875–890. https://doi.org/10.1007/s11430-019-9525-6

Yang, B., Morse, A. P., Shaw, R. H., & Paw U, K. T. (2006). Large-eddy simulation of turbulent flow across a forest edge. Part II: Momentum and turbulent kinetic energy budgets. *Boundary-Layer Meteorology*, *121*(3), 433–457. https://doi.org/10.1007/s10546-006-9083-3

Yang, B., Raupach, M. R., Shaw, R. H., Paw U, K. T., & Morse, A. P. (2006). Large-eddy simulation of turbulent flow across a forest edge. Part I: Flow statistics. *Boundary-Layer Meteorology*, *120*(3), 377–412. https://doi.org/10.1007/s10546-006-9057-5

Yue, W., Parlange, M. B., Meneveau, C., Zhu, W., van Hout, R., Katz, J., et al. (2007). Large-eddy simulation of plant canopy flows using plant-scale representation. *Boundary-Layer Meteorology*, *124*, 183–203. https://doi.org/10.1007/s10546-007-9173-x

Zellweger, F., De Frenne, P., Lenoir, J., Vangansbeke, P., Verheyen, K., Bernhardt-Römermann, M., et al. (2020). Forest microclimate dynamics drive plant responses to warming. *Science*, *368*(6492), 772–775. https://doi.org/10.1126/science.aba6880

Zeng, P., & Takahashi, H. (2000). A first-order closure model for the wind flow within and above vegetation canopies. *Agricultural and Forest Meteorology*, *103*(3), 301–313. https://doi.org/10.1016/S0168-1923(00)00133-7

Zeri, M., Rebmann, C., Feigenwinter, C., & Sedlák, P. (2010). Analysis of periods with strong and coherent CO_2 advection over a forested hill. *Agricultural and Forest Meteorology*, *150*(5), 674–683. https://doi.org/10.1016/j.agrformet.2009.12.003

Zhao, F., Yang, X., Schull, M. A., Román-Colón, M. O., Yao, T., Wang, Z., et al. (2011). Measuring effective leaf area index, foliage profile, and stand height in New England forest stands using a full-waveform ground-based lidar. *Remote Sensing of Environment*, *115*(11), 2954–2964. https://doi.org/10.1016/j.rse.2010.08.030

Zhong, J., Cai, X., & Bloss, W. J. (2016). Coupling dynamics and chemistry in the air pollution modelling of street canyons: A review. *Environmental Pollution*, *214*, 690–704. https://doi.org/10.1016/j.envpol.2016.04.052

Zhong, J., Nikolova, I., Cai, X., Mackenzie, A. R., & Harrison, R. M. (2018). Modelling traffic-induced multicomponent ultrafine particles in urban street canyon compartments: Factors that inhibit mixing. *Environmental Pollution*, *238*, 186–195. https://doi.org/10.1016/j.envpol.2018.03.002

Zhu, J., Zhang, G., Wang, G. G., Yan, Q., Lu, D., Li, X., & Zheng, X. (2015). On the size of forest gaps: Can their lower and upper limits be objectively defined? *Agricultural and Forest Meteorology*, *213*, 64–76. https://doi.org/10.1016/j.agrformet.2015.06.015